A STUDY OF K-BAND BACKSCATTERING COEFFICIENTS OF SYMMETRICAL TARGETS

By

LAVERN ANDREW YARBROUGH

Bachelor of Science
Oklahoma Agricultural and Mechanical College
Stillwater, Oklahoma
1951

Master of Science
Oklahoma Agricultural and Mechanical College
Stillwater, Oklahoma
1951

Submitted to the faculty of the Graduate School of Oklahoma State University of Agricultural and Applied Sciences in partial fulfillment of the requirements for the degree of
DOCTOR OF PHILOSOPHY
August, 1957

A STUDY OF K-BAND BACKSCATTERING
COEFFICIENTS OF SYMMETRICAL
TARGETS

Thesis Approved:

Harald Fristoe
Thesis Adviser

A. Naeter

Albert G. Umm

Paul A. McCollum

Wilson J. Bentley

Dean of the Graduate School

PREFACE

Scientists have studied the concepts of the back-scattering of electromagnetic energy from objects for many years. Spheres with sizes comparable to the wavelength of the impinging energy have been investigated both theoretically and experimentally. Metal spheres have been used extensively as a means of reference in conjunction with radar system calibration and reflection comparison. These spheres, usually constructed of aluminum, are treated as prefect conductors while actually they do not have infinite conductivity. Interest has been directed toward treating these as possessing dielectric constants that are complex and to verify the effects of these by laboratory measurements. The formal solution by classical theory does not present a concise method of numerical computation for this case of complex dielectric constant, therefore experimental equipment and techniques are invaluable in the determination of back-scattering coefficient values. The investigation discussed utilizes the synchrodyne principle of operation in the k-band using a modified pyramidal horn adapted to an image plane.

This very important problem of electromagnetic back-scattering deserves much attention and future investigation. The area has been only slightly touched but affords many interesting problems and is of great value in the understanding

and development of further work in the fields of physics, chemistry, meteorology and radio engineering. The experimental phase of this study was performed, under U. S. Air Force Contract, Project 4026, Task 40241, Wright Air Development Center, Air Research and Development Command, Wright-Patterson Air Force Base, Ohio, with project administration under Mr. William Shively, Chief of Chaff Systems.

Many persons through encouragement, advice and suggestions were instrumental in the completion of this research. It is impractical to acknowledge fully my indebtedness to all of these persons.

I wish to express my appreciation for the policies of the United States Air Force which has permitted me the opportunity to pursue graduate studies at Oklahoma State University and particularly to Major General Ralph P. Swofford, former Commandant, USAF Institute of Technology, Wright-Patterson Air Force Base, Dayton, Ohio, for supporting the extension of my study time to complete the educational program and to Major General Lucian K. Lacy, Commandant, USAF Institute of Technology for his continuing support of policies permitting this assignment. Also I wish to thank Brigidier General Ralph L. Wassell, Commander, Directorate of Nuclear Systems, Air Research and Development Command Headquarters, Detachment Number One, Wright-Patterson Air Force Base, Ohio for permitting me to be released from his program and his further support in the Civilian Institution assignment under which the study was completed.

The author wishes to express his appreciation to Doctor Harold T. Fristoe, Professor, School of Electrical Engineering, Oklahoma State University, for his guidance in the overall preparation of this paper; to Doctor Attie L. Betts, Head of Department of Electrical Engineering, Washington State College and former member of the faculty at Oklahoma Agricultural and Mechanical College and to Professor Paul McCollum, member of the faculty at Oklahoma State University, for their many suggestions concerning the detailed information developed in the early stages of this research.

The completion of the educational program culminating in this research has been possible at Okalhoma State University due to the policies of that institution and the policy administration and the encouragement of Professor Albrecht Naeter, Head of the School of Electrical Engineering.

I wish to express appreciation to members of the Advisory Committee for invaluable guidance, advice, support and constructive criticism throughout this program.

Presentation of the subject analysis without some background on the equipment would be incomplete. Furthermore this background offers an opportunity to stress the manner in which the new type of equipment and technique was conceived, developed and employed as a result of basic research.

If the conditions for the conception of new equipment and measurement techniques are to exist and flourish, the principles of conception and development must be understood. The defense of the United States and the moving forward of

scientific development is dependent upon the advancement of basic research.

While an officer in the Signal Corp during World War II, Doctor A. L. Betts, became interested in the radar problems confronting the Armed Services. Later he made a proposal and was awarded a contract from the Wright Air Development Center of the USAF Air Research and Development Command to investigate the reflection of electromagnetic energy from metallic strips. At U. S. Air Force Cambridge Research Center, USAF Air Research and Development Command, interest existed in this same area. Through the efforts of Doctor Roy C. Spencer, Mr. Ralph Hiatt, Mr. Herman Poehler and 1st. Lt. Phillip Blacksmith of AFCRC this research was possible. They provided the necessary equipment and knowledge, as needed to expedite the program.

An examination of new military applications for the analysis of electromagnetic reflective properties of materials draws the conclusion that the use of the equipment and techniques exhibited in this research, and other applications, may represent new and important contributions to the techniques of electronic warfare and related areas.

A word of thanks is due to Doctor Franklin A. Graybill and Mr. David L. Weeks of the School of Mathematics at Oklahoma State University for their guidance and assistance in the reduction of the data by statistical methods. In conclusion I wish to express my sincere gratitude to my wife, Evelyn, for her assistance and encouragement during the preparation of this manuscript.

TABLE OF CONTENTS

LIST OF TABLES

LIST OF ILLUSTRATIONS

LIST OF PLATES

CHAPTER I

INTRODUCTION

Lord Kelvin made a statement that applies so well to help describe the value gained in performing research measurements and using measurement methodology. His statement[1] was;

> When you can measure what you are speaking about and express it in numbers, you know something about it, and when you cannot measure it, when you cannot express it in numbers, your knowledge is of a meagre and unsatisfactory kind. It may be the beginning of knowledge, but you have scarcely in your thought advanced to the stage of a science.

Investigators[2] have devoted considerable effort to the theoretical and experimental study of the scattering from a conducting sphere when it is illuminated by a plane electromagnetic wave. It is known that a redistribution of the field's energy occurs in the vicinity of the sphere. This process involves the internal dissipation of a given amount of the energy in the form of heat due to the characteristics of the metal and the external reradiation of some of the energy in the form of a distributed scattered field due to the geometrical configuration.

---

[1] Thomas B. Crumpler and John H. Yoe, Chemical Computations and Errors, John Wiley and Sons, Inc., New York, 1950, p1.

[2] C. J. Bowkamp, Diffraction Theory, Phillips Research Laboratories, N. V. Phillips' Gloeilampenfabrieken, Eindhaven, Netherlands, May 1955.

The dicussion will be primarily restricted to the particular aspect of the problem describing an improved method for determining backscattering coefficients and methods of analysis of the recorded data. The method of measurement will be applied to conducting spheres with equal radii constructed from iron, aluminum and brass. The measured values will be compared with calculated backscattering values. An introduction to the related theory will be developed before explaining the particular examples in order to present a more complete subject analysis.

There are not very many methods for performing exact solutions for the scattering of electromagnetic waves and the possibility of extending this list is limited. Exact methods have been applied to configurations of finite dimensions such as spheres, infinitely thin circular discs and prolate spheroids. Classical methods of approximations and variational methods of calculations have been applied with limited success.

Modern radar employment demands the facility to distinguish between operational targets and then to analyze the target. The analysis of the target requires that it's conductivity and back-scattering coefficient be carefully defined. Mie's[3] contribution in 1908 involved an infinite series of spherical-mode functions each of which must be represented by an infinite series. Considering a sphere with a complex

---

[3] C. J. Bowkamp.

index of refraction, and since the spherical-mode functions have amplitude coefficients determined by the boundary conditions at the sphere's surface, a complete mathematical solution becomes impractical. The complete theory of the problem was presented by Stratton in 1941 and Goldstein in 1945. An investigation by Aden[4] in 1952 further developed and utilized a part of the solution to the problem. Many others have contributed throughout the years, both theoretically and experimentally, with no small difficulty in determining the reflection from a sphere.

The Problems of scattering, reflection and diffraction of electromagnetic waves by spherical particles are important to the fields of physics, chemistry, meteorology and radio engineering. Perhaps the most important problems being those considering a monochromatic[5] plane wave impinging on a homogeneous isotropic sphere embedded in an infinite homogeneous medium.

About fifty years ago when Rayleigh, Mie and Debye made their formal solutions to this problem and since, when Stratton and others developed and showed applications for these, the form is always an infinite series involving Bessel functions of half and odd integer orders. Calculations

---

[4]A. L. Aden, "Electromagnetic Scattering from Metal and Water Spheres", Naval Technical Report Number 106, Cruft Laboratory, Harvard University, Cambridge, Massachusetts, 1 August 1950.

[5]C. J. Bowkamp.

yielding data are very laborious for some of the practical applications. This arises from the slow convergence of the series which requires the inclusion of a large number of terms. This places great importance on good experimental apparatus and techniques. An experimental method of obtaining reliable values has been a major handicap. Spheres constructed from two different metals such as iron and aluminum would normally indicate indistinguishable readings for backscattering coefficients. The system explained in this thesis did show different values for these. For example, spheres made of these two metals with radii approximately equal to the wavelength of the impinging energy produced values of reflected power requiring attenuator settings in the receiver line of 28.85 db for iron and 29.16 for aluminum to obtain the reference level. An analysis of this difference is also the subject of this Thesis. The reduction of the data to obtain these values was accomplished on probability paper to obtain a preliminary check on the results. Then a final analysis was performed by the statistical method of Analysis of Variance.

This is the first time an arrangement has been successfully adapted to an image system for the purposes of making back-scattering coefficient measurements at a K-band frequency. A method for accomplishing scattering measurements for antennas in terms of the standing waves[6] in the space between

---

[6]Donald D. King, Measurements At Centimeter Wavelengths, D. Van Nostrand Company, Inc., 1952, p. 295.

source and scatterer has been demonstrated for an image system. This method is different from the method used in the described experimentation, in that the measuring apparatus is connected to a movable sampling probe placed in the space between source and scatterer to permit a sampling of the reflection field of the scatterer. This probe causes field distortion and removes energy from the field. The method described overcomes this disadvantage by using a common modified electromagnetic horn for transmitting and receiving.

The term K-band is used in this thesis to mean the particular frequency of operation of the transmitter. This frequency was 25,162.5 megacycles per second as described in the following chapter.

CHAPTER II

RESEARCH EQUIPMENT AND METHOD OF MEASUREMENT

Introduction to Measurement Techniques

The general problem of scattering behavior of electromagnetic energy from metallic and nonmetallic objects has been investigated primarily considering radar reflection characteristics. Using the radar set as a measuring apparatus, the radar cross section, K, sometimes called the echoing area or back-scattering cross section, is related to the power by the following equation;

$$\frac{K}{4\pi} = \frac{\text{Power reflected toward the source per unit solid angle}}{\text{Incident power density}}$$

$$\frac{K}{4\pi} = \frac{(4\pi)^2 \, r^4}{G^2 \, \lambda^2} \cdot \frac{P_r}{P_t} \qquad (2\text{-}1)$$

where r = distance from radar to target

G = Radar Antenna gain

λ = Wavelength

P_r = Received Power

P_t = Transmitted Power

The radar method of measurement has many applications but also has serious limitations. Two limitations of most interest are the requirements for elaborate apparatus and the minumum range restriction.

An equivalent transmission-line[1] circuit may be used to describe some methods of accomplishing back-scattering measurements. Where the parameters of a space transmission line are the parameters of phase constant, $\beta = \frac{2\pi}{\lambda}$ radians; attenuation constant, $\alpha = \frac{\ln r}{r}$ nepers per meter or $\alpha = \frac{\log r}{r}$ decibels per meter; and characteristic impedance, $R_o = 377$ ohms, the system may be represented by the following block diagram.

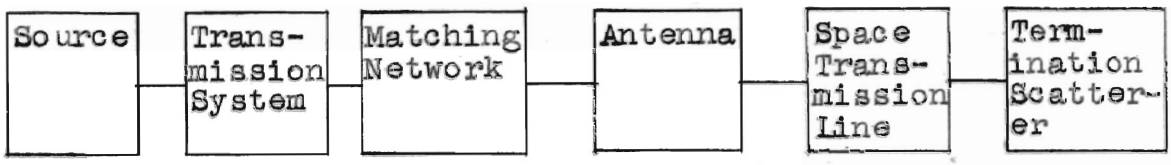

The matching network is used to eliminate standing waves in the absence of a scatterer. This leaves only traveling waves in the space transmission line region, which are generated by the source and radiated at the antenna. The placement of a scatterer in the antenna field results in the presence of standing waves in the space between the scatterer and the antenna and on the antenna feeder. The antenna may be considered from the point of view of it's transformer action or a discontinuity between the attached transmission line and free space. The propagation of waves in the space beyond the transition region between the line and free space is described by the phase constant β corresponding to the velocity of light. The amplitude of the wave is inversely proportional to the distance from the source.

The apparatus and procedure described in this paper

---

[1]Donald D. King, Measurements At Centimeter Wavelengths, D. Van Nostrand Company, Inc., 1952, p. 291.

were established to give maximum sensitivity and stability and to produce a more precise method of measurement of backscattering from objects than has been developed by previous methods. External disturbances were eliminated, or their magnitudes established by performing the tests in a room of adequate size with it's interior constructed of low reflection material so that uncertainties were fully controlled. The experimental measurement errors were reduced to $\pm$ 0.125 db compared to a reliable overall gain measurement of 111.3 db.

This experimentation with the image-plane may be extended to include backscattering values for all basic geometric configurations from different aspects. The information gathered could be used to great advantage. One example would be that of obtaining the backscattering from a particular aircraft or missile. The vehicle may be reduced to the basic geometric configurations, these in turn may be measured on the image-plane by the technique described in this thesis, then the resulting measured values could be combined to produce the overall backscattering values. The mathematical approach[2] to this procedure has been formulated but the results become very extended and complicated. The inadequate sensitivity of equipments and the methods of measurements employed have restricted previous experimentation.

---

[2]K. M. Siegel and H. A. Alperin, Studies in Radar Cross-sections, Willow Run Research Center, Engineering Research Institute, University of Michigan. Reports I through XI.

This system could possibly be used to obtain backscattering values from non-rigid configurations such as a ribbon of metal if the image-plane were inverted to permit the ribbon to hang from it. Perhaps the measurements could be made in a laboratory test box. This would require one of adequate size and lined with an absorbent material. These are problems of interest and perhaps will be investigated in the near future. Research could be conducted on many objects to help gain more knowledge about radar cross sections and their analytical solution.

Conductivity has demonstrated it's effects when considering the surface-wave transmission characteristics of a metal wire with finite conductivity. It was shown by Sommerfeld's calculations[3] in 1899 that the conditions for the mode of propagation of surface waves are satisfied by the very slight retardation provided by the finite conductivity of a metal wire. This concept may be extended to include retardations provided by finite conductivity of metal objects placed on the image plane and irradiated by electromagnetic waves. The results obtained from the experimentation that was performed utilizing a K-band source, synchrodyne principle, horn antenna, image plane and scatterers constructed from iron, aluminum and brass show good correlation with the theoretical predictions. When reference is made to conductivity, concerned with backscattering coefficients the term is meant to include all considerations of energy loss in relation to the

---

[3] Sommerfeld, Annual Physik, p. 81, 1135, 1926.

object under test. Factors such as phase shift, external medium loss, ground plane attenuation, conductivity of the metal and others are included.

The Transmit-Receive System.

The equipment and it's arrangement to make possible the reflection measurements described are unique. Only with the equipment of the prescribed sensitivity, stability, accuracy and physical arrangement are measurements of this type possible. Since the measured values were to be absolute and the variations were to be small in magnitude, every precaution had to be observed in the details of calibration to give full control of all influencing factors. The apparatus will be explained in order to define the conditions under which the data were observed. Figure 1 shows a block diagram of the laboratory arrangement. This arrangement of the equipment was made from component assemblies available in the Antenna laboratory of the US Air Force Cambridge Research Center, Bedford Air Force Base, Massachusetts, therefore, it has no particular identification.

The transmitter-receiver system employed the synchrodyne principle of operation. Reference may be made to the block diagram in Figure 1 to observe frequencies from the different stages. The crystal-controlled oscillator in the exciter section supplies a stable output signal of 5.787037 mc $\pm$ 0.0001%. This frequency is multiplied in this section to produce an output frequency of 833.333 mc = f_o, to drive a SMC-11 klystron multiplier. The output frequency of the SMC-11 is f_1 = 5000 mc $\pm$ 0.0001%, which is channeled to the receiver local oscillator and to the SAC-9 klystron mixer stage. The synchrodyne crystal-controlled oscillator

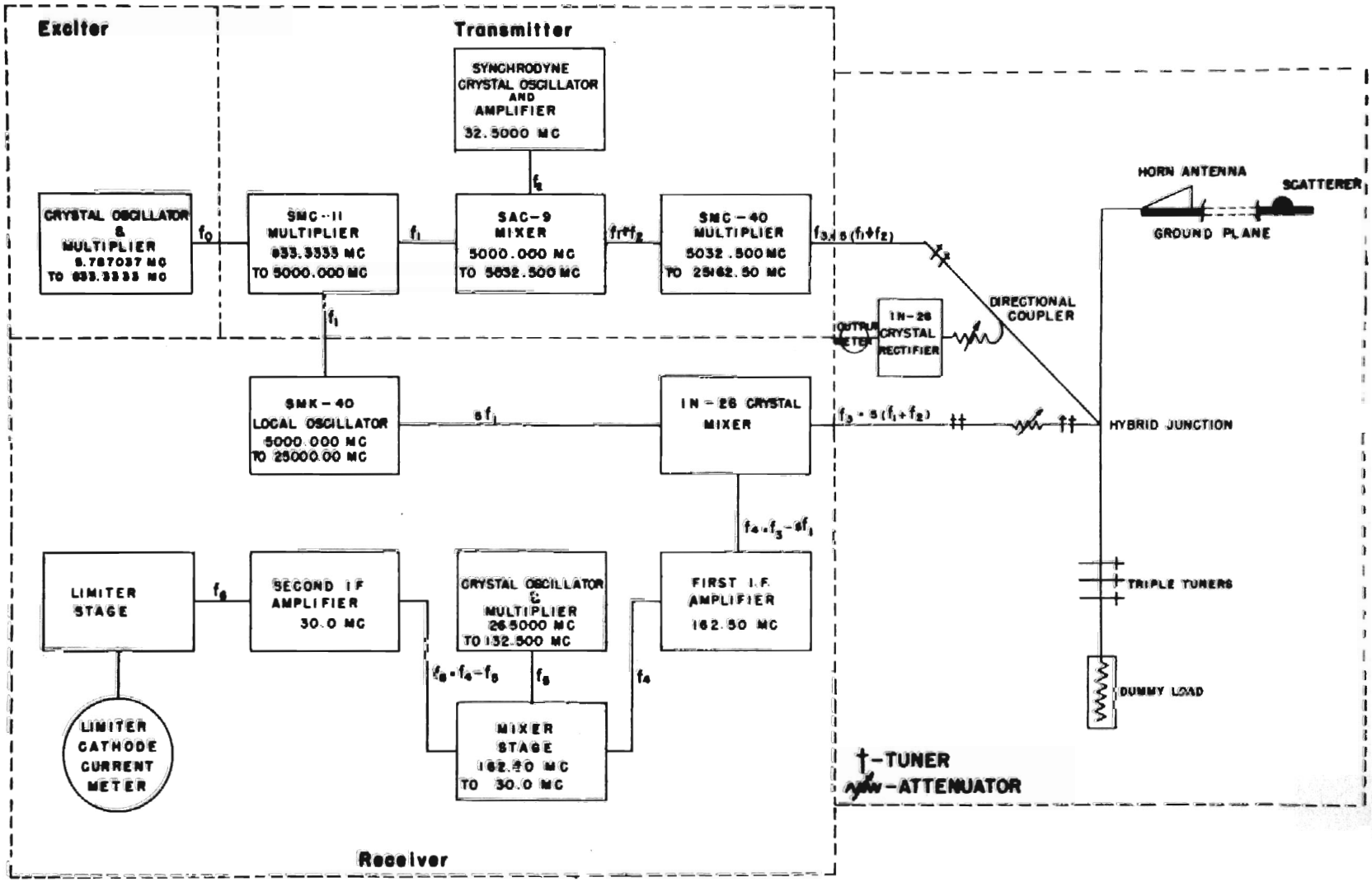

Figure 1. Block diagram of K-band reflection measuring equipment with a schematic of the waveguide and image plane assembly.

through amplifier stages, simultaneously supplies a 32.5000 mc signal, f_2, to the synchrodyne amplifier klystron, which is of the SAC-9 type. The selective tuning of the center and output cavities of the SAC-9 produces an output frequency of $f_1 + f_2 = 5032.500$ mc. This signal is applied to the input of a transmitting multiplier klystron which produces a continuous output wave of $f_3 = 5(f_1 + f_2) = 25,162.50$ mc. This signal is applied to the hybrid junction then to the horn antenna, where it is radiated. The directional coupler, attenuator, IN-26 crystal and output meter are provided to permit the monitoring of the output power. It is essential that the power remain constant. The power output of this system was measured to be 37.5 milliwatts for a reading on the output meter of 200 milliamperes. The output signal is propagated down the image plane and impinges upon the sphere which reradiates part of the incident energy. The reflected signal frequency is f_3, the same as the output signal and it is received by the horn. The reflected signal is coupled from the horn to the hybrid junction, then through a double tuner, an attenuator and another double tuner to an IN-26 crystal mixer stage. The two sets of double tuners are set to produce the desired conditions and are not disturbed throughout the measurements. The variable attenuator is the one mentioned previously, used to produce a decibel reading for back-scattered values of objects. This was carefully calibrated with the klystron source at 25162.50 mc and the

PRD 650-A Power Measurement Bridge. The received signal, f_3 = 25,162.50 mc, is mixed with a 25,000 mc signal that is generated by the SMK-40 and by multiplication. The remainder of the receiver section is a double-superheterodyne receiver. The output of the IN-26 crystal mixer is $f_4 = f_3 - 5f_1 = 162.50$ mc. This signal, f_4, is then coupled to a mixer through the first intermediate frequency amplifier stages. A crystal-controlled oscillator generates a frequency of 26.5000 mc which is multiplied to give an input to the mixer of 132.500 mc. The mixer output frequency becomes $f_6 = f_4 - f_5 = 30.$mc. The 30.0 mc frequency is coupled to a limiter stage through the second intermediate frequency amplifier stages. A meter is placed in the limiter's cathode circuit and it's scale is calibrated to read reflected power values in conjunction with the variable attenuator in the receiver input line.

Power requirements were supplied by a central power rack placed at the rear of the ground plane, (see Plate I). All of these power supplies were carefully regulated.

Plate I.

Pictorial view of the central power rack and connecting assemblies.

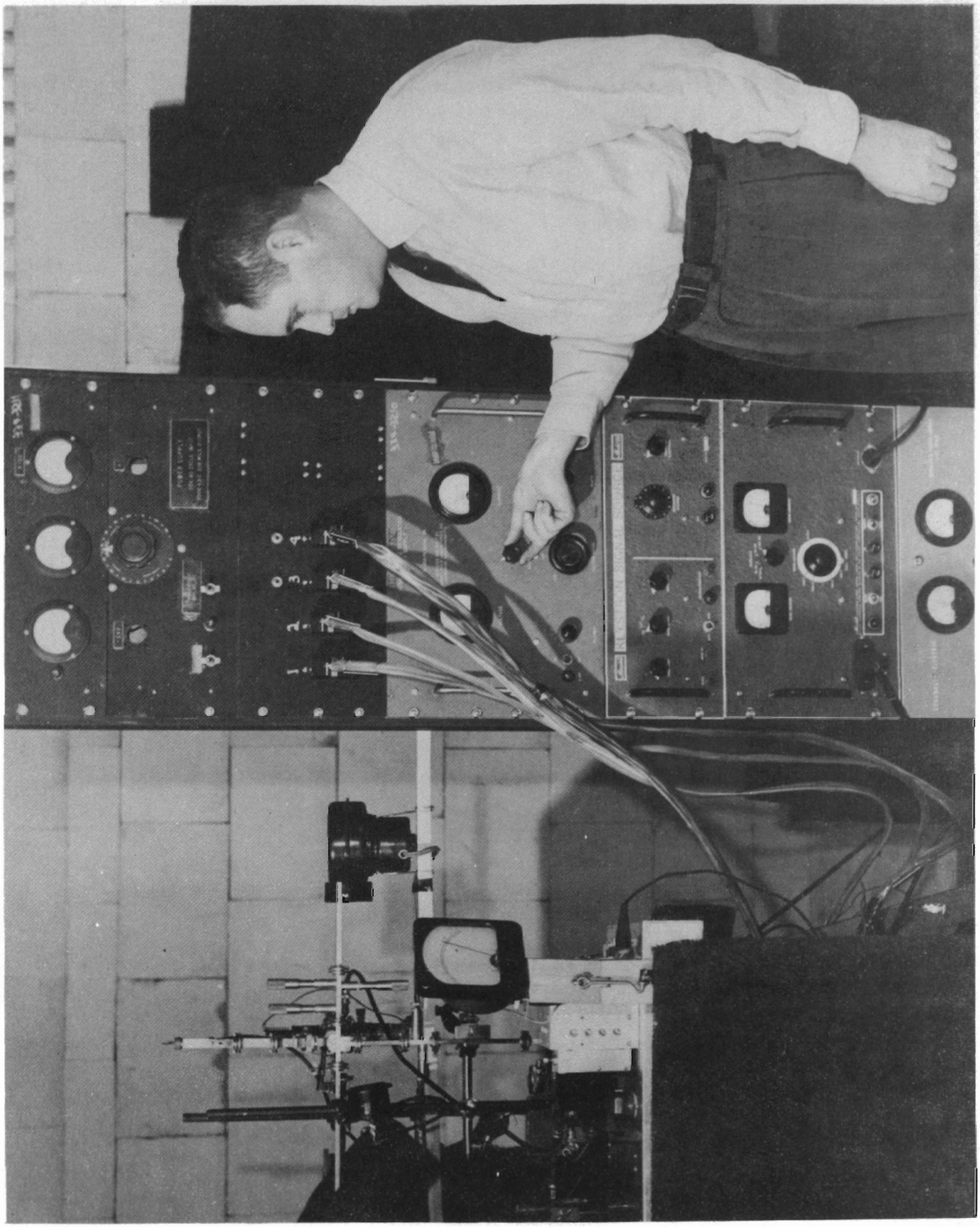

The Hybrid Junction Analysis

The Hybrid Junction, commonly called magic tee, (Refer to Plate II), was one of the more critical components in the equipment. Special attention had to be given to keep it physically and electrically stable. Sufficient clamping was provided to permit stationary placement and to prevent any physical deformation. The temperature of the dark room was kept constant preventing any expansion and contraction of the elements due to temperature changes. The triple tuners, with micrometer handles attached, were used to match the impedance of the dummy load to that of the horn. These were very critical in adjustment but remained in adjustment considerably well after they had been tuned to the desired position.

The condition for balance of the hybrid is that the side arm terminations be equal. If unbalanced operation is desired the degree of match obtained is of great importance. In this research the condition of unbalance with a matched standard is utilized. The attenuation[4] between the two side arms is

$$A = 20 \log_{10} P_2 - 6 \text{ db} = 10 \log_{10} \frac{P4}{P_2} \qquad (2\text{-}2)$$

This corresponds to a power level in the detector arm of $\frac{P_2^2}{4}$ x (incident power in generator arm), producing conditions particularly suitable for small reflection determination. These relations apply to input and output when the hybrid

---

[4] Donald D. King, pp. 229-230.

Plate II.

View of the equipment assembly with the hybrid junction connections.

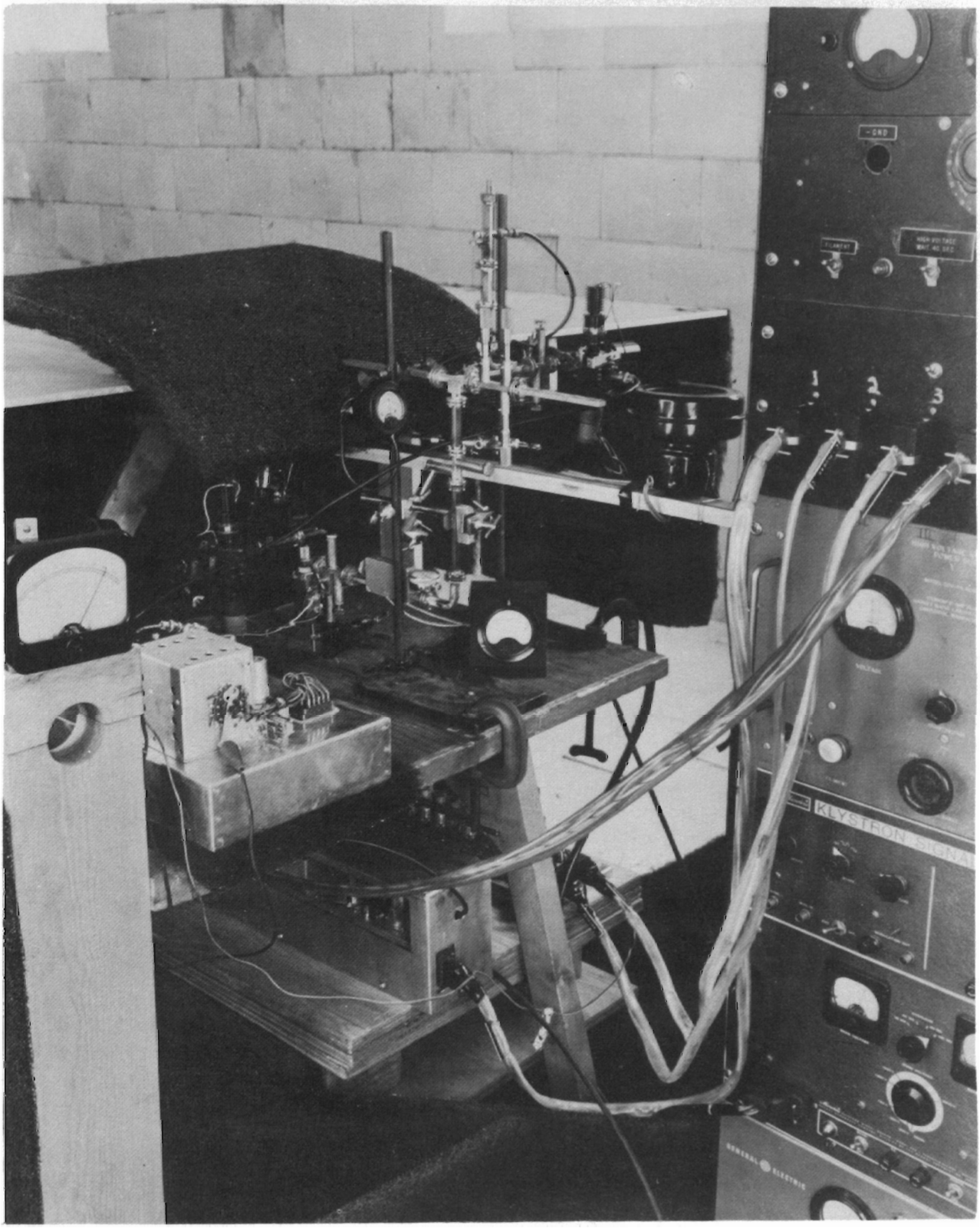

appears matched looking into any arm with the three remaining arms properly matched. Stub tuners with micrometer handles attached were used to facilitate precise tuning. A useful fact in securing proper adjustment is that the magic tee unbalance signal is insensitive to the phase of the reflections.

The magic tee, when carefully tuned, presents the frequency dependence of the unknown reflection coefficient, also it presents precise reflection data.

The magic tee was constructed by combining E-type and H-type junctions, as shown in Figure 2. The illustration

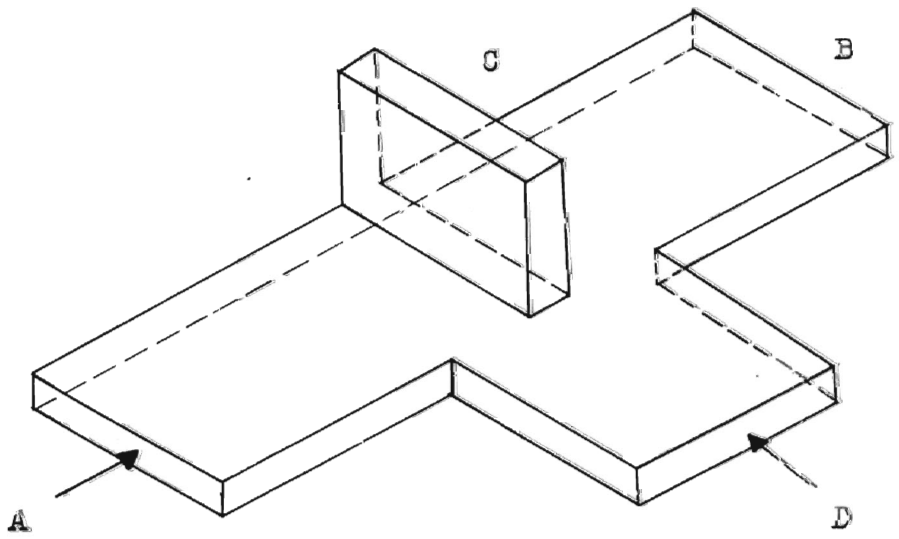

Figure 2. The magic tee.

shows that the magic tee had two input signals applied to it. The oscillator signal generated by the SMK-40 klystron multiplier tube was fed into arm D, and the echo signals from the horn antenna were fed into arm A. The principle of

operation may be explained by considering the H-type and E-type junctions separately then superimposing the two in combination.

The H-type T-Junction

The H-type T-junction[5] shown in Figure 3, is constructed by joining rectangular waveguides with an arm (labelled D) connected along the narrow dimension of the main waveguide. The H-type junction is so called because the arm of the junction extends from the main waveguide in the plane in which the H lines lie in the main waveguide, with the resultant shape forming a T.

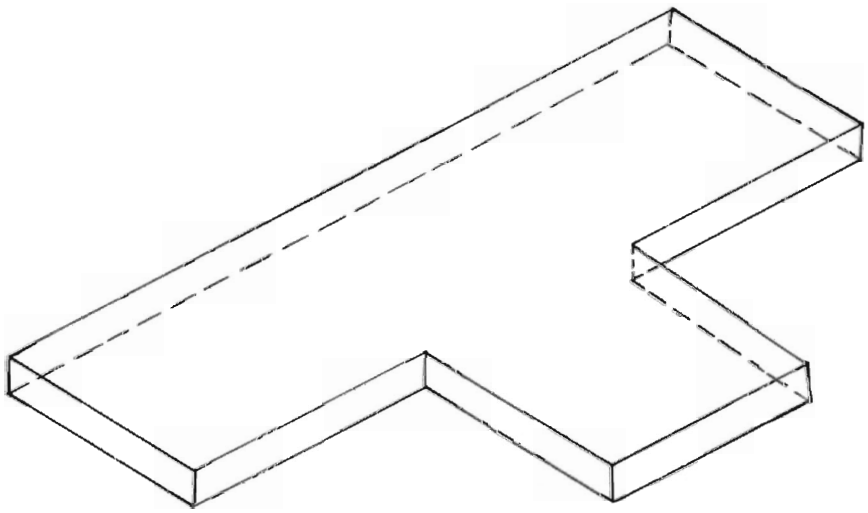

Figure 3 The H-type T-junction.

Figure 4 is a top view representation of an H-type T-junction, showing a signal being fed into arm A. The figure

---

[5] John E. Marchesano, "Hybrid Junctions", Philco Tech Rep Division Bulletin, Volume 5, Number 5, September and October 1955, Philadelphia, Pennsylvania, pp. 2-11.

shows the tails of the E field arrows as crosses, with lines joining the points of the equipotential lines. The energy moves normally along the main waveguide until it approaches the junction. At the junction, the E field will have to change in order to conform to the discontinuity. The potential difference between the upper and the lower walls of the main waveguide at the A entrance end causes a potential difference to exist at the entrances to B and D. This condition results in the presence of an E field in both of these arms, and energy will move out of them without change of phase.

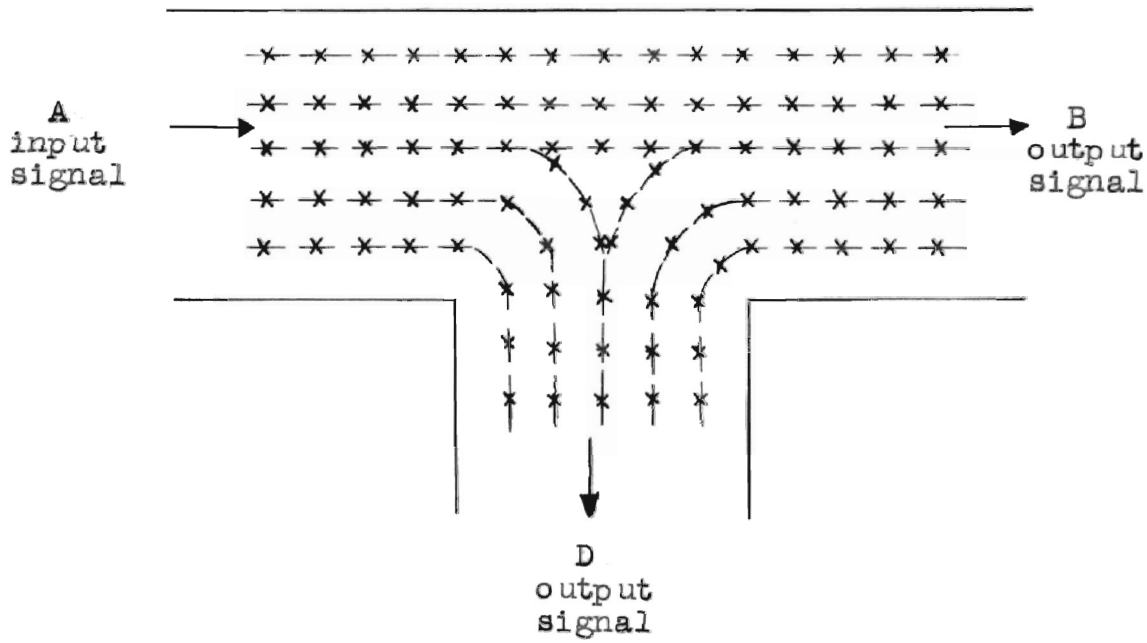

Figure 4. E fields in an H-type T-junction with a signal fed into arm A.

Figure 5 is a pictorial representation of the contour described by the E field as it progresses through the junction. Note that the condition of zero E field at the surface of the narrow guide walls is always met. The E-type and the H-type junctions are symmetrical, the same conditions apply for both if the signal is fed into arm B. If the energy is fed into arm D, in-phase outputs are obtained from arms A and B. These facts may be stated as follows; When a signal is fed into any arm of an H-type T-junction, outputs will be obtained from the remaining two arms and the outputs will be in phase with the input signal.

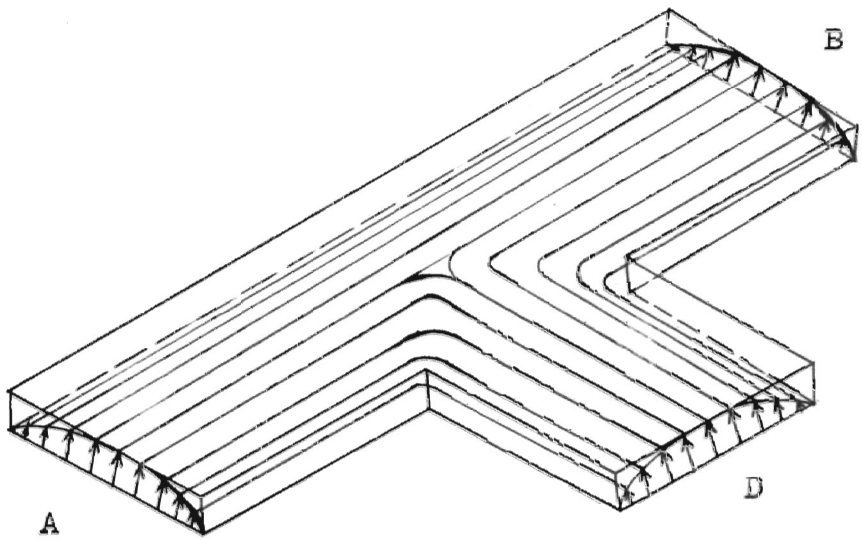

Figure 5. Pictorial representation of the surface described by the E field in Figure 4.

The E-type T-Junction

The E-type T-junction, shown in Figure 6, is constructed by joining rectangular waveguides with an arm (labelled C) connected across the wide dimension of the main waveguide. The E-type T-junction is so called because the arm of the junction extends from the main waveguide in the same direction as the E lines in the waveguide, with the resultant shape forming a T.

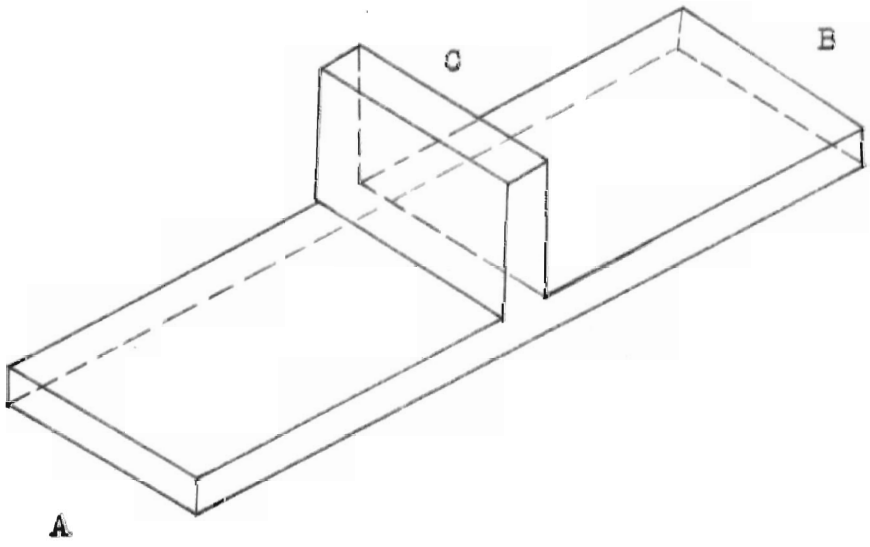

Figure 6. The E-type T-junction.

Figure 7 is a cutaway front view of the E-type T-junction shown in Figure 6. The drawing shows a signal being fed into arm A. The energy travels normally along the waveguide until it approaches the junction, where the fields must change to conform to the discontinuity. Arrows are used to show the direction and distortion of the E field, the direction of the arrows being from a positive to a negative potential.

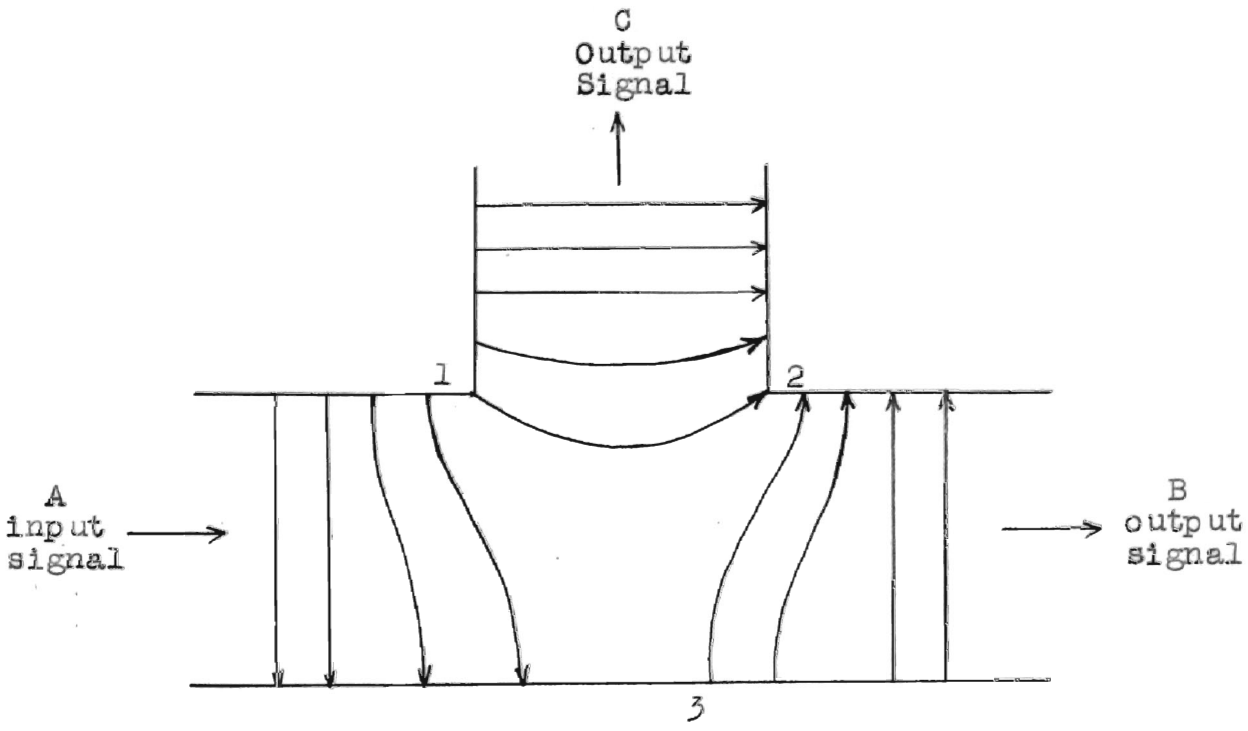

Figure 7. E Fields in an E-type T-junction.

When the E field arrives at point 1, a positive charge will exist there. This charge induces, electrostatically, a negative charge at point 2, and an E field will exist between the two points as shown in the illustration. The induced negative charge at point 2 will, in turn, induce a positive charge on the wall below it, causing an E field between points 2 and 3, as indicated. This new E field now proceeds out through B and C. Note that the E field did not change polarity in going from arm A to arm C, but that it did change polarity in going from arm A to arm B. Thus the following conclusion with reference to Figure 7 may be stated: When a signal is fed into arm A of an E-type T-junction, the output from arm B will be 180° out-of-phase

with the input signal, and the output from arm C will be in-phase with the input signal.

Operation of the Magic Tee

Consider the operation of the magic tee when a signal is fed into D, as shown in Figure 8. From the operation of the H-type T-junction, it can be seen that signals will travel out through arms A and B in phase. However, no signal will travel out through arm C, because there is no potential difference at the input to arm C. The reason for this lack of potential can be found by referring to Figure 8.

First, however, a brief explanation of the figure is in order. When a signal is applied to arm D, an E field will appear across this arm, and it's components will have different magnitudes as shown by the associated vectors labelled 1. If one visualizes this E field progressing to the junction, and then out through arms A and B, a solid volume will be described as shown in Figure 5 for the H-type T-junction. However, instead of showing the volume, slices of it have been drawn only at important points to indicate the shape of the field at those points. The large arrows indicate the direction in which the energy flows in passing through the junction. With this in mind, consider the slices labelled 2 and 3. Because of the symmetry of the magic tee, the energy will divide equally into arms A and B, and the E fields on both sides of arm C will be identical in shape. Since the potentials on both sides of arm C are the same, no potential difference will be impressed at the input of this arm, and no signal will travel out through arm C.

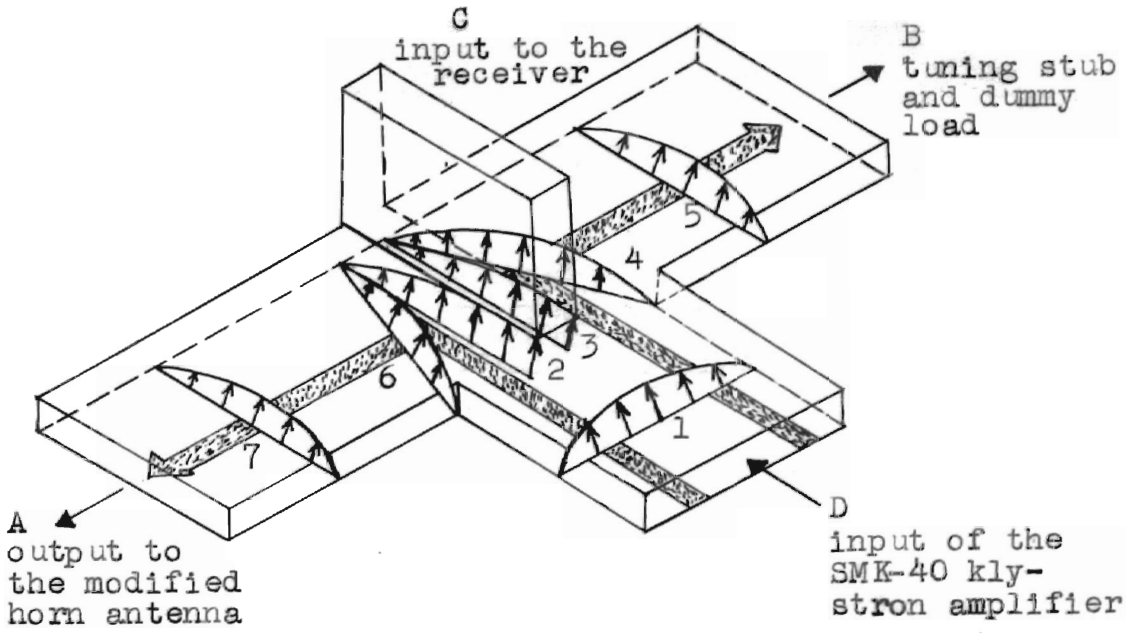

Figure 8. E fields in a magic tee with a signal fed into arm D.

The bending of the arrows is due to the fringing effect at the opening of the arm. E field slices 4 and 6 indicate the shape the field takes as it goes around the corners of the junction. E field slices 5 and 7 show the field returned to it's normal shape as it is propagated out through arms A and B. The result of applying a signal to arm D may be stated as follows: When an input signal is applied to arm D of a magic tee, the outputs from arms A and B will be in-phase with the input signal, and no output will be obtained from arm C.

Finally, consider the operation of the magic tee when a signal is applied either to arm A or B. Because of the symmetry of the magic tee, the operation will be the same for

application to either arm. Assuming that the signal is applied to arm A, as indicated in Figure 9, it will be found that outputs will be obtained from arms C and D, but not from B. The reason for this may be determined by referring to Figure 9 and recalling the rules for the operation of basic T-junctions. In order to determine the resulting outputs, it will first be assumed that arm D is not present, making the magic tee a simple E-type junction. It is known that the output from arm C will be in-phase with the input signal, whereas the output from arm B will be displaced 180°. Next assume that arm C is not present, making the magic tee a simple H-type T-junction. It is known that the outputs from arms B and D will be in phase with the input signal. Now, when the resulting fields are combined in the magic tee, it can be seen that the two component fields in arm B are opposite in phase, causing a cancellation of the signal and zero output from arm B. These facts may be stated as follows: When a signal is applied either to arm A or arm B of a magic tee, outputs that are in-phase with the input signal will be obtained from arms C and D, but no output will be realized from the remaining arm.

The above explanation applies to the operation of the magic tee for the application in this research, since the oscillator signal was applied to arm D and the reflection signals received by the modified pyramidal horn antenna were applied to arm A.

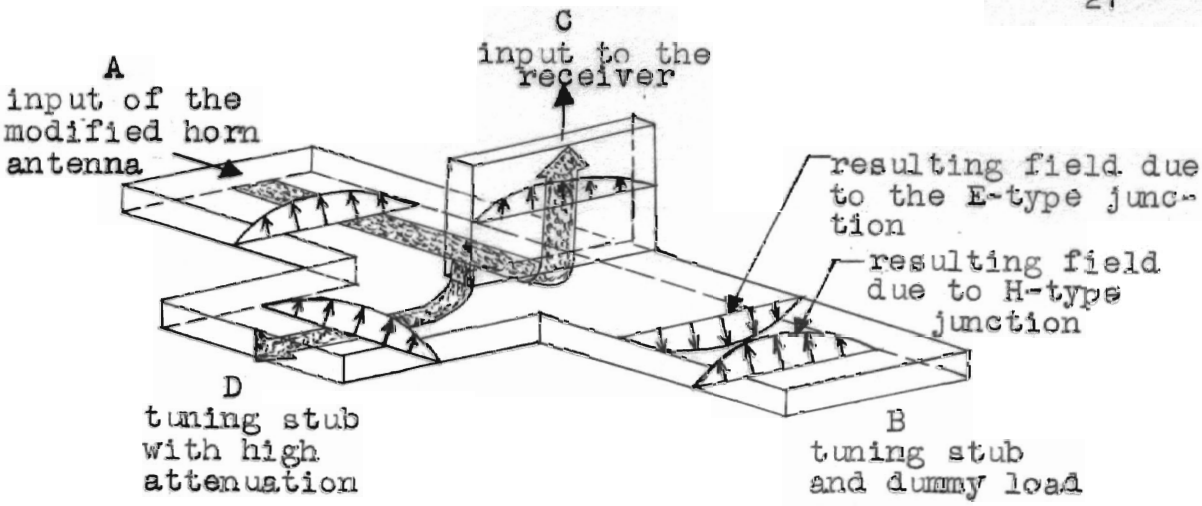

Figure 9. E fields in a magic tee with a signal fed into arm A.

The term magic tee is applied to the hybrid junction having very valuable properties from it's four outputs. Using the illustration in Figure 10, an analytical development will be done, on the basis of these properties.

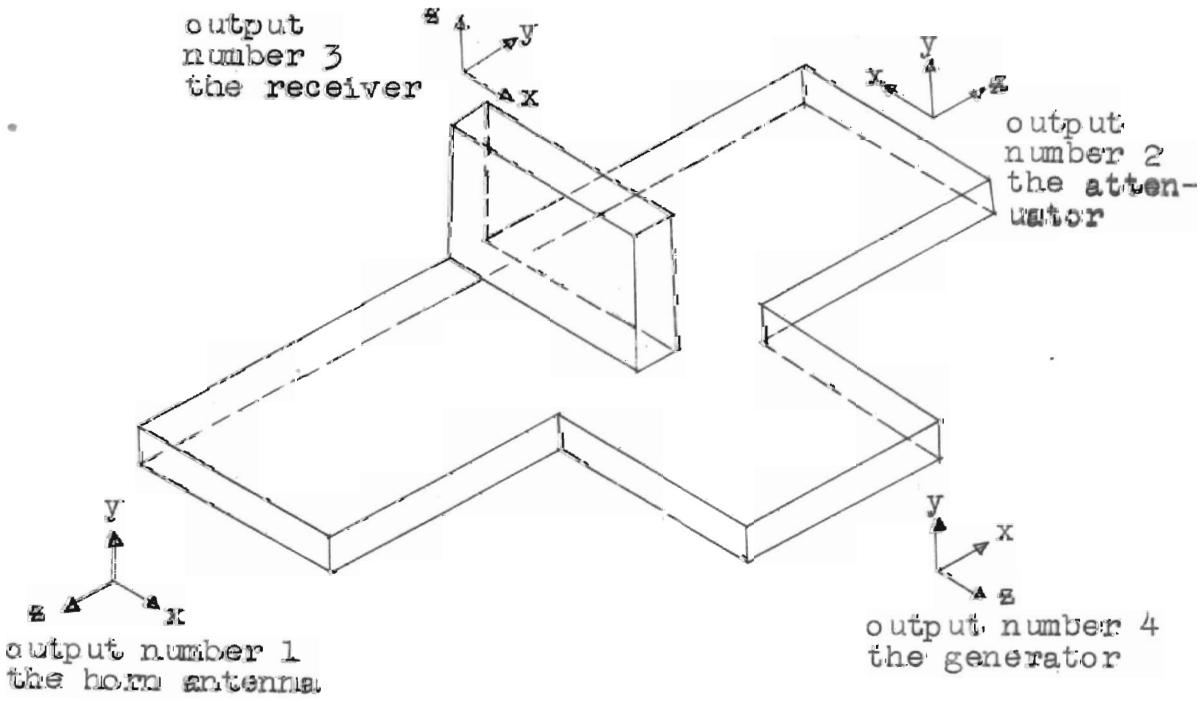

Figure 10. The magic tee with axes established and connections indicated.

The important properties of symmetry and transmission of waves through the magic tee are considerations that apply to the application in these measurements. The wave from the klystron multiplier was traveling into output 4. It's electric field was along the vertical in the y-direction as shown. Symmetrically we have coupling into outputs 1 and 2 but none in output 3. By matching outputs 1 and 2 an equal power division results and no power flows out of output 3. Equal reflected waves are produced by outputs 1 and 2 since they are terminated in equal impedances. These combine and flow out of output 4.

Consider the magic tee from the analysis of standing waves of different symmetries. According to the method of Slater[6] there is no unique way to determine reference planes. Arbitrarly choose symmetrically placed planes in outputs 1 and 2 and set up two anti-symmetrical and two symmetrical standing waves. One of each of these standing waves will have V = 0 and the others I = 0 at the reference planes in outputs 1 and 2.

Choose the reference plane in output 4 such that it has zero voltage across it when the symmetric function has zero voltage across the planes in outputs 1 and 2. Choose the reference plane in output 3 so that it has zero voltage

---

[6]John C. Slater, Microwave Electronics, D. Van Nostrand Co., Inc., New York, 1950, pp. 62-168.

across it when the anti-symmetric function has zero voltage across the reference planes in outputs 1 and 2.

Use a first subscript to represent the output to be considered. Use a second subscript to denote the anti-symmetric solutions by 1 and 2 for the case of zero voltage at the plane 1 and 2, and denote the symmetric solutions by 3 and 4 for the case of zero current on these planes. These conditions produce the following relations;

$$V_{11} = V_{21} = V_{31} = V_{41} = 0, \qquad I_{11} = -I_{21}, \; I_{41} = 0 \tag{2-3}$$

$$V_{12} = -V_{22}, \qquad V_{42} = 0, \qquad I_{12} = I_{22} = I_{42} = 0 \tag{2-4}$$

$$V_{13} = V_{23} = V_{33} = V_{43} = 0, \qquad I_{13} = I_{23}, \; I_{33} = 0 \tag{2-5}$$

$$V_{14} = V_{24}, \qquad V_{34} = 0, \qquad I_{14} = I_{24} = I_{34} = 0 \tag{2-6}$$

Voltages and currents at the different reference planes become

$$V_1 = C_2 V_{12} + C_4 V_{14}, \qquad V_2 = -C_2 V_{12} + C_4 V_{14}, \tag{2-7}$$

$$V_3 = C_2 V_{32}, \qquad V_4 = C_4 V_{44} \tag{2-8}$$

$$I_1 = C_1 I_{11} + C_3 I_{13}, \qquad I_2 = -C_1 I_{11} + C_3 I_{13} \tag{2-9}$$

$$I_3 = C_1 I_{31} + C_2 I_{32}, \qquad I_4 = C_3 I_{43} + C_4 I_{44} \tag{2-10}$$

where C represents a constant.

Using these, set up the equations

$$\frac{I_3}{V_3} = \frac{I_{32}}{V_{32}} + \frac{C_1}{C_2}\frac{I_{31}}{V_{32}} = \frac{I_{32}}{V_{32}} + \frac{I_{31}}{V_{32}}\frac{V_{12}}{I_{11}}\left(\frac{I_1 - I_2}{V_1 - V_2}\right) \tag{2-11}$$

$$\frac{I_4}{V_4} = \frac{I_{44}}{V_{44}} + \frac{C_3}{C_4}\frac{I_{43}}{V_{44}} = \frac{I_{44}}{V_{44}} + \frac{I_{43}}{V_{44}}\frac{V_{14}}{I_{13}}\left(\frac{I_1 + I_2}{V_1 + V_2}\right) \tag{2-12}$$

Assuming the four outputs to have equal characteristic impedances, let

$$\frac{I_1}{V_1} z_o = Y_1 \tag{2-13}$$

$$\frac{I_2}{V_2} z_o = Y_2 \tag{2-14}$$

$$\frac{I_3}{V_3} z_o = Y_3 \tag{2-15}$$

$$\frac{I_4}{V_4} z_o = Y_4 \tag{2-16}$$

$$-jb_3 = \frac{I_{32}}{V_{32}} z_o \tag{2-17}$$

$$-jb_4 = \frac{I_{44}}{V_{44}} z_o \tag{2-18}$$

$$\alpha_3 = -\frac{I_{31}}{V_{32}} \frac{V_{12}}{I_{11}} \tag{2-19}$$

$$\alpha_4 = -\frac{I_{43}}{V_{44}} \frac{V_{14}}{I_{13}} \tag{2-20}$$

and we get

$$Y_3 = -jb_3 - \alpha_3 \left(\frac{Y_1 V_1 - Y_2 V_2}{V_1 - V_2} \right) \tag{2-21}$$

$$Y_4 = -jb_4 - \alpha_4 \left(\frac{Y_1 V_1 + Y_2 V_2}{V_1 + V_2} \right) \tag{2-22}$$

Solving for the ratio $\frac{V_1}{V_2}$ in each equation, the results from the equation for Y_3 become

$$V_1 (Y_3 + jb_3 + \alpha_3 Y_1) = V_2 (Y_3 + jb_3 + \alpha_3 Y_2)$$

$$\frac{V_1}{V_2} = \left(\frac{Y_3 + jb_3 + \alpha_3 Y_2}{Y_3 + jb_3 + \alpha_3 Y_1} \right) \tag{2-23}$$

and from the equation for Y_4

$$V_1(Y_4 + jb_4 + \alpha_4 Y_1) = -V_2 (Y_4 + jb_4 + \alpha_4 Y_2)$$

$$\frac{V_1}{V_2} = -\left(\frac{Y_4 + jb_4 + \alpha_4 Y_2}{Y_4 + jb_4 + \alpha_4 Y_1}\right) \qquad (2\text{-}24)$$

Now

$$\frac{Y_3 + jb_3 + \alpha_3 Y_2}{Y_3 + jb_3 + \alpha_3 Y_1} = \frac{-Y_4 - jb_4 - \alpha_4 Y_2}{Y_4 + jb_4 + \alpha_4 Y_1}$$

and

$$Y_1 Y_2 + \frac{(Y_3 + jb_3)}{\alpha_3} \quad \frac{(Y_4 + jb_4)}{\alpha_4} +$$

$$\frac{1}{2}\left(Y_1 + Y_2\right)\left[\frac{Y_3 + jb_3}{\alpha_3} + \frac{Y_4 + jb_4}{\alpha_4}\right] = 0 \qquad (2\text{-}25)$$

which is an equation of the admittances for the magic tee.

The condition holding for the transmission characteristics of this experimentation was $Y_1 = Y_2$. From the admittance equation this gives

$$\left(Y_1 + \frac{Y_3 + jb_3}{\alpha_3}\right) \left(Y_1 + \frac{Y_4 + jb_4}{\alpha_4}\right) = 0 \qquad (2\text{-}26)$$

In this equation the second factor is zero since energy was fed into output 4, meaning no energy feeds to output 3. For this

$$Y_1 + \frac{Y_4 + jb_4}{\alpha_4} = 0$$

$$-Y_4 = jb_4 + \alpha_4 Y_1 \qquad (2\text{-}27)$$

This shows the admittance to be independent of Y_3. Since the output lines were tuned to make b_3 equal b_4 equal zero and make α_3 equal α_4 equal 1, we have $-Y_4 = Y_1$. This indicates if terminals 1 and 2 are a perfect match, $Y_1 = Y_2 = 1$ and there occurs a match looking in at output 3. This follows since outputs 1 and 2 show equal impedances and therefore the total power is divided between them equally, leaving no power for output 3. There is no effect of the admittance in output 3 on the admittance as seen in output 4.

The condition holding for the reception characteristics is

$$\frac{Y_3 + jb_3}{\alpha_3} = \frac{Y_4 + jb_4}{\alpha_4} \qquad (2\text{-}28)$$

From the admittance equation we can get

$$\left(\frac{Y_4 + jb_4}{\alpha_4} + Y_1\right) \qquad \left(\frac{Y_4 + jb_4}{\alpha_4} + Y_2\right) = 0 \qquad (2\text{-}29)$$

Output 1 is the horn connection and the terminal for input power. If in the derivation all terms of $\frac{Y_3 + jb_3}{\alpha_3}$ are replaced by Y_3 and all terms of $\frac{Y_4 + jb_4}{\alpha_4}$ are replaced by Y_4 the result will be complete symmetry between the two sets of outputs.

Power having been chosen as the factor of most importance in these measurements, the power flow relations may be considered according to the following,

$$P_1 = G_1 \left|V_1\right|^2 \qquad P_3 = G_3 \left|V_3\right|^2,$$

$$P_2 = G_2 \left|V_2\right|^2, \qquad P_4 = G_4 \left|V_4\right|^2 \qquad (2\text{-}30)$$

From the admittance relationships a value for the ratio $\frac{V_1}{V_2}$ was determined and in like manner the following relations would hold,

$$V_3 = \frac{V_{32}}{V_{12}} \left(\frac{V_1 - V_2}{2}\right) \text{ and } V_4 = \frac{V_{44}}{V_{14}} \left(\frac{V_1 + V_2}{2}\right) \qquad (2\text{-}31)$$

The quantities $\frac{V_{32}}{V_{12}}$ and $\frac{V_{44}}{V_{14}}$ may be evaluated by considering the fact that the total power flow from all the outputs must equal zero.

$$R_e \sum_{kab} C_a \; V_{ka} \; \bar{C}_b \; \bar{I}_{kb} = R_e \sum_{ab} C_a \; C_b \sum_{k} V_{ka} \; \bar{I}_{kb} = 0 \qquad (2\text{-}32)$$

where a and b are the series 1 to 4 and k the outputs 1 to 4, and the following must hold

$\sum_{k} V_{ka} \; \bar{I}_{kb} = 0$ for the above to be true using arbitrary values for the C's. The only case where this needs to hold is for $a \neq b$. The combinations of a and b that are not trivial are

$$2 \; I_{11} \; V_{12} + I_{31} \; V_{32} = 0 \qquad (2\text{-}33)$$

$$2 \; I_{13} \; V_{14} + I_{44} = 0 \qquad (2\text{-}34)$$

combining these with

$$\alpha_3 = - \frac{I_{31}}{V_{32}} \quad \frac{V_{12}}{I_{11}} \text{ and } \alpha_4 = \frac{-I_{43}}{V_{44}} \quad \frac{V_{14}}{I_{13}}$$

the result is

$$\frac{V_{32}}{V_{12}} = \sqrt{\frac{2}{\alpha_3}} \quad \text{and} \quad \frac{V_{44}}{V_{14}} = \sqrt{\frac{2}{\alpha_4}} \; . \qquad (2\text{-}35)$$

Now with the relationships of V_1, V_2, V_3 and V_4 the equations for the respective powers become

$$P_1 = G_1 \left| \frac{Y_3 + jb_3}{\alpha_3} + Y_2 \right|^2 \qquad (2\text{-}36)$$

$$P_2 = G_2 \left| \frac{Y_3 + jb_3}{\alpha_3} + Y_1 \right|^2 \qquad (2\text{-}37)$$

$$P_3 = \frac{G_3}{2\alpha_3} \left| Y_2 - Y_1 \right|^2 \qquad (2\text{-}38)$$

$$P_4 = \frac{G_4}{2\alpha_4} \left| 2\left(\frac{Y_3 + jb_3}{\alpha_3}\right) + Y_1 + Y_2 \right|^2 \qquad (2\text{-}39)$$

This form is convenient to use when power is fed into the output arm 4 of the magic tee. For the case of $Y_1 = Y_2$ the equations for the powers are

$$P_1 = G_1 \left| \frac{Y_3 + jb_3}{\alpha_3} + Y_1 \right|^2 \qquad (2\text{-}40)$$

$$P_2 = G_1 \left| \frac{Y_3 + jb_3}{\alpha_3} + Y_1 \right|^2 \qquad (2\text{-}41)$$

$$P_3 = \frac{G_3}{2\alpha_3} \left| Y_1 - Y_1 \right|^2 = 0 \qquad (2\text{-}42)$$

$$P_4 = \frac{2G_4}{\alpha_4} \left| \frac{Y_3 + jb_3}{\alpha_3} + Y_1 \right|^2 \qquad (2\text{-}43)$$

Using the real part of the equation

$$-Y_4 = jb_4 + \alpha_4 Y_1$$

the expression for the conductance is

$$-G_{14} = \alpha_4 G_1 \qquad (2\text{-}44)$$

which produces

$$P_1 = 1$$

$$P_2 = 1$$

$$P_3 = 0$$

$$P_4 = -2$$

This shows the power flowing into output 4 is equally

divided between outputs 1 and 2 and gives no power to output 3. Since this verifies the statement concerning symmetry and power relations, the conditions assumed for the transmission and reception characteristics are valid.

The Modified Pyramidal Horn Antenna

The horn used in this research was adapted for ground plane use by reducing it's effective aperture to one-half the size that would be used for free space conditions without the ground plane, (see Plate III). This means the horn has it's aperture reduced electromagnetically 3 db down from that of a full-sized pyramidal horn when working in free space. The principle of images was verified in the gain measurements. Figure 11a illustrates the full-sized free space horn and it's dimensions. Figure 11b shows the modified pyramidal horn adapted for ground plane employment and it's values. The full-sized pyramidal horn was modified by cutting away the lower horn flare such that the section of waveguide was in line with the bottom of the horn. Thus the lower wall of the waveguide and the bottom of the horn are in the same plane.

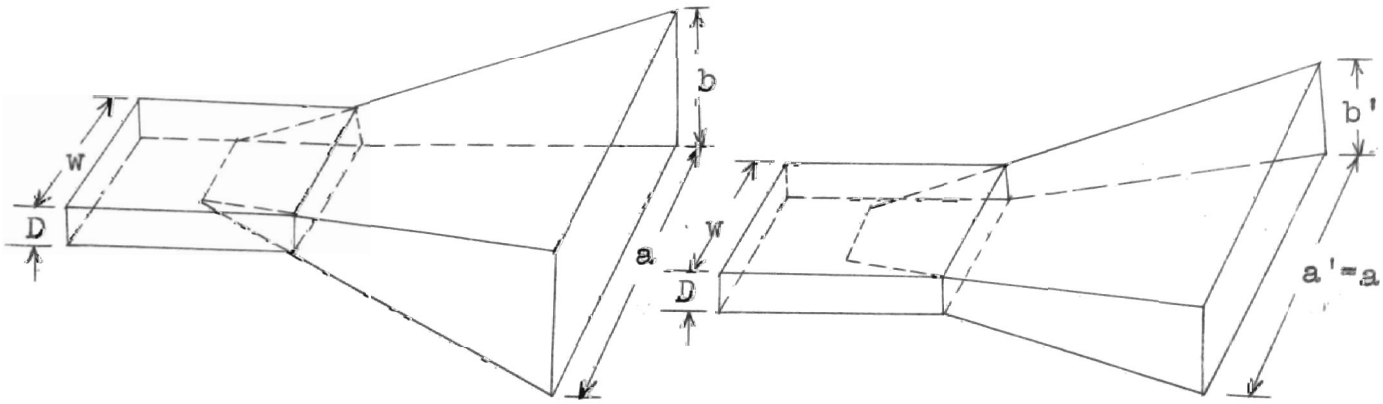

a. Full-sized pyramidal horn. b. Modified pyramidal horn.

Figure 11. The pyramidal horn antenna.

Plate III.

The modified pyramidal horn
mounted on the image plane.

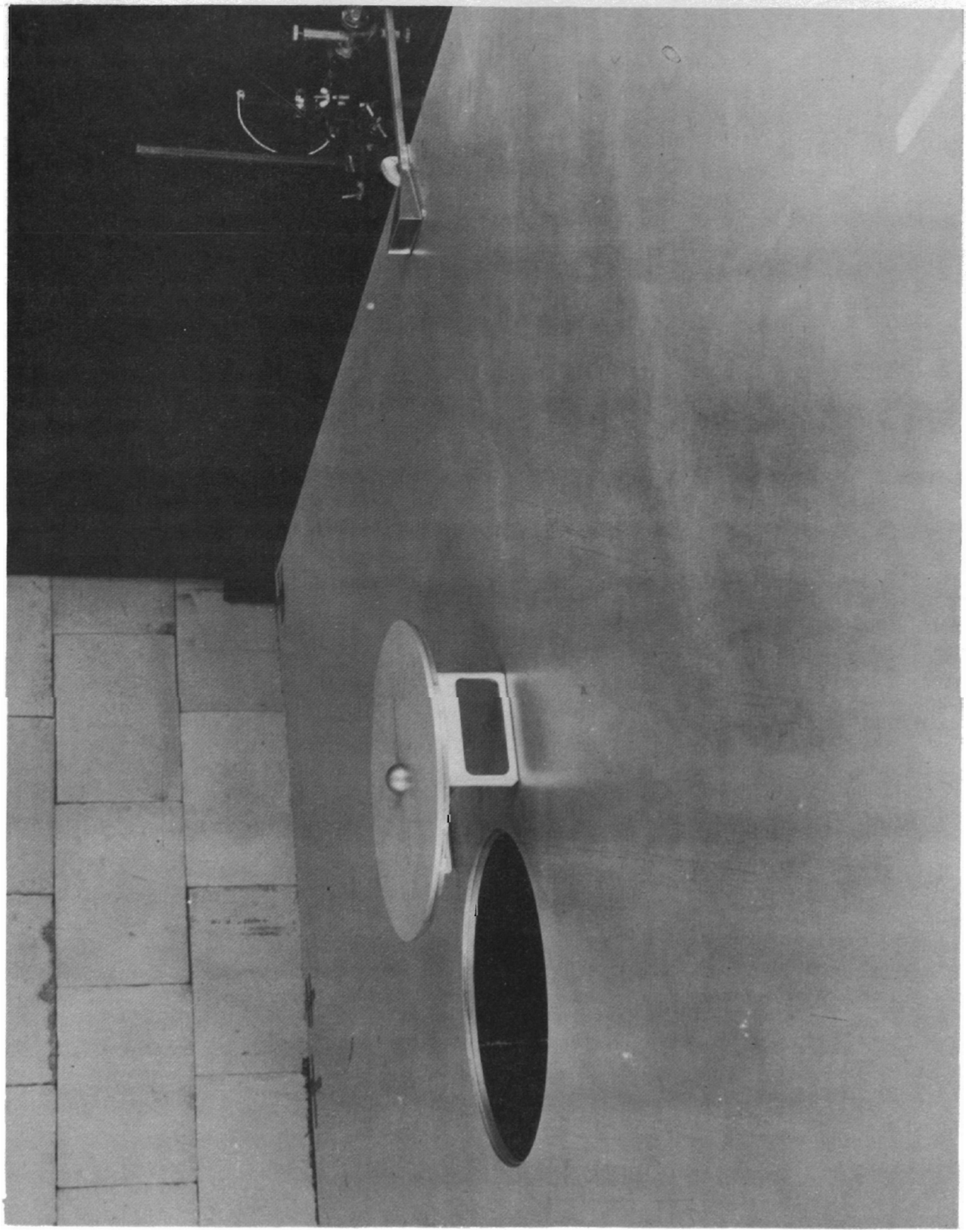

Radiation patterns in either the E-plane or the H-plane for pyramidal horns show these planes to present practically no dependence on the flare angle imposed in the other plane. This means these patterns closely resemble the E-plane and H-plane patterns of the sectoral horns[7]. Appropriate choice of flare angles produces near matched impedance of horn to free space and results in nearly complete suppression of standing waves[8] along with increased radiated energy. With this choice of flare angles the equiphase surface at the mouth of the horn is essentially a plane. This produces a radiation that is exactly the same as that of a rectangular waveguide with the same dimensions as that of the horn aperture[9]. This approximation holds up to flare angles of about 50°. The shape of the beam in any of the planes is dependent on the mode of the wave being fed into it and on the width of the mouth in that plane. Assuming a plane wave front exists at the horn aperture and the TE_{10} field is the unique distribution present, the angle between nulls[10] in the E-plane is

$$\theta = 2 \sin^{-1} \frac{\lambda}{b} \qquad (2\text{-}45)$$

and the angle between nulls in the H-plane is

$$\theta = 2 \sin^{-1} \frac{3\lambda}{2a} \qquad (2\text{-}46)$$

---

[7] Samual Silver, Microwave Antenna Theory and Design, MIT Radiation Laboratory Series, Volume 12, McGraw-Hill Book Company, Inc., New York, 1951, pp. 588-589.

[8] R. I. Sarbacher and W. A. Edson, Hyper and Ultra-High Frequency Engineering, 8th Printing, John Wiley and Sons, Inc., New York, 1950, p. 403.

[9] Ibid., p. 406.

[10] Reich, Ordung, Krauss, Skalink, Microwave Theory and Techniques, D. Van Nostrand Company, Inc., 1953, p. 427.

where a and b are the horn aperture dimensions as shown in Figure 11 and λ is the wavelength of the signal.

Although the pyramidal horn gives only moderate directivity when compared to more elaborate radiating elements it proved very satisfactory for this application. The dimensions are not very critical, it is simple to construct and the frequency bandwidth is large. The throat dimensions and cutoff frequency of the waveguide determine the lowest frequency of operation while the appearance of higher modes and the resulting deterioration of the radiation pattern determine the highest frequency. Normally there is little change over a bandwidth of ten per cent for directivity and power gain, although both are functions of frequency.

Referring to Figure 11b and Figure 12, the values for the dimensions of the modified pyramidal horn are; W = 0.420 inches, D = 0.170 inches, a = 2.000 inches, b' = 0.750 inches, ℓ'_a = 2.75 inches, ℓ'_b = 2.66 inches, h_o = 2.625 inches, ϕ = 31.65°, θ = 21.70°, λ = 0.4693 inches.

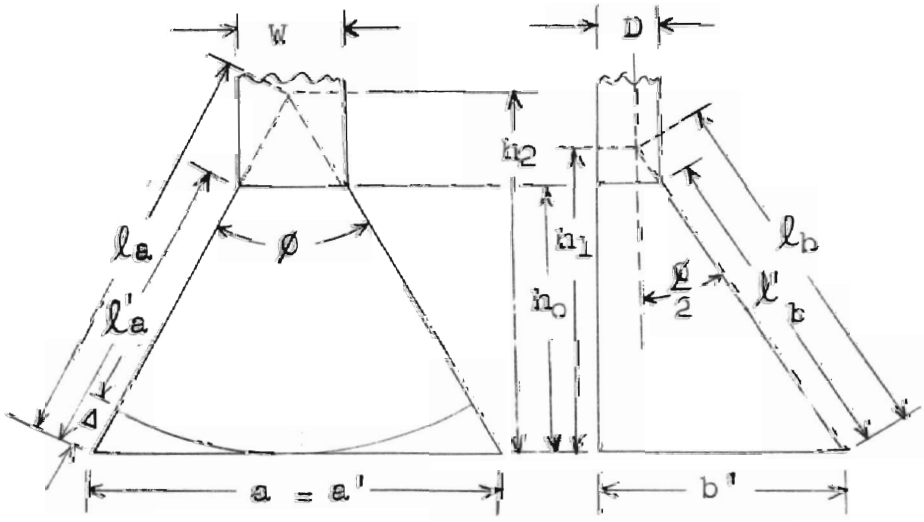

Figure 12. Modified pyramidal horn dimensions.

It can be seen that the dimensions used are well within the required limits to produce a horn that satisfies the requirements of this instrumentation. The literature[11,12,13,14] lists the design data and curves to obtain optimum design horns. The optimum design horn provides maximum gain for a fixed horn length with an apparent source of radiation located back of the throat as indicated in Figure 12.

The wave tends to assume a spherical shape as it enters the throat of the horn. The portion of the spherical wave appearing at the horn aperture is limited to a small solid angle[15] and hence may be considered essentially plane if the dimensions of ℓ_a and ℓ_b are kept to values that are but a little larger than h_2 and h_1, respectively. If the relations exist, $\ell_a - h_2 \leq \frac{\lambda}{4}$ and $\ell_b - h_1 \leq \frac{\lambda}{4}$, the desired conditions are met. The approximate expression for the quantity $\ell_a - h_2$ is

$$\ell_a - h_2 = \frac{a^2}{8\ell_a} \qquad (2\text{-}47)$$

and that for $\ell_b - h_1$ is

$$\ell_b - h_1 = \frac{b^2}{8\ell_b} \qquad (2\text{-}48)$$

---

[11] Helmut E. Schrank, "Design of Optimum Horns for Rectangular Waveguide", Electronic Design, Vol. 12, No. 11, Nov. 1954, p. 18.

[12] Sergei A. Schelkunoff, Electromagnetic Waves, D. Van Nostrand Company, Inc., New York, 1953, pp. 363-365

[13] Silver, p. 413.

[14] George C. Southworth, Principles and Applications of Waveguide Transmissions, D. Van Nostrand Company, Inc., 1950, p. 413.

[15] Donald G. Fink, Radar Engineering, First Edition, McGraw-Hill Book Company, Inc., 1947, p. 232.

These arise from the relationship for the separation of an arc and it's chord. The sine of the flare angles become limited to

$$\sin \frac{\phi}{2} = \frac{a}{2\ell_a} = \frac{\lambda}{a} \qquad (2\text{-}49)$$

$$\sin \frac{\theta}{2} = \frac{b}{2\ell_b} = \frac{\lambda}{b} \qquad (2\text{-}50)$$

The quantities a sin $\frac{\phi}{2}$ and b sin $\frac{\theta}{2}$ should not exceed the operating wavelength. The equations for these also imply that the beamwidths $\frac{\lambda}{a}$ and $\frac{\lambda}{b}$, respectively, expressed in radians, must be smaller than the sine of the flare angle. For an optimum pyramidal horn[16], such that minimum beamwidth with a minimum side-lobe level for a given length, may be produced, the relationships in Figure 12 may be used. These demonstrate further the restrictions that are imposed. The difference in path length for a wave reaching the aperture at the side of the horn and one reaching the aperture at the horn axis is indicated by the length Δ. Uniformity of the field over the entire aperture is limited to values of Δ equal to a small fraction of a wavelength. Considering the narrowing of beamwidth with increasing values of ϕ and a, ϕ may take values up to ones that make the ratio $\frac{h_2}{h_2+\Delta}$ differ appreciably from unity, which would result in a non-uniform distribution of the field across the aperture. If Δ_m is selected to represent the maximum value, resulting from the largest flare angle at which maximum directivity occurs, the following relations will hold.

---

[16] John D. Kraus, Antennas, McGraw-Hill Book Company, Inc., 1950, p. 473.

$$\Delta_m = \frac{h_2}{\cos \frac{\phi}{2}} - h_2$$

$$h_2 = \frac{\Delta_m \cos \frac{\phi}{2}}{1 - \cos \frac{\phi}{2}} \qquad (2\text{-}51)$$

and $$\phi = 2 \cos^{-1} \frac{h_2}{h_2 + \Delta_m} \qquad (2\text{-}52)$$

Similar relationships may be shown for the flare angle θ.

Following this design criteria, the higher modes of transmission in the horn must be suppressed when the most uniform aperture illumination exists. This can be controlled by proper selection of waveguide dimensions at the throat of the horn.

Expressing the full-sized pyramidal horn in terms of the gains of E-plane and H-plane sectoral horns the following development[17,18] may be applied to horn design. Using the Fresnel integrals

$$C(x) = \int_0^x \cos \left(\frac{\pi q^2}{2}\right) dq \qquad (2\text{-}53)$$

and

$$S(x) = \int_0^x \sin \left(\frac{\pi q^2}{2}\right) dq \qquad (2\text{-}54)$$

the E-plane sectoral horn gain is

$$G_E = \frac{64\, a \ell_b}{\pi \lambda b} \left[C^2\left(\frac{b}{\sqrt{2\lambda \ell_b}}\right) + S^2\left(\frac{b}{\sqrt{2\lambda \ell_b}}\right)\right] \qquad (2\text{-}55)$$

and the H-plane sectoral horn gain is

$$G_H = \frac{4\pi\, b \ell_a}{\lambda a} \left\{ \left[C(u) - c(v)\right]^2 + \left[S(u) - s(v)\right]^2 \right\} \qquad (2\text{-}56)$$

---

[17] Schelkunoff, Chapter IX.

[18] Silver, p. 587.

where

$$u = \frac{1}{\sqrt{2}} \left[\frac{\sqrt{\lambda \ell_a}}{a} + \frac{a}{\sqrt{\lambda \ell_a}} \right]$$

and $$v = \frac{1}{\sqrt{2}} \left[\frac{\sqrt{\lambda \ell_a}}{a} - \frac{a}{\sqrt{\lambda \ell_a}} \right]$$

The resulting gain for the pyramidal horn becomes

$$G = \frac{\pi}{32} \left(\frac{\lambda}{b} G_H \right) \left(\frac{\lambda}{a} G_E \right) . \qquad (2\text{-}57)$$

The modified pyramidal horn physically met all of the requirements with respect to dimensions (Figure 12). The lower plate of the horn was beveled at the aperture to assure a close fit on the surface of the ground plane and to provide a smooth transition from horn to image plane.

For purposes of calculations and data analysis it is desirable to know the gain of the horn. The transmission and reception of the radiated energy may be calculated using the radiated pattern on an absolute basis[19]. This can be done by assuming a standard uniform radiator such that the effective gain for the antenna is defined as the following.

For the transmitting gain;

G_{et} is the quantity that expresses the power per unit solid angle in the direction of maximum radiated power in terms of the power delivered to the horn.

---

[19] Silver, p. 580.

For the receiving gain;

G_{er} is the quantity that expresses the maximum power delivered to a load matched to the waveguide of assumed zero loss when the power per unit solid angle incident on the horn aperture is known.

The effective gain accounts for losses resulting from heating in the horn and those due to reflections resulting from a mismatched horn. The G_e will be identical for the horn whether it be used for transmitting or receiving since the losses can be assumed to be the same. G_e was determined for a full sized pyramidal horn with the dimensions shown in Figure 12. This was done by comparing it to a gain standard on reception. The experimental setup utilized is shown in Figure 13.

The field across the pattern mount was assumed to be uniform, this provides conditions for an accurate gain

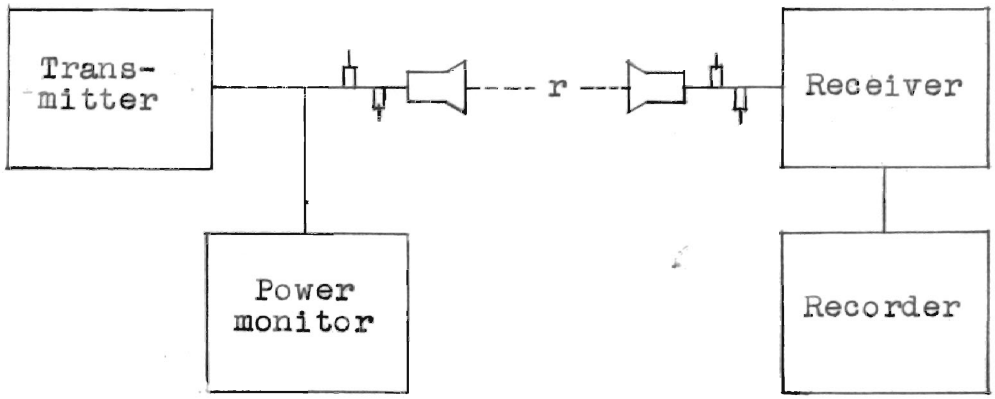

Figure 13. Setup for the determination of the gain of the horn antenna.

comparison. The horn was rotated in azimuth and elevation to give an indication of maximum received power, P_u, and this power was recorded on the pattern indicator tape. This horn was removed from the mount and the standard horn was used to replace it. The standard horn was rotated in azimuth and elevation to produce a maximum power reading, P_s, which was also recorded on the same power indicator tape. Since the gain of the standard horn is known, the gain of the pyramidal horn, by comparison, is also known. These values were read from the calibration chart accompanying the standard horn and the calibration equipment. The effective gain of this horn can be calculated from $G_u = \frac{P_u}{P_s} G_s$. The standard horn was now replaced with the modified pyramidal horn of the dimensions shown in Figure 12. This horn was rotated in azimuth and elevation to produce a maximum power reading. This value was recorded on the same tape with the other two patterns. This reading was also converted to gain, using the aforementioned calibration chart, and the result compared with that of the full-sized pyramidal horn of similar dimensions. The standard horn exhibited a gain of 17 db, the full-sized pyramidal horn showed a gain of 20.3 db and the modified pyramidal horn indicated a gain of 17.3 db. Radiation patterns that were recorded for the three horns used to obtain data for the gain measurements are shown in Figure 14. These patterns are of the horizontal plane with the vertical plane peaked for maximum energy received.

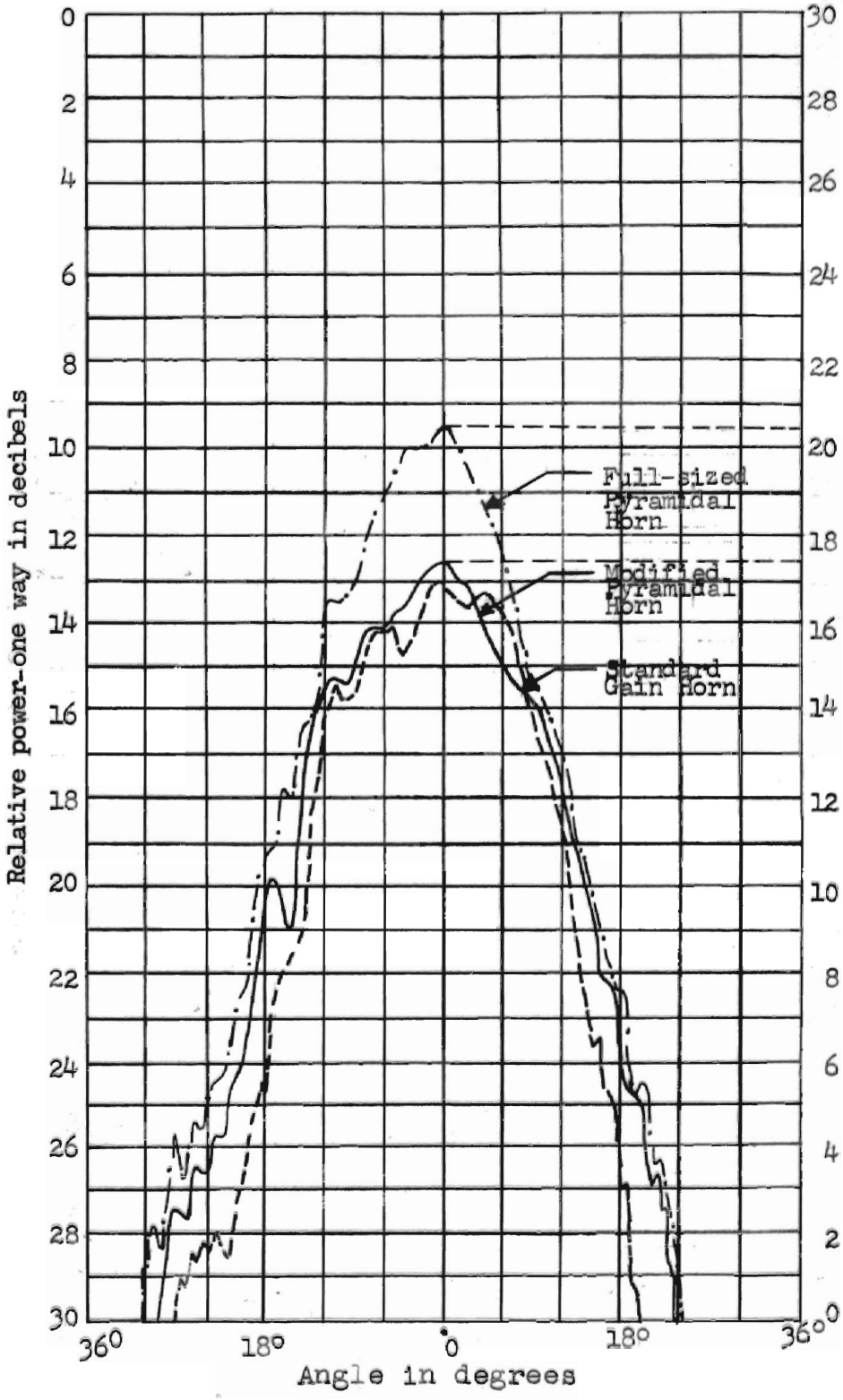

Figure 14. Radiation patterns for the three horns used in the gain measurement.

Certain precautions were observed while making these measurements. These were the following.

a. The matched gain standard was directive and had a gain comparable to that of the other two horns.

b. Field distribution was assumed to be uniform.

c. The transmitter power was monitored to assure constant radiated energy.

d. The same detection system was used for all three horns.

e. The detection system was matched to the transmission line.

f. All readings were reduced to square law values at the detection system.

The values of the gains measured are the results of the directive properties of the horns due to the concentration of energy in the direction of the apertures.

The values from Figure 14 show the modified pyramidal horn adapted for ground-plane employment to produce a gain that is 3 db down from that produced by the full-sized pyramidal horn when operating in free space conditions. When mounted on the ground plane, the modified pyramidal horn, under the conditions of this experimentation would exhibit a gain equal to the full-sized modified pyramidal horn operating in free space.

Image Plane

The image plane has been used in various arrangements in backscattering measurements, scale-model work and in

airborne antenna problems. The existance of a plane of symmetry permits the use of the equivalent image system, which replaces one-half of the component under investigation. The plane of symmetry should show an infinite, perfectly conducting surface. Aluminum and copper[20] have proven to have conductivities such that they are satisfactory for use as image planes. Moderate surface impedances may be neglected in the low-Q system since the image surface supports traveling waves that are distributed over a large surface area. The conditions of image plane operation may be analyzed by observing the existance of standing waves on the plane. Standing waves will appear at the extreme edges of the plane, since these are discontinuities in the path of the outgoing wave. If these standing waves are allowed to exist during a backscattering measurement, erroneous values will be recorded since these waves interact with the object under test, causing undesirable impedance data to be observed. Methods have been devised to overcome this undesirable feature of the image plane. The placement of the hairflex used in this experimentation was selected because of it's practicality and excellent results. This method of reducing edge effects on a rectangular plane by placement of hairflex is most useful. Methods to reduce these effects that may be used also,are to avoid circular image surfaces and increase the size of the plane to better approach the

---

[20]King, p. 253.

infinite surface condition. Both of these were observed and utilized. The interaction between scatterer and image plane are controlled by the degree of coupling between them and the equivalent Q of the scatterer. The latter is determined by the characteristics and the dimensions of the object while the first is determined by the amount of energy directed along the plane's surface.

The image plane should be tested for performance previous to making measurements. The appearance of standing waves over a large portion of the plane indicate undesirable operation. The conditions of operation of the image plane were determined previous to these tests. The condition of propagation with a vertical component of the E-vector normal to the image-plane surface with a plane wave front existing at the object under test was assumed to prevail to a good approximation.

An approximate minimum distance, R, that a scatterer may be placed from the horn aperture, when making a back-scattering measurement in the far zone, may be solved for. R can be used to determine a minimum size image plane to employ. This solution shows the receiving horn antenna aperture and it's gain to be functions of it's side dimensions. When a minimum phase error is prescribed, a minimum range in terms of the horn side dimensions and the scatterer dimensions is determined. This development may be done by the following method.

Define the following quantities;

Sr = received signal strength

S_o = transmitted signal strength

P_r = received power

P_o = transmitted power

K = scattering cross section of the target

A_{eff} = Effective area of the antenna aperture

G = Antenna Gain

R = distance of travel of the signal

Based on the concepts[21] used to derive the radar equation

$$S_r = \frac{S_o K}{4\pi R^2} \qquad (2\text{-}58)$$

$$S_o = \frac{P_o G}{4\pi R^2} = \frac{1}{2} R_e (\bar{E} \times \bar{H}) \qquad (2\text{-}59)$$

$$P_r = S_r A_{eff} \qquad (2\text{-}60)$$

$$P_r = \frac{P_o G}{4\pi R^2} \frac{K}{4\pi R^2} A_{eff} \qquad (2\text{-}61)$$

Assume a square horn aperture and

$$A_{eff} = \ell_1 \ell_2 = \ell^2 \qquad (2\text{-}62)$$

and $$G' = \frac{4\pi}{\lambda^2} \ell^2 \qquad (2\text{-}63)$$

now $$P_r = \ell^2 \frac{P_o 4\pi}{4\pi R^2} \frac{\ell^2}{\lambda^2} \frac{K}{4\pi R^2}$$

$$P_r = \frac{P_o}{4\pi} \left(\frac{\ell}{R}\right)^4 \frac{K}{\lambda^2} \frac{P_o}{4\pi} K_\lambda \left(\frac{\ell}{R}\right)^4 \qquad (2\text{-}64)$$

where $K_\lambda = \frac{K}{\lambda^2}$

---

[21] Donald E. Kerr, Propagation of Short Radio Waves, First Edition, McGraw-Hill Book Company, Inc., 1951, p. 29.

The phase error, ϕ, may be determined by referring to the following diagram.

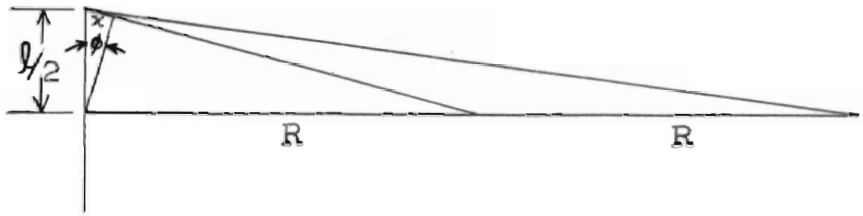

$$\frac{x}{\ell/2} = \frac{\ell/2}{2R} \qquad (2\text{-}65)$$

$$x \approx \frac{\ell^2}{8R} \qquad (2\text{-}66)$$

$$\phi \approx \frac{2\pi x}{\lambda} \approx 2\,\frac{\ell^2}{8R} \approx \frac{\pi}{4} \quad \frac{\ell^2}{R} \approx \frac{\pi}{4}\left(\frac{\ell}{R}\right)^2 R \qquad (2\text{-}67)$$

Assume a scatterer placed according to the following

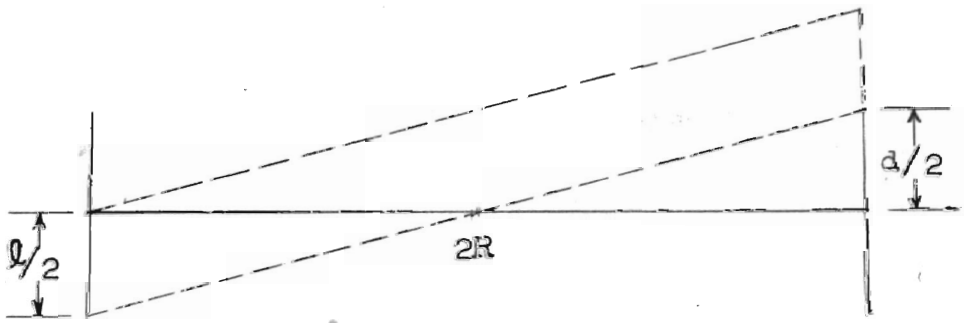

$$x \approx \frac{\left(\frac{\ell + d}{2}\right)^2}{2R} \qquad (2\text{-}68)$$

$$2x = \frac{\left(\frac{\ell + d}{2}\right)^2}{R}$$

Assume $2x < \frac{\lambda}{4}$

so that

$$\frac{\left(\frac{\ell + d}{2}\right)^2}{R} < \frac{\lambda}{4}$$

$$\frac{(\ell + d)^2}{\lambda} = R_{\min} \qquad (2\text{-}69)$$

This is the minimum range to operate for the defined conditions of a uniformily illuminated square aperture for the horn with a prescribed radar phase error of $\frac{\lambda}{4}$ prevailing. The minimum range for this research differs only slightly from that derived above. The conditions for far zone measurements were adequately met.

The image plane used in this study was constructed from a solid sheet of aluminum which was coated with aluminum lacquer possessing high conductivity, (see Plate III). The plate insert was set and remained stationary during the measurements. The plane was 183.3 cm wide, 122 cm long and 0.9 cm thick, (see Plate IV). The mats used to shield objects external to the image plane and reduce edge effects, were loosely spun mats of animal hair with each individual hair coated with a layer of pigmented neoprene. This material gives less than 0.2% reflection at the frequency used. More details concerning this material is included in the section "Control Features of the System".

Plate IV.

View of the image plane showing arrangement for measurements.

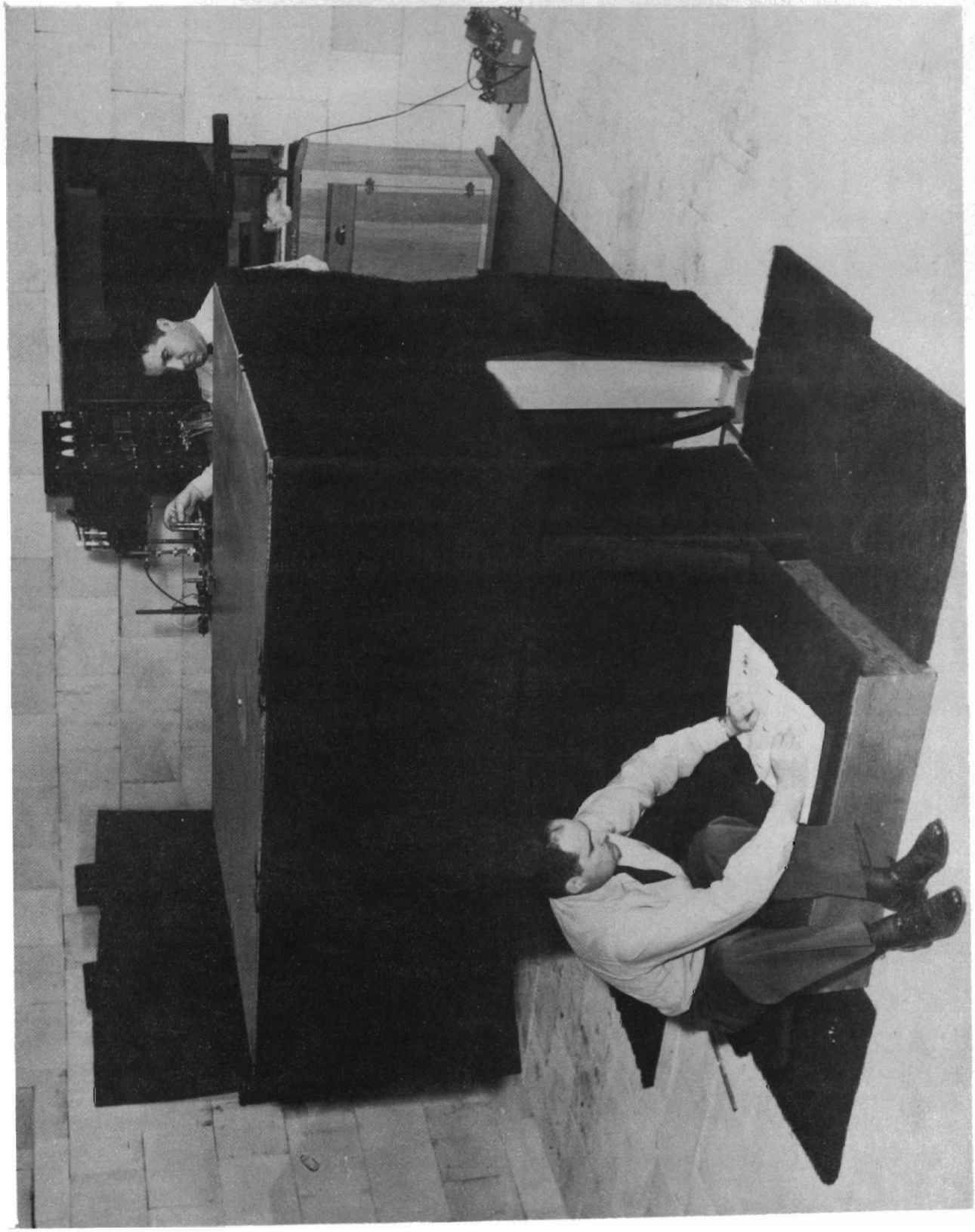

Specimen for test.

The scattering objects were constructed from three different materials with known specifications. These materials consisted of the following;

Aluminum Alloy-24ST	Army Specification QQ -A-362
Brass - Naval Hard	Army Specification QQ -B-636
Steel - Cold Rolled	Army Specification MIL-S-7079

Samples in the form of rectangular bars approximately 4.25 inches long by 0.187 inches square were submitted to the Electricity and Electronics Division of the National Bureau of Standards, United States Department of Commerce in Washington, D. C. for measurements of resistivity. These were made for each bar at a temperature of 20.00° Centigrade. These were dc values but values at higher frequencies may be considered to have relative quantities that are in the same proportions. This fact is utilized in the analysis. The results were determined such that they were probably accurate to one per cent.

The results that were tabulated are contained in the following table.

TABLE I

RESISTIVITY VALUES FOR METALS

Sample Number	Material	Resistivity Microhn-CM
1	Copper	1.72
2	Copper	1.73
3	Aluminum	5.71
4	Aluminum	5.73
5	Brass	6.87
6	Brass	6.86
7	Iron	13.3
8	Iron	13.3

The geometric configurations tested were spheres, (Refer to Plates V and VI). All dimensions were machined with tolerances of $\pm$ 0.001 inches. The placement of the spheres on the image plane was determined by setting them in three different positions, each $\frac{\lambda}{4}$ apart in line with the horn aperture. The position that produced the median reading was the one used. This position did not produce the maximum nor the minimum reading. The reading used was the resultant reading when the outgoing wave and the image-plane edge and others returns were in quadrature. This produced a reliable value to be used in the analysis. The target placement was in all cases 67.5 cm or 67.5 cm $\pm \frac{\lambda}{4}$.

Plate V.

Spheres used as specimen for measurements.

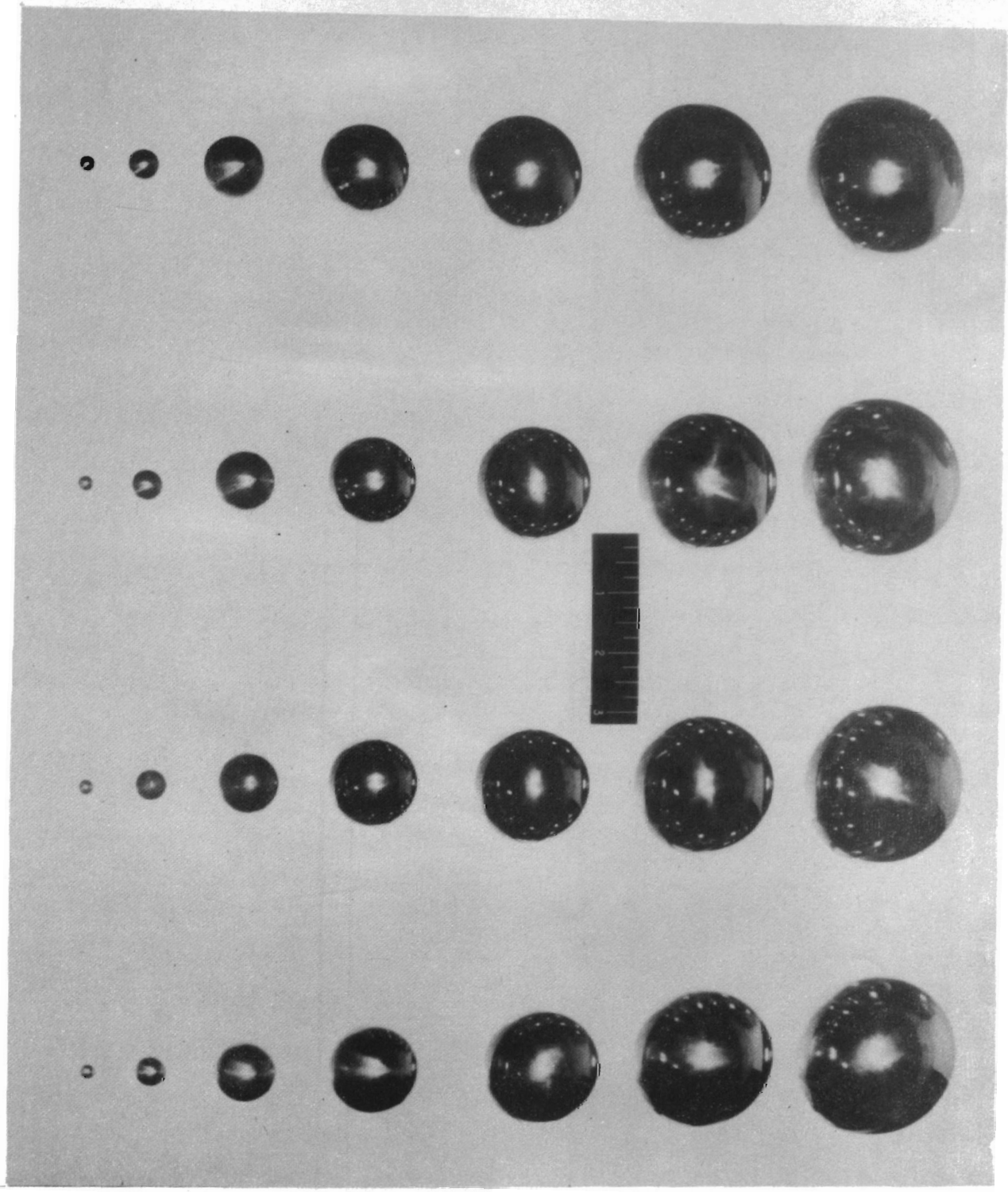

Plate VI.

View of hemisphere and modified horn antenna on the image plane.

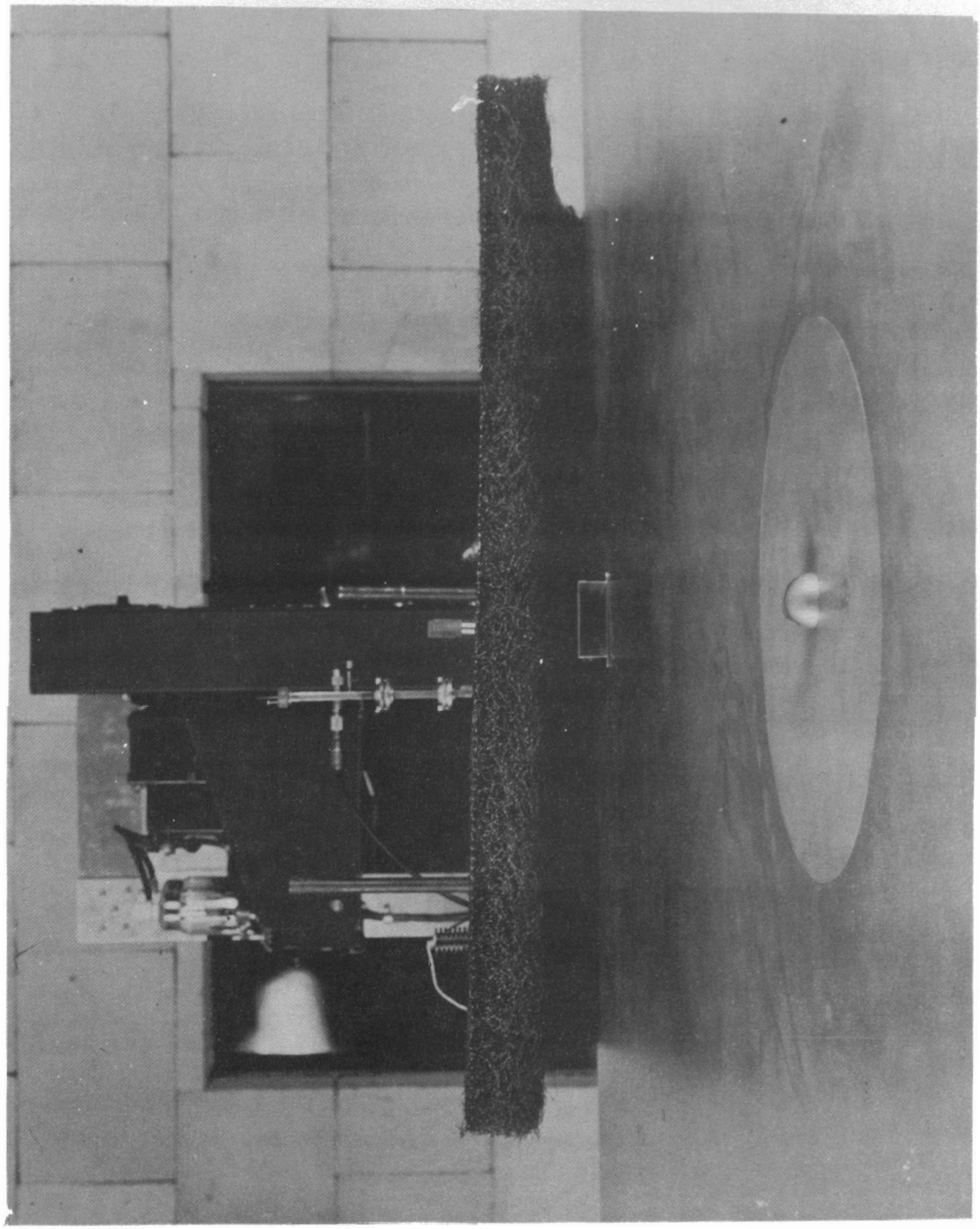

Control Features of the System

The room used for this research was 40 feet long and 25 feet wide. The front end of the ground plane was located about 12 feet from the back wall. It was lined with blocks of McMillan absorbent material (see Plate VII). This material produced about 4.0 per cent reflection at the frequency used. Tests to determine the characteristics of this material and to compare them with other materials available, were performed by the Naval Research Laboratory[22], on samples furnished by the Air Force Cambridge Research Center. The samples were representative of the material used throughout construction. They were subjected to Navy standard tests. These blocks were approximately 12" x 18" x 7". They were formed from a base made of a layer of pigmented hair plus a thick center section of pigmented foam plastic with a top surface made of cones. The cones were covered by a section of polyfoam to give a flat outer surface. The polyfoam was coated with a thin layer of white paint.

Navy specifications for broadband absorbent material for darkroom use calls for a reflection of less than two per cent in power at all points and an average reflection of less than one percent in power for the frequency band specified. The reflection was measured for angles of incidence nearly normal to the sample surface and in order to give a

---

[22]"Tests of Absorbent Material", Naval Research Laboratory Problem Number R11-4; Report on, Forwarding of, Naval Research Laboratory Washington, D. C., 24 June 1954.

standard condition, measurements were made with the absorbers backed by a metal surface. In the band of interest in this experimentation, 3000 to 60,000 megacycles per second, a double horn set-up for free space measurements was used. The samples used failed to meet the Navy specifications, but gave best results in the K-band region. The results are shown in Figure 15, page 59. It was determined that at the low frequencies large reflections arose from discontinuities in the samples and from insufficient attenuation. At the very high frequencies surface reflections from the paint layer were too high.

Figure 15 also shows the performance of representative 1,000 megacycles per second and higher frequency absorbent material manufactured according to Navy specifications and design. This material was a loosely spun mat of animal hair with each individual hair coated with a layer of pigmented neoprene. The overall thickness was 4 3/4 inches. This hairflex material is used to reduce edge effects and equipment reflections as shown in Plate VII. It is the material referred to in the section on the image plane.

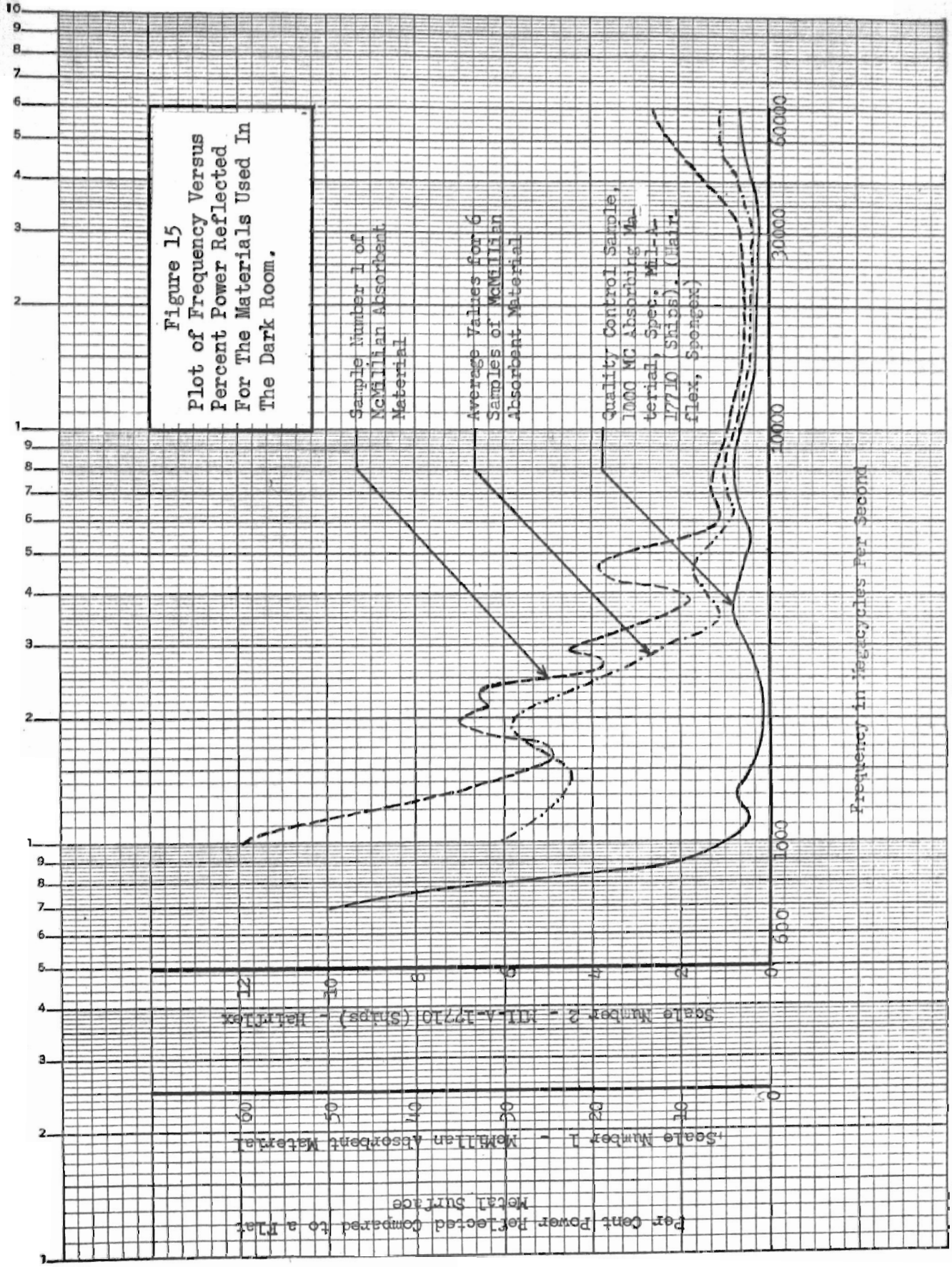
Figure 15
Plot of Frequency Versus
Percent Power Reflected
For The Materials Used In
The Dark Room.
Sample Number 1 of
McMillan Absorbent
Material
Average Values for 6
Samples of McMillan
Absorbent Material
Quality Control Sample,
1000 MC Absorbing Ma-
terial, Spec. Mil-R-
17210 (Ships). (Hair-
flex, Sponge)
Frequency in Megacycles Per Second
Per Cent Power Reflected Compared to a Flat
Metal Surface
Scale Number 1 - McMillan Absorbent Material
Scale Number 2 - MIL-A-17210 (Ships) - HairFlex

Plate VII.

Overall equipment placement in the dark room.

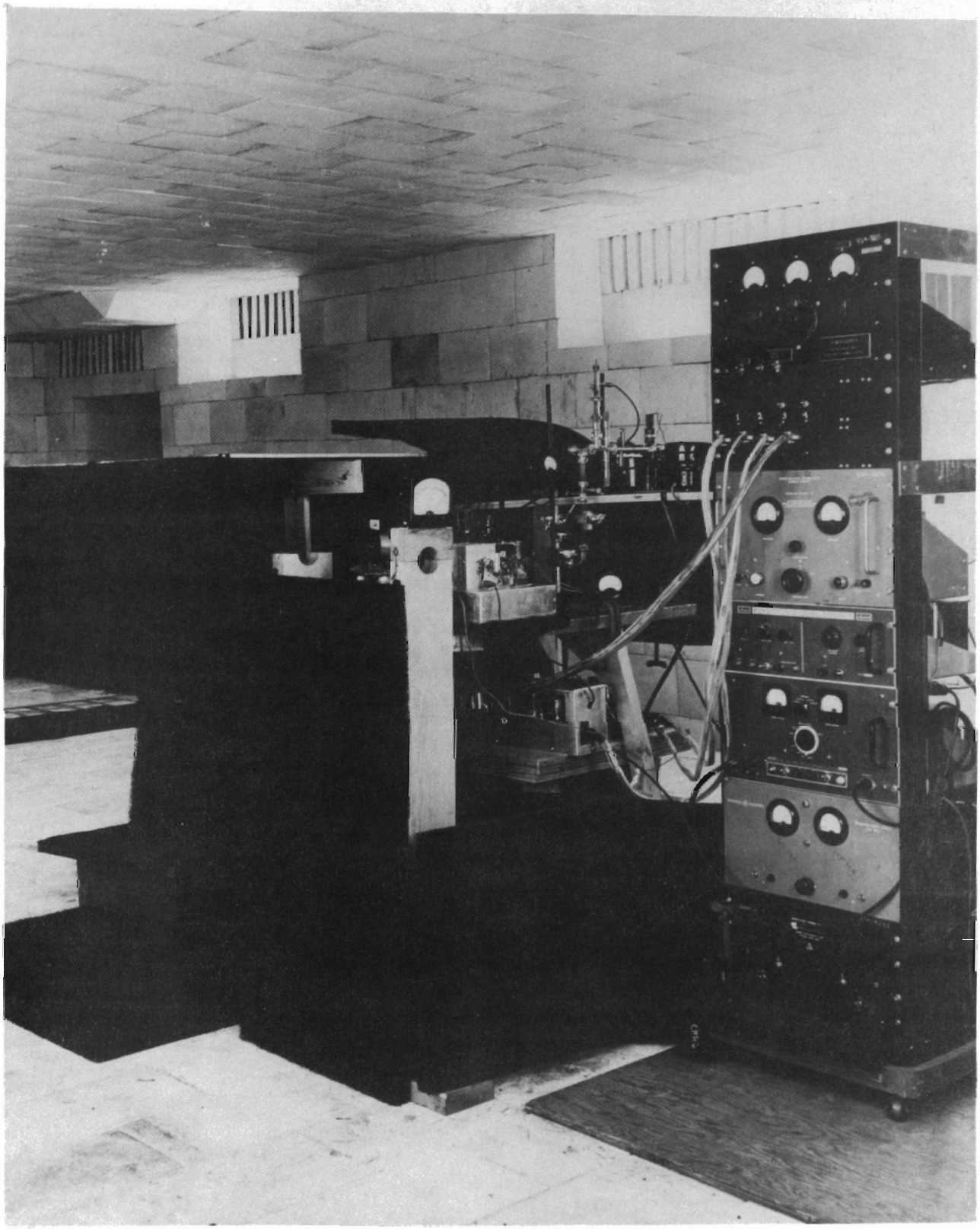

Calibration of the System

Referring to Plate IV the procedure used to make static measurements was the following:

1. The system had power applied for about one hour before attempting any tuning.

2. The receiver controls were set and were not changed from these settings throughout the period of measurements.

3. The attenuator that was used in conjunction with the directional coupler was set and remained in this position.

4. Changes in the output power level of the klystrons were made by changing the beam voltages.

5. The crystal current of the mixer stage was set at a convenient reading, about 200 microamperes, since the crystal operated best at this value. This value was maintained throughout the experiment.

6. The system was balanced to obtain an optimum reading on the limiter cathode meter with no target on the ground plane.

7. A visual check was made to see that the crystal mixer current and power output level (indicated in milliamperes) were at the desired levels.

8. A target was placed in the desired position.

9. Attenuation was put in the receiver line to bring the signal to a convenient point on the meter in the cathode of the limiter. This meter was calibrated in milliwatts of power. The attenuator reading and the limiter cathode meter reading were recorded.

10. Readings for the same target were made a sufficient

number (at least ten) of times to assure the desired accuracy as indicated by repetitions in readings.

The scattering and absorption parameters of an object in an electromagnetic field involve the concepts[23] of total scattered power and total absorbed power.

Total scattering power is

$$P_s = Q_s \; i \; . \qquad (2\text{-}71)$$

Total absorbed power is

$$P_a = Q_a \; i \; . \qquad (2\text{-}72)$$

Total power removed from the incident wave is

$$P_t = P_s + P_a \qquad (2\text{-}73)$$

Where i is the power density incident upon the object

Q_s is the total scattering cross section

and Q_a is the total absorbed cross section.

Back-scattering cross section K has been defined by the equation

$$K = 4\pi \; r^2 \; \frac{s}{i} \qquad (2\text{-}74)$$

Where: r is the distance from the scatterer at which s is evaluated.

s is the far zone scattered field power density in the direction of the transmitter.

and i is the plane wave power density incident upon the scatterer.

Equation (2-74) defines the ability of a scatterer to reradiate

---

[23] A. L. Aden, "Electromagnetic Scattering from Metal Spheres and Water Spheres", Cruft Laboratory, Harvard University, Cambridge, Massachusetts. Naval Technical Report No. 106.

energy in the direction of the source. This cross section for a given object is dependent upon the polarization, wavelength, angle of incidence of the impinging radiation, and the material, shape and dimensions of the scattering object. Power values are involved in the quantities to be determined and the powers indicated would be convenient values to use in a solution, therefore, measurements of these were made.

Absolute values of microwave power are difficult to determine. A measuring set was selected as a reference or standard to calibrate all components and measure powers desired. The PRD Type 650-A Universal Power Bridge was selected for this purpose. This instrument directly indicates the equivalent power in milliwatts that a bolometer element absorbs when microwave power is incident upon it. This instrument and the K-band source were used to calibrate the attenuators used in the system. When making a reading of the output power, the PRD 650-A was coupled to the transmitter output line with a Sperry Model 412 directional coupler, which is of the branch guide type giving a high degree of coupling. This provided a facility to monitor the output power for a constant value.

The gain of the overall system was calibrated to be 117.2 decibels with a 37.5 milliwatt transmitter output power. The receiving system was adjusted to produce a reading of 0.200 millamperes on the limiter's cathode meter indicating this to be the balance point. The magic tee produced a loss of 3 decibels on transmission and another 3 decibel loss on receiving, therefore the total usable gain for the

overall system is reduced to 111.2 decibels.

To illustrate the method of using the calibration, we may use the following information.

1. It was desired to keep the reading above the noise range, including the leakage signal of the system, therefore, the desired backscattering value in decibels was read from the scale of the calibrated attenuator at the 0.6 milliampere level on the limiter's cathode meter.
2. The total power level that was possible to be read was one that was down 91.5 decibels from the transmitter output power of 37.5 milliwatts. This results from 117.2 db - 6 =111.2 db. $\log_{10} \frac{37.5}{0.100}$ = 25.7 db and 117.2 db - 25.7 db = 91.5 db.
3. Using the following information the reading was accomplished.

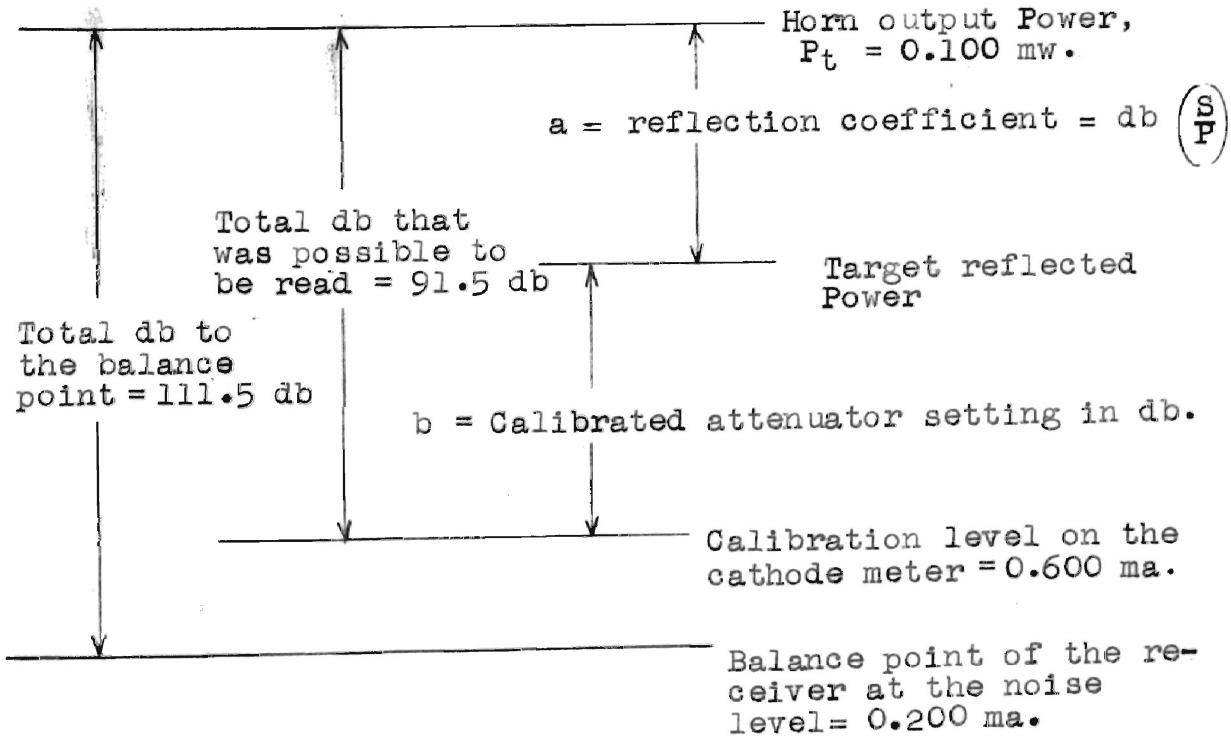

$$a + b = -91.5 \text{ db}$$

$$K = k \frac{P_r}{P_t} \qquad (2\text{-}75)$$

$$\frac{K}{k} = \frac{P_r}{P_t} = K'$$

$$db(K') = db\ (P_r) - db\ (P_t) \qquad (2\text{-}76)$$

The attenuator used in conjunction with the reflection coefficient readings had a calibration in db that was linear over the range of interest. This curve of db versus scale reading is shown in Figure 16, page 67.

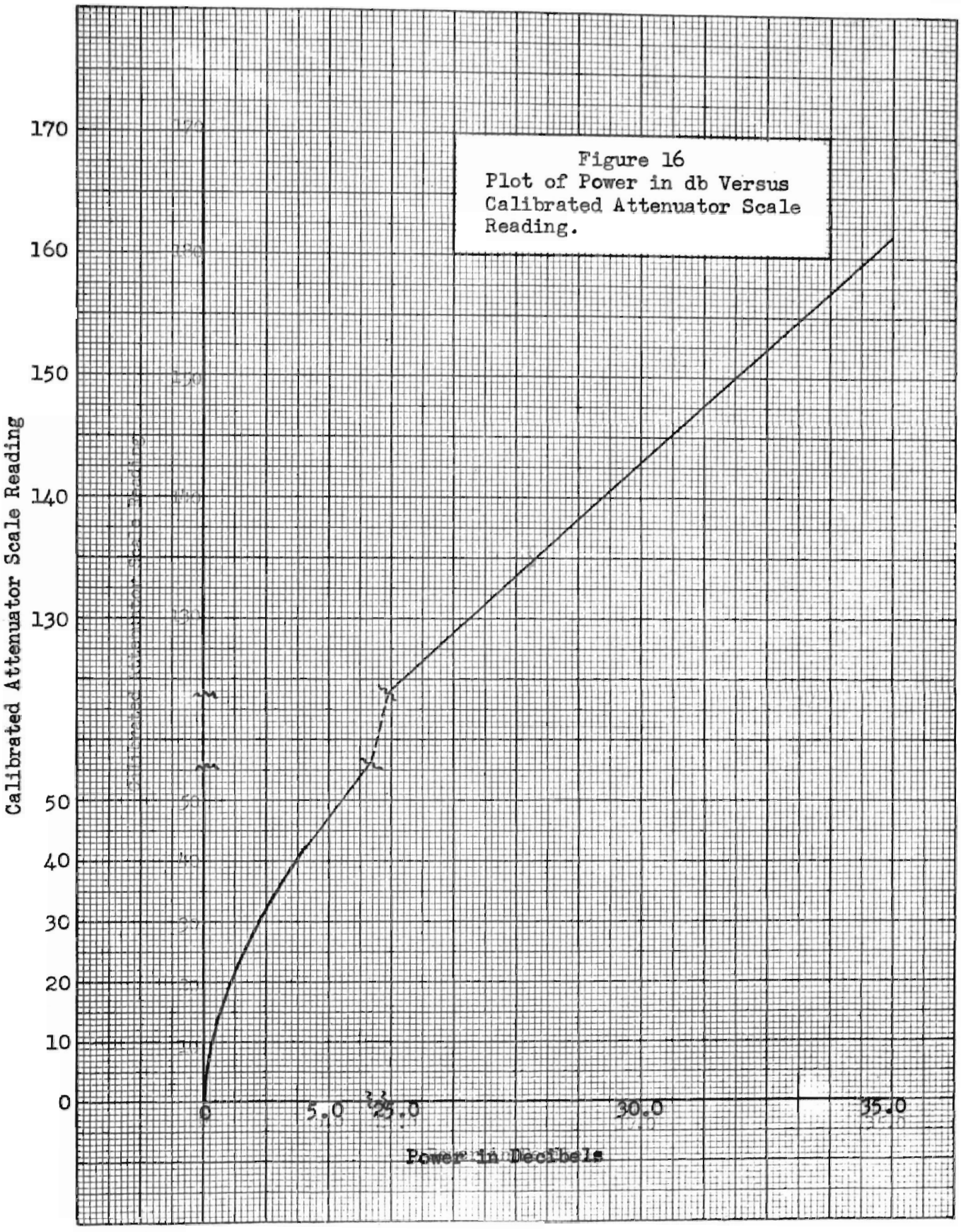

Figure 16
Plot of Power in db Versus Calibrated Attenuator Scale Reading.

CHAPTER III

ANALYSIS AND RESULTS OF MEASUREMENTS

Introduction

It has been shown[1] that for the case of refraction in a conducting medium when the conductivity increases, due to an increase in frequency, the planes of constant phase align themselves parallel to the planes of constant amplitude. The propagation is into the conductor in a direction normal to the surface.

The depth of penetration may be measured by the factor

$$\delta = \sqrt{\frac{2}{\omega \mu_1 \sigma_1}} \qquad (3\text{-}1)$$

where δ is the depth of penetration, ω is the angular frequency, μ_1 is the permeability and σ_1 is the conductivity. This equation relates the distance within a conductor of a point at which the amplitude of the electric vector is equal to $\frac{1}{e}$ or 36.79 per cent of it's value at the surface, to the frequency, permeability and conductivity. The phase lag is 180 degrees at this distance. An increase in permeability, conductivity or frequency gives a decrease in the depth of penetration. Skin effect appears as a phenomenon showing a tendancy for concentration of currents on the surfaces of conductors nearest to the producing field sources. When a

---

[1] Julius Adams Stratton, Electromagnetic Theory, First Edition, Second Impression, McGraw-Hill Book Company, Inc., New York 1941, p. 504.

high frequency source produces an electric field, E, in the proximity of a conductor, the applied E causes current to flow in the conductor. This current flow causes a magnetic field, H, to be produced at right angles to the E field. The magnetic field varies causing an electric field, E_1, to be induced in a direction opposite to E. The farther into the conductor this phenomenon is observed the smaller the net field present to cause flow of current and consequently the greater the observed skin effect. These considerations may be used to help develop the theory of waves with the accompanying phase delays in the conductor of finite conductivity. Charges and currents experiencing time variations cause fields which have corresponding variations and result in phase delays permitting electromagnetic effects to be treated as wave phenomenon. The observed effects of the changes between the points of locations of the fields and the currents and charges travel outward from the latter with finite velocity according to the conductor's configuration and dielectric constant and the surrounding medium's permeability. A change in electric field produces a change in magnetic field in the dielectric medium. Any medium with finite permeability will show an electric field produced when an existing magnetic field changes. In the case considered the electromagnetic horn's energy is a source of waves that are transmitted down the image plane and impinge upon the spherical conductor. The conductivity of the conductor causes the wave energy that passes into the conductor to be attenuated at a given rate while an impedance mismatch

at the discontinuities between the air medium and the conductor causes some of the energy to be reflected.

Although the above concepts[2] are, in general, made for plane solids it may be extended to conductors of other shapes so long as the value of δ calculated is much smaller than any curvatures of the surfaces.

The results of analytical developments[3] show that the reflection coefficients of the metals are practically independent of the angle of incidence and differ slightly from unity at the highest radio frequencies. The reflection coefficients may be defined as the ratio of the energy flows in the incident and reflected waves.

Hagen and Rubens[4] verified in the infrared region of the spectrum that at normal incidence the following formula is valid for the reflection coefficient as long as the concern is only with metals at wavelengths between 10^{-3} centimeters and 3×10^{13} cycles per second. This is the case of macroscopic electromagnetic theory:

$$R = 1 - 4.22 \times 10^{-4} \sqrt{\frac{f \; K_{m1} \; K_{e2}}{\sigma_1}} \qquad (3\text{-}2)$$

where; f is the frequency in cycles per second.

K_{m1} is the magnetic permeability, $\left(\frac{\mu_1}{\mu_2} = \frac{\mu_1}{\mu_o}\right)$, of the conductor

---

[2]Simon Ramo and John R. Whinnery, Fields and Waves in Modern Radio, John Wiley and Sons, Inc., New York, 1953, pp. 204-210.

[3]Stratton, p. 508.

[4]Hagen and Rubens, Annual Physik, 11, 1903, p. 873.

K_{e2} is the specific inductive capacity, (e_{2/e_o}), of the dielectric.

For the air-metal surfaces used in this investigation $K_{m1}=1$, $K_{e2}=1$ and the following tabulated results may be obtained for the metals tested at a frequency of 25,162.5 mc.

TABLE II

VALUES OF REFLECTION COEFFICIENTS FOR THE METALS

METAL	CONDUCTIVITY (Calculated from inverse of Resistivity, p. 47)	REFLECTION CO-EFFICIENT $R=1-4.22 \times 10^{-4}\sqrt{\frac{f}{\sigma_1}}$
Aluminum	1.75×10^9 mhos per cm	0.998501
Brass	1.46×10^9 mhos per cm	0.998249
Iron	0.752×10^9 mhos per cm	0.997557

These calculated values of the reflection coefficients indicate the effects of the metals' conductivities upon their ability to reflect incident electromagnetic energy.

Summary of a Mathematical Derivation of Radar Cross-Section.

The case at hand involving a good conductor may be considered from the application of Maxwell's Equations. These may be stated in differential equation form as

$$\bar{\nabla} \cdot \bar{D} = \rho \qquad (3\text{-}3)$$

$$\bar{\nabla} \cdot \bar{B} = 0 \qquad (3\text{-}4)$$

$$\bar{\nabla} \times \bar{E} = \frac{-\partial \bar{B}}{\partial t} \qquad (3\text{-}5)$$

$$\bar{\nabla} \times \bar{H} = \bar{\iota} + \frac{\partial \bar{D}}{\partial t} \qquad (3\text{-}6)$$

where $\bar{\nabla}$ is the Del operator, ρ is the density of charge, $\bar{D}$ is the electric displacement, $\bar{B}$, is the magnetic induction,

$\bar{E}$ is the value of the electric field and $\bar{H}$ is the value of the magnetic field.

Ohms law for a conductor is

$$\bar{\iota} = \sigma \bar{E} \qquad (3\text{-}7)$$

where $\bar{\iota}$ is the vector current density,

and σ is the conductivity.

Substituting equation (3-7) in equation (3-6)

$$\bar{\nabla} \times \bar{H} = \sigma \bar{E} + \frac{\partial \bar{D}}{\partial t} . \qquad (3\text{-}8)$$

Since the divergence of the curl is equal to zero, by taking the divergence of both sides of equation (3-8)

$$\bar{\nabla} \cdot \bar{\nabla} \times \bar{H} = 0 = \frac{\sigma}{E} \bar{\nabla} \cdot \bar{D} + \frac{\partial (\bar{\nabla} \cdot \bar{D})}{\partial t} .$$

From equation (3-3)

$$\bar{\nabla} \cdot \bar{D} = \rho$$

and

$$\frac{\sigma}{E} \rho + \frac{\partial \rho}{\partial t} = 0 . \qquad (3\text{-}9)$$

The solution[5] of this differential equation is

$$\rho = \rho_0 e^{-\sigma (t/\epsilon)} \qquad (3\text{-}10)$$

where ϵ is the dielectric constant.

This indicates that charge density existing in a good conductor must decay exponentially with time.

In this development it is desirable to consider the electric and magnetic fields existing in the imperfect conductor as waves. Assuming sinusoidal time variations for the transmitted energy, the following equations may be written from equations (3-5) and (3-6) respectively,

$$\bar{\nabla} \times \bar{E} = -j\omega\mu\bar{H} \qquad (3\text{-}11)$$

$$\bar{\nabla} \times \bar{H} = (\sigma + j\omega\epsilon) \bar{E} = j\omega\epsilon \left[1 + \frac{\sigma}{j\omega\epsilon} \right] \bar{E} \qquad (3\text{-}12)$$

---

[5] Ramo and Whinnery, p. 234.

which treats the conductor as a dielectric with a complex dielectric constant of $\epsilon_c = \left[1 + \frac{\sigma}{j\omega\epsilon}\right]$. For the case of the uniform plane wave of sinusoidal form represented by the time function $e^{j\omega t}$, positively and negatively traveling wave components may be formulated.

$$E_x = E\, e^{j\omega(t - \frac{z}{v})} + E'\, e^{j\omega(t + \frac{z}{v})} \qquad (3\text{-}13)$$

or

$$E_x = E\, e^{-jkz} + E'\, e^{jkz} \qquad (3\text{-}14)$$

where

$k = \frac{\omega}{v} = \omega\sqrt{\mu\epsilon}$ meters^{-1}, z is the direction of travel and v is the velocity of light.

k is the phase change per unit length for each component and for a given frequency may be considered as a constant of the medium.

The propagation constant, γ, for a uniform plane wave now becomes

$$\gamma = jkc = j\omega\sqrt{\mu\epsilon_c}$$

$$\gamma = \alpha + j\beta = j\omega\sqrt{\mu\epsilon\left[1 + \frac{\sigma}{j\omega\epsilon}\right]} \qquad (3\text{-}15)$$

and

$$\alpha = \omega\sqrt{\frac{\mu\epsilon}{2}\left[\sqrt{1 + \frac{\sigma}{\omega^2\epsilon^2}} - 1\right]} \qquad (3\text{-}16)$$

$$\beta = \sqrt{\frac{\mu\epsilon}{2}\left[\sqrt{1 + \frac{\sigma}{\omega^2\epsilon^2}} + 1\right]} \qquad (3\text{-}17)$$

$$e^{-\gamma z} = e^{-\alpha z}\; e^{-j\beta z}$$

These equations show attenuation due to a loss of energy from current flow in the imperfect conductor.

The ratio of electric to magnetic field for the uniform plane wave is complex which shows there exists a phase difference between them. This ratio is called the intrinsic impedance and is

$$\eta_c = \sqrt{\frac{\mu}{\epsilon}} = \sqrt{\frac{\mu}{\epsilon\left(1 + \frac{\sigma}{j\omega\epsilon}\right)}}$$

The reflection coefficient, p, when considering the

passage of a wave from a perfect dielectric onto a conducting medium is a complex value. It indicates the incident and reflected waves differ in phase as,

$$p = \frac{\eta_c - \eta}{\eta_c + \eta}$$

The result of this analysis shows the magnitude of the reflection coefficient differs from unity because some of the incident energy is transmitted into the conductor, and there is a phase shift of incident to reflected energy upon reflection from the conductor.

The principle methods of attack for the mathematical solution of scattering by finite bodies have been discussed and summarized by Mentzner[6]. These include: the exact solutions which may yield for the diffracted field an abritrarily high accuracy, which may result from the classical solutions, integral equation formulation and application of Green's Function subject to boundary conditions; approximate solutions which may result from methods such as geometrical optics, physical optics, application of Babinet's Principle and the variational principles.

Successful theoretical treatment has been applied to the sphere by a number of authors for the general and specific cases. The summary of a development to be shown here follows the methods illustrated by Kerr[7] as summarized from Stratton's[8] elaboration.

---

[6]J. R. Mentzer, Scattering and Diffraction of Radio Waves, Pergamon Press, London and New York, 1955.

[7]Donald E. Kerr, Propagation of Short Radio Waves, McGraw-Hill Book Company, Inc., First Edition, 1951, p. 445.

[8]Stratton, p. 563.

The radar cross section properties and their relations to the properties of the target are to be considered when a plane wave front exists at the target and free space is the medium existing external to the sphere. Consider the closed domain of an isotropic, homogeneous medium free of sources with any one of the field vectors $\bar{E}$, $\bar{B}$, $\bar{D}$, and $\bar{H}$ satisfying the differential equation

$$\bar{\nabla}^2 \bar{C} - \mu\epsilon \frac{\partial^2 \bar{C}}{\partial t^2} - \mu\sigma \frac{\partial \bar{C}}{\partial t} = 0 . \qquad (3\text{-}20)$$

Since this equation exhibits linearity, the vector $\bar{C}$ may be assumed to have the time factor $e^{-j\omega t}$. $\bar{\nabla}^2$ operating on $\bar{C}$ gives

$$\bar{\nabla}^2 \bar{C} = \bar{\nabla} \bar{\nabla} \cdot \bar{C} - \bar{\nabla} \times \bar{\nabla} \times \bar{C} \qquad (3\text{-}21)$$

and letting $k^2 = \epsilon\mu\omega^2 + j\sigma\mu\omega$, the result is

$$\bar{\nabla} \cdot \nabla \bar{C} - \bar{\nabla} \times \bar{\nabla} \times \bar{C} + k^2 C = 0 \qquad (3\text{-}22)$$

Resolving $\bar{C}$ into the rectangular components x, y, and z produces the three independent equations

$$\bar{\nabla}^2 C_x + k^2 C_x = 0 \qquad (3\text{-}23)$$

$$\bar{\nabla}^2 C_y + k^2 C_y = 0 \qquad (3\text{-}24)$$

$$\bar{\nabla}^2 C_z + k^2 C_z = 0 \qquad (3\text{-}25)$$

Let a solution of the above be a scaler function ψ and $\bar{a}$ represent a unit length constant vector, to get the equation

$$\bar{\nabla}^2 \psi + k^2 \psi = 0 \qquad (3\text{-}26)$$

with the three independent vector solutions of

$$L = \bar{\nabla} \psi \qquad (3\text{-}27)$$

$$M = \bar{\nabla}\psi \times \bar{R} = \frac{1}{k} \bar{\nabla} \times \bar{N} \qquad (3\text{-}28)$$

$$N = \frac{1}{k} \bar{\nabla} \times \bar{M} \qquad (3\text{-}29)$$

where $\bar{R} = \bar{i}_r R$ R is the position vector from the spherical coordinates R, θ, ϕ. When $\bar{C} = \bar{L}$, $\bar{M}$, or $\bar{N}$, equation (3-21) is satisfied by equations (3-27), (3-28) and (3-29) subject to equation (3-26).

Fields $\bar{E}$ and $\bar{H}$ may be represented by the vectors $\bar{M}$ and $\bar{N}$ since each is proportional to the curl of the other. Since we have charge-free density that is everywhere zero in the homogeneous, isotropic medium with conductivity σ,

$$\bar{E} = \frac{j\omega\mu}{k^2} \bar{\nabla} \times \bar{H} \qquad (3\text{-}30)$$

$$\bar{H} = \frac{\bar{I}}{j\omega\mu} \bar{\nabla} \times \bar{E} \qquad (3\text{-}31)$$

Assume the vector potential can be expanded in characteristic vector function form of

$$\bar{A} = \frac{j}{\omega} \sum_n (a_n \bar{M}_n + b_n \bar{N}_n + c_n \bar{L}_n) \qquad (3\text{-}32)$$

where a_n, b_n, and c_n are functions of the current distribution.

$\bar{\nabla} \cdot \bar{M} = \bar{\nabla} \cdot \bar{N} = 0$ can be shown to hold since $\bar{M}$ and $\bar{N}$ are solenoidal and $\bar{E}$ and $\bar{H}$ may be expressed as

$$\bar{E} = -\sum_n (a_n \bar{M}_n + b_n \bar{N}_n) \qquad (3\text{-}33)$$

$$\bar{H} = \frac{k}{j\omega\mu} \sum_n (a_n \bar{N}_n + b_n \bar{M}_n) \qquad (3\text{-}34)$$

$$\psi_{\substack{e \\ o}} m\ n = \begin{matrix}\cos \\ \sin\end{matrix} m\ \phi\ p_n^m (\cos\theta)\ z_n (kR) \qquad (3\text{-}35)$$

Equation (3-35) can be shown to be solutions of the scalar wave equation where $p_n^m (\cos\theta)$ are the Legendre polynomials and $z_n (kR)$ are spherical Bessel functions determined by the range of R being considered. Solutions that are even or odd in ϕ are described by e and O respectively.

The Bessel function of the first kind may be used where the field remains finite. This applies inside the sphere of radius a, that is $R \leq a$, and is

$$z_n(kR) = \psi_n(kR) = \sqrt{\frac{\pi}{2\,kR}}\, J_{n+\frac{1}{2}}(kR) \qquad (3\text{-}36)$$

The Hankel function of the second kind may be used outside the sphere, $R \geq a$, where the field is a traveling wave and appears as

$$z_n(kR) = h_n^{(2)}(kR) = \sqrt{\frac{\pi}{2\,kR}}\, H^{(2)}_{n+\frac{1}{2}}(kR) \qquad (3\text{-}37)$$

and writing $\bar{M} = \bar{m}\, e^{j\omega t}$ and $\bar{N} = \bar{n} e^{j\omega t}$ to remove the time factor, then substitute equation (3-35) into equations (3-28) and (3-29), the result becomes

$$\bar{m}_{e_{o}^{m}\,n} = \mp \bar{i}_\theta \frac{m}{\sin\theta}\, z_n(kR)\, p_n^m(\cos\theta) \begin{matrix}\sin\\ \cos\end{matrix} m\phi - \bar{i}_\phi\, z_n(kR)\, \frac{d\, p_n^m(\cos\theta)}{d\,\theta} \begin{matrix}\cos\\ \sin\end{matrix} m\phi \qquad (3\text{-}38)$$

$$\bar{n}_{e_{o}^{m}\,n} = \bar{i}_r \frac{n(n+1)}{kR}\, z_n(kR)\, p_n^m(\cos\theta) \begin{matrix}\cos\\ \sin\end{matrix} m\phi + \bar{i}_\theta \frac{1}{kR}\frac{d}{dR}\left[R\, z_n(kR)\right] \frac{d\, p_n^m(\cos\theta)}{d\theta} \begin{matrix}\cos\\ \sin\end{matrix} m\phi \mp \bar{i}_\phi \frac{m}{kR\sin\theta}\frac{d}{dR}\left[R\, z_n(kR)\right] p_n^m(\cos\theta) \begin{matrix}\sin\\ \cos\end{matrix} m\phi \qquad (3\text{-}39)$$

The form of the incident plane wave to be represented, if the z - axis is the positive direction of propagation, is

$$\begin{pmatrix}\bar{E}\\ \bar{H}\end{pmatrix} = \bar{a} \begin{pmatrix}E_o\\ H_o\end{pmatrix} e^{-jkR\cos\theta} \qquad (3\text{-}40)$$

where $z = R\cos\theta$ and $\bar{a}$ represents a unit vector with components along the x- and y- axes.

Vector functions may be used to express the plane wave traveling along the z -axis through free space and polarized

on the x-axis. This is the plane wave incident on the sphere and is to be denoted by using superscript i. The following form, using $\eta_o = 120\pi$ ohms, satisfies these conditions.

$$\bar{E}^i = \bar{i}_x \; E_o \; e^{j(\omega t - kz)}$$

$$\bar{E}^i = E_o \; e^{j\omega t} \sum_{n=1}^{\infty} (-j)^n \frac{2n+1}{n(n+1)} (\bar{m}_{o1n} + j\bar{n}_{e1n}) \qquad (3\text{-}41)$$

$$\bar{H}^i = \bar{i}_y \frac{E_o}{\eta_o} \; e^{j(\omega t - kz)}$$

$$\bar{H}^i = -\frac{E_o}{\eta_o} \; e^{j\omega t} \sum_{n=1}^{\infty} (-j)^n \frac{2n+1}{n(n+1)} (\bar{m}_{e1n} - j\bar{n}_{o1n}) \qquad (3\text{-}42)$$

Using the prime to indicate differentiation with respect to the argument kR the following quantities are obtained.

$$\bar{m}_{e_{on}} = \pm \; \bar{i}_\theta \frac{1}{\sin\theta} \psi_n(kR) P_n'(\cos\theta) \begin{matrix}\cos\\ \sin\end{matrix} \phi - \bar{i}_\phi \psi_n(kR) \frac{dP_n'(\cos\theta)}{d\theta} \begin{matrix}\sin\\ \cos\end{matrix} \phi \qquad (3\text{-}43)$$

$$\bar{n}_{e_{on}} = \bar{i}_r \frac{n(n+1)}{kR} \psi_n(kR) P_n'(\cos\theta) \begin{matrix}\sin\\ \cos\end{matrix} \phi + \bar{i}_\theta \frac{[kR\psi_n(kR)]'}{kR} \frac{dP_n'(\cos\theta)}{d\theta} \begin{matrix}\sin\\ \cos\end{matrix} \phi \pm \bar{i}_\phi \frac{[kR\psi_n(kR)]}{kR} \frac{P_n'(\cos\theta)}{\sin\theta} \begin{matrix}\cos\\ \sin\end{matrix} \phi \qquad (3\text{-}44)$$

The energy division at the sphere consists of reradiated energy in the form of a scattered field and energy dissipated in the form of heat inside the sphere. The determination of these has been the basis for much investigation and has become one of the most important problems of electrodynamics. If we let s denote the scattered field and t the transmitted, the scattered field will have a solution involving Hankel functions of the second order, $h_n^{(2)}$. It behaves as a spherical wave for large R and the transmitted

field will involve radial Bessel functions of the first order. Denoting these changes in equations (3-43) and (3-44) by $\bar{m}_{eln}^{(2)}$ and $\bar{n}_{eln}^{(2)}$ and assume the propagation constant, k_1, of the sphere to be $k_1^2 = \omega^2 \mu_1 \epsilon_1 - j\omega\mu_1\sigma_1$, the scattered field ($R \geq a$) and the transmitted field ($R \leq a$) become,

$$\bar{E}^s = E_o\, e^{j\omega t} \sum_{n=1}^{\infty} (-j)^n \frac{2n+1}{n(n+1)} \left(a_n^s\, \bar{m}_{on}^{(2)} + j b_n^s\, \bar{n}_{en}^{(2)} \right) \quad (3\text{-}45)$$

$$\bar{H}^s = \frac{E_o}{\eta_o}\, e^{j\omega t} \sum_{n=1}^{\infty} (-j)^n \frac{2n+1}{n(n+1)} \left(b_n^s\, \bar{m}_{en}^{(2)} - j a_n^s\, \bar{n}_{on}^{(2)} \right) \quad (3\text{-}46)$$

$$\bar{E}^t = E_o\, e^{j\omega t} \sum_{n=1}^{\infty} (-j)^n \frac{2n+1}{n(n+1)} \left(a_n^t\, \bar{m}_{on} + j b_n^t\, \bar{n}_{en} \right) \quad (3\text{-}47)$$

$$\bar{H}^t = -\frac{k}{\omega \mu_1} E_o\, e^{j\omega t} \sum_{n=1}^{\infty} (-j)^n \frac{2n+1}{n(n+1)} \left(b_n^t\, \bar{m}_{en} - j a_n^t\, \bar{n}_{on} \right) \quad (3\text{-}48)$$

When equations (3-41) and (3-42) describe the incident wave, the boundary conditions for continuity of $\bar{E}$ and $\bar{H}$ tagential components at the sphere's surface ($R = a$) are

$$\bar{i}_r \times (\bar{E}^i + \bar{E}^s) = \bar{i}_r \times \bar{E}^t \quad (3\text{-}49)$$

$$\bar{i}_r \times (\bar{H}^i + \bar{H}^s) = \bar{i}_r \times \bar{H}^t \quad (3\text{-}50)$$

The expansion coefficients a_n^s, b_n^s, a_n^t, b_n^t, may be represented by two pairs of inhomogeneous equations. a_n^s, b_n^s, represent the external field and are the ones to be considered. The size of the sphere may be defined as

$$\rho = ca = \frac{2\pi a}{\lambda}$$

where c is the constant $\frac{2\pi}{\lambda}$ and a is the radius. Further assume $\mu_1 = \mu_o$ and a complex refractive index of η_c to be

$$\eta_c = \sqrt{\epsilon_c} = \frac{k_1}{k} = \sqrt{\epsilon_1 - j\frac{\sigma_1}{\omega\epsilon_o}} \cdot \qquad (3\text{-}51)$$

The resulting expansion[9] may be expressed as

$$a_n^s = \frac{\psi_n(\rho)\left[\eta_c \rho \psi_n(\eta_c\rho)\right]' - \psi_n(\eta_c\rho)\left[\rho\psi_n(\rho)\right]'}{h_n^{(2)}(\rho)\left[\eta_c \rho \psi_n(\eta_c\rho)\right]' - \psi_n(\eta_c\rho)\left[\rho h_n^{(2)}(\rho)\right]'} \qquad (3\text{-}52)$$

$$b_n^s = \frac{-\eta_c^2 \psi_n(\eta_c\rho)\left[\rho\psi_n(\rho)\right]' - \psi_n(\eta_c\rho)\left[\rho\psi_n(\rho)\right]'}{\eta_c^2 \psi_n(\eta_c\rho)\left[\rho h_n^{(2)}(\rho)\right] - h_n^{(2)}(\rho)\left[\eta_c\rho\psi_n(\eta_c\rho)\right]'} \qquad (3\text{-}53)$$

The development to this point shows the incident wave excites partial oscillations in the sphere with a_n being the amplitudes of those of the magnetic type and b_n being the amplitudes of those of the electric type. A resonance condition may be observed whenever the impressed frequency approaches a characteristic frequency ω_{ns} of the free oscillations.

Using the concept of total radiation being the sum of the primary and secondary fields at any point outside the sphere, it may be formulated as the following.

$$\bar{E} = \bar{E}_i + \bar{E}_r \qquad (3\text{-}54)$$

$$\bar{H} = \bar{H}_i + \bar{H}_r \qquad (3\text{-}55)$$

Integrating the Poynting vector over the surface of the scattering sphere may be done by developing the radial component of the total complex flow vector to produce the net

---

[9] Kerr, p. 448.

outflow of energy.

$$S_R = \frac{1}{2} \text{ Re } (\bar{E} \times \bar{H}^*) = \frac{1}{2} \text{ Re } (E_\theta H_\phi^* - E_\phi H_\theta^*) \qquad (3\text{-}56)$$

$$S_R = \frac{1}{2} \text{ Re} \Big[(E_\theta^i H_\phi^{i*} - E_\phi^i H_\theta^{i*}) + (E_\theta^s H_\phi^s - E_\phi^s H_\theta^s) + (E_\theta^i H_\phi^{s*} - E_\phi^i H_\theta^{s*} + E_\theta^s H_\phi^{i*} - E_\phi^s H_\theta^{s*}) \Big] \qquad (3\text{-}57)$$

where * is used to indicate conjugate multiplication.

If P_a is the power loss in the dielectric of the sphere, $-P_a$ will represent the net outflow. The net outflow of energy in the incident wave as found by integrating the first term of equation (3-57) is zero. The total power of the incident wave that is scattered, P_s, is a positive value that can be obtained by integrating the second term of equation (3-57). The third term represents the sum of the absorbed and scattered energies and may be denoted as P_t.

$$P_t = P_a + P_s = -\frac{1}{2} \text{ Re} \int_0^{2\pi} \int_0^{\pi} (E_\theta^i H_\phi^{s*} - E_\phi^i H_\theta^{s*} + E_\theta^s H_\phi^{i*} - E_\phi^s H_\theta^{i*}) R^2 \sin\theta \, d\theta \, d\phi . \qquad (3\text{-}58)$$

This integration may be performed at very large R, using equations (3-38) and (3-39), the necessary orthogonal relations of the Legendre functions and the following z_n (kR) asymptotic expansions.

$$\psi_n(kR) \approx \frac{1}{kR} \cos\left(kR - \frac{n+1}{2}\pi\right) \qquad (3\text{-}59)$$

$$h_n^{(2)}(kR) \approx \frac{j^{n+1}}{kR} e^{-jkR} \qquad (3\text{-}60)$$

The result for P_t becomes

$$P_t = \frac{-\pi E_0^2}{\eta_0 k^2} \text{ Re} \sum_{n=1}^{\infty} (2n+1)(a_n^s + b_n^s) \qquad (3\text{-}61)$$

The commonly called radar cross-section given by the term, $\frac{1}{2}\mathrm{Re}(E_\theta^s H_\phi^{s*} - E_\phi^s H_\theta^{s*})$, in the equation for S_R, may be computed for large R and $\theta = \pi$, to be

$$S_R^s(\pi) = \frac{E_o^2}{2\eta_o (kR)^2}\left[\sum_{n=1}^{\infty} (-1)^n (n+\tfrac{1}{2})(a_n^s - b_n^s)\right]^2 . \quad (3\text{-}62)$$

This summary of the referenced works has been done to demonstrate the rigor and possible difficulties involved in obtaining numerical answers for the desired values. This places a premium on good equipments and techniques adaptable for producing reliable values.

Reduction and Analysis of the Observed Data

Statistical methodology[10] will be utilized to interprete the data, employing developed theory and devised methods with adequate statements on their limitations. The mathematics employed is arithmetic supplemented with symbols to provide an intelligible exposition.

The development of this bit of scientific knowledge has the standing question always applied to experimental techniques. Are the techniques adequate to furnish the demanded precision of results, and in what respects need they be improved? In which does the most hopeful point of attack lie, in the laboratory methods or in the experimental material?

To better define the problem and the procedure used, a few pertinent statements will be very helpful. The possession or lack of an attribute will distinquish two classes of individuals making up the populations. In this particular case the attribute is the distinquished differences in the backscattering values for the spheres constructed from the different metals. The record of sampling consists of the numbers of individuals found to have or lack the attribute under investigation. The aim is to determine the population parameter that lies within the stated interval. Any probability involved is the probability that the sample drawn has lead

---

[10] George W. Snedecor, Statistical Methods, Fourth Printing, The Iowa State College Press, Ames Iowa, 1950 pp. 60-65.

to the correct conclusion. In this practice of sampling it is assumed that for each sample the population parameter lies within the 0.95 confidence interval for that sample. This means an average of 95 per one hundred of the assertions are correct. The experimentation is performed on the basis that the sampling is completely randomized. The estimates in this work are unbiased and consistent, which means the expected value is the population parameter and this parameter tends toward the true value as the size of sample increases.

The estimates, confidence statements and test of hypothesis are sufficient to summarize the information in the data. The facts of the sampling will be reported along with the relation of the findings to the problem set up, to permit making decisions and drawing conclusions. The data is presented in tabular form to display all of the desired information about the statistics of the investigation. The sampled population is specified by the description of the circumstances surrounding the experiment as explained in the section entitled Control Features of the System. Assuming the sample is a source of information that has been randomly drawn, the result will be to have the unbiased estimate, the confidence interval and the test of the sampler's hypothesis, which will provide a complete analysis and evaluation.

In the analysis of variance of the completely randomized experiment, using the infinite theory concept, $n \to \infty$, the following relationships may be stated.

1. The sample values are; x_1, x_2, x_3 ..... x_n.

2. The arithmetic mean; $\bar{x} = \frac{1}{n} \sum x_i$.

3. Corrected sum of squares of deviation from the mean;

$$\sum x^2 = \sum x_i^2 - \frac{(\sum x_i)^2}{n} = \sum (x_i - \bar{x})^2.$$

4. Correction factor as a term subtracted from $\sum x^2$ to give the deviation, c.f. $= \frac{(\sum x_i)^2}{n}$.

5. Estimate of Variance; $s_x^2 = \frac{1}{n-1} \sum (x_i - \bar{x})^2$.

6. The Standard Deviation of Means; $s_{\bar{x}} = \sqrt{\frac{s_x^2}{n}}$

7. Distribution of t, ${}_{n-1}t_{0.05}$; values were taken from the t-tables for the type 1 error with the probability that we reject the hypothesis is 0.05 or one out of twenty.

8. F is used to show the usage of the F-test and the required F tables. The F-test suffices for the multiple range test when there are only two treatments.

9. Fiducial limits;

a. $\ell_1 = \bar{x} - {}_{n-1}t_{0.05} s_{\bar{x}}$

b. $\ell_2 = \bar{x} + {}_{n-1}t_{0.05} s_{\bar{x}}$

10. The Probability Level is indicated as PrL values. The population mean, μ, lies between the confidence limits ℓ_1 and ℓ_2, and the probability of being mislead by the sampling is only 0.05.

The Observed Data and Methods of Reduction .

The following tables summarize the experimentation, data reduction and analysis. The data compaerd is for spheres constructed of iron (Fe), aluminum (Al), and Brass (Br) with radii of 0.492 inches.

TABLE III. OBSERVED DATA
RECORDED FROM THE EXPERIMENTATION

Observation Number	Iron(Fe)	Aluminum(Al)	Brass(Br)
Group 1			
1	136.0	139.0	142.0
2	140.0	136.0	142.0
3	140.0	140.0	143.0
4	141.0	140.0	144.0
5	140.0	138.0	143.0
6	137.0	140.0	145.0
7	138.0	139.0	143.0
8	136.0	142.0	143.0
9	135.0	139.0	143.0
10	137.0	139.0	143.0
Group 2			
1	134.5	140.0	142.
2	134.0	143.0	144.0
3	135.0	140.0	144.0
4	140.0	142.5	142.5
5	143.0	142.0	142.5
6	143.0	136.0	140.5
7	143.0	139.0	140.0
8	136.5	142.0	138.0
9	137.0	136.0	136.5
10	136.0	136.5	136.0

TABLE IV CONDENSED COMPUTATIONS

GROUP 1

	Iron (fe)	Aluminum(Al)	Brass (Br)
$\sum x_1$	1380.0	1392.0	1431.0
n	10.	10.	10.
$\bar{x}$	138.00	139.20	143.10
$\sum x_1^2$	190480.	193788.	204783.
c.f.	190440.0	193766.4	204776.1
$\sum(x_1-\bar{x})^2$	40.	21.6	6.9
$s_{\bar{x}}^2$	4.44	2.40	0.77
s_x	2.11	1.55	0.88
$s_{\bar{x}}$	0.21	0.16	0.09
$_{n-1}t_{0.05}$	2.262	2.262	2.262
$_{n-1}t_{0.05}\,s_{\bar{x}}$	0.48	0.36	0.20
ℓ_1	137.52	138.84	142.90
ℓ_2	138.48	139.56	143.30

GROUP 2

	Iron (Fe)	Aluminum(Al)	Brass (Br)
$\sum x_1$	1382.0	1397.0	1406.5
n	10.	10.	10.
$\bar{x}$	138.20	139.70	140.65
$\sum x_1^2$	191115.50	195228.50	197901.25
c.f.	190992.40	195160.90	197824.23
$\sum(x_1-\bar{x})^2$	123.10	67.60	77.02
$s_{\bar{x}}^2$	13.68	7.51	8.56
s_x	3.70	2.74	2.93
$s_{\bar{x}}$	0.37	0.27	0.29
$_{n-1}t_{0.05}$	2.262	2.262	2.262
$_{n-1}t_{0.05}\,s_{\bar{x}}$	0.84	0.61	0.66
ℓ_1	137.36	139.09	139.99
ℓ_2	139.04	140.31	141.31

TABLE V. ANALYSIS OF VARIANCE FOR GROUP 1

Source	Degree of Freedom(df)	Sum of Squares(ss)	Mean Square(ms)
Total(based on n-1)	29	210.70	
Treatments (based on n-1)	2	142.20	71.10
Error	27	68.50	2.54

Estimate of Standard Error of Treatment Mean, $SEM = \sqrt{\frac{EMS}{10}} = 0.504$

TABLE VI. MULTIPLE RANGE TEST FOR GROUP 1

Metal	Fe	Al	Br
Means	138.0	139.2	143.1

TABLE VII. CONFIDENCE INTERVALS FOR GROUP 1

	Al	Br	Fe
Al	X	+2.44; +5.36	-2.66; +0.26
Br	X	X	-6.56; -3.46
Fe	X	X	X

The values of confidence intervals are based on aluminum. For example; the first entry in the second column of Table V is Brass minus aluminum. The confidence limits are from -2.44 to + 5.36, etc.

TABLE VIII. ANALYSIS OF VARIANCE FOR GROUP 2

Source	Degree of Freedom(df)	Sum of Squares(ss)	Mean Square(ms)
Total(based on n-1)	29	298.25	
Treatments (based on n-1)	2	30.52	15.26
Error	27	267.73	9.92

Estimate of Standard Errof of Treatment Mean, $SEM = \sqrt{\frac{EMS}{10}} = 0.996$

TABLE IX. MULTIPLE RANGE TEST FOR GROUP 2

Metal	Fe	Al	Br
Means	138.20	139.70	140.65

TABLE X. CONFIDENCE INTERVALS FOR GROUP 2

	Al	Br	Fe
Al	X	-1.95;+3.85	-4.40;+1.40
Br	X	X	-5.35;+0.45
Fe	X	X	X

TABLE XI. ANALYSIS OF VARIANCE FOR COMBINED GROUPS 1 AND 2

Source	Degree of Freedom(df)	Sum of Square(ss)	Mean Square(ms)
Total(based on n-1)	59	514.05	
Treatments (based on n-1)	2	146.36	73.18
Error	54	336.23	6.23

Estimate of Standard Error of Treatment Mean, $SEM=\sqrt{\frac{EMS}{10}}=0.558$

TABLE XII. MULTIPLE RANGE TEST FOR COMBINED GROUPS 1 AND 2

Metal	Fe	Al	Br
Means	138.1	139.5	141.9

TABLE XIII. CONFIDENCE INTERVALS FOR COMBINED GROUPS 1 AND 2

	Al	Br	Fe
Al	X	+0.82;+3.98	-2.98;+0.18
Br	X	X	-5.38;-2.22
Fe	X	X	X

It can be observed from the multiple range test that in all cases the values of the means for iron and brass have been derived from two distinct populations. The mean for aluminum is always more than that for iron and less than that for brass. This may be observed also from the groupings in the tables of multiple range tests. This analysis shows, in addition to iron and brass belonging to different populations, a trend in values placed in the following order; iron, aluminum, and brass.

A preliminary analysis was made at the time of experimentation using the probability paper reduction method[11]. The results were identical with those of the above method. This probability method and an introduction to probability will be reviewed to show it's utility of application to this type of reduction and to indicate the similarity in the results to that of the Analysis of Variance Method.

If a probabilistic model[12] is accepted to give a satisfactory mathematical theory of the phenomenon under investigation, the theory for making applications of various kinds can be employed. The applications of probability theory may be roughly classified under the headings; Description, Analysis and Prediction.

The set of statistical data has been collected and it is desired to describe the characteristic features of this

---

[11]Captain Lavern A. Yarbrough, Laboratory Instruction Manual, ITUSAF, Revised Edition 1955, Wright-Patterson AFB, Ohio, AF-WP-(B)-O-1, pp. 58-61.

[12]Harold Cramer, The Elements of Probability Theory, John Wiley and Sons, Inc., New York, 1955.

material as briefly and concisely as possible. The first step will be to register the data in a convenient table, and to work out a graphical representation of the material. Compute a small number of numerical quantities, which may serve as descriptive characteristics of the material, and which give in a condensed form, as much as possible of the relevant information contained in the data.

Assuming the statistical data can be regarded as observed values of certain random variables then some information about the probability distributions[13] is known and the mathematical expressions of these probability distributions give useful guidance in convenient tabular and graphical arrangements. Descriptive characteristics may be had by calculating from the data estimated values of the parameters appearing in the expressions of the probability distributions. Descriptive characteristics are usually employed as a preliminary step of a statistical investigation. This in turn is used in arriving at the final step of an inquiry involving the analysis or the prediction.

Powerful tools for a scientific analysis of statistical data can be realized in the concepts and methods of probability theory[14]. Usually the data observed may be regarded as arriving at certain inferences regarding the probability distribution of variables.

Prediction, in it's broadest definition, would be the

---

[13]Thomas B. Crumpler and John H. Yoe, Chemical Computations and Errors, John Wiley and Sons, Inc., New York, 1950, pp. 174-196.

[14]Cramer, all.

ultimate practical aim of science. It relates to the ability to answer questions, such as the following. What can be expect to happen under certain conditions?

Description, Analysis and Prediction cannot always be distinctly defined, for instance, the descriptive treatment of statistical material may be inseparably connected with the estimation or comparison of analytical nature. These do serve to introduce a convenient method of presenting some of the essential aspects of the applications of mathematical probability.

A simple, convenient and versatile method of display of a reduction of statistical data can be found in the use of probability graph paper[15]. The following example reduction using the data in this research, will demonstrate it's use.

Referring to Table III, Group 1, page 86, the ten readings have been recorded in the experiment and this number of readings has been determined to be adequate to show a desirable statistical display. Any number of readings could be used, primarily enough readings are desired to give a good display. Ordinarily this number will be approximately ten or more. These values are tabulated according to their rank in the set. Each rank is then assigned a percentage dependent upon the number of times it occurs in the set and the order of occurance. Referring to the tabulation(Table III, Group 1), 135 is the lowest ranking value in the set for the iron sphere. It appears one time, therefore, it is assigned a proportional

---

[15]Yarbrough, pp. 58-61.

precentage of 9.09. The value 136 is the next ranking value. It occurs two times in the set, therefore, it is assigned the proportional percentage of 18.18 plus the preceding percentage, or a total percentage of 27.27. Each reading is assigned a per cent value based on the desired divisions of the abscissa. This is arrived at by dividing the abscissa by a convenient number to produce a desirable grouping of the distribution in the vacinity of the most probable value. The maximum percentage calibration on the abscissa of the probability graph paper is 99.99. Each reading in the set is assigned it's corresponding percentage by the above method. For this display the abscissa has been divided into eleven divisions. Table III, Group 1 yields the results tabulated in Table XIV, for the iron sphere with a radius of 0.492 inches.

Having arrived at the values stated, according to rank and percentages, a plot of this information can be made on probability graph paper (see Figure 17 page 99). The ordinate is divided linearly into a number of increments which permits the choice of a variety of scales. In this case the scale has been calibrated to provide a convenient display of the respective ranks as shown on the graph. Each rank value is plotted as the ordinate versus it's corresponding percentage as the abscissa. After these are plotted, the best straight line is drawn through all points. At the 50 per cent calibration on the abcissa the most probable value

can be read on the ordinate from the point of intersection of the straight line and the 50 per cent line. In this case, iron yields a reading of 137.81, as is indicated on the graph, at the intersection of the curve for iron and the 50% calibration of the abscissa. The possibility arises that a particular value may be widely displaced from the straight line plot. When this occurs it can be assumed that this value does not satisfy the statistical sample and it can be eliminated from the considerations. The probability graph is a most useful means of arriving at an approximate most probable value when required to determine a quantity from a statistical tabulation. This case occurs often in the scientific processes of instrumentation.

If a probabilistic model is accepted to give a satisfactory mathematical theory of the phenomenon under investigation, this theory can be used in making an application. This method gives an approximation that is well within the limits of the ability of an observer to read values from plots on the probability paper.

TABLE XIV. IRON SPHERE WITH RADIUS = 0.492 INCHES

Value	Rank	Number of Occurance Times	Assigned Percentage
135	1	1	9.09
136	2	2	27.27
137	3	2	45.45
138	4	1	54.54
140	5	3	81.81
141	6	1	90.90

The method used to arrive at the most probable value for iron may be used to obtain the most probable values for aluminum and brass. Referring to Table III, Group 1, the required readings can be made available to permit tabulation in the form of Table XIV. Tables XV and XVI are derived from data for the aluminum sphere and the brass sphere, respectively.

TABLE XV. ALUMINUM SPHERE WITH RADIUS = 0.492 INCHES

Value	Rank	Number of Occurance Times	Assigned Percentage
136	1	1	9.09
138	2	1	18.18
139	3	4	54.54
140	4	3	81.81
142	5	1	90.90

TABLE XVI. BRASS SPHERE WITH RADIUS = 0.492 INCHES

Value	Rank	Number of Occurance Times	Assigned Percentage
142	1	1	9.09
143	2	7	72.72
144	3	1	81.81
145	4	1	90.90

The curves for aluminum and brass are plotted in Figure 17, page 99 along with the plot for iron for purposes of comparisons. The most probable value for aluminum, as read from the graph is 139.00 while that for brass is 143.10

The probability graph reduction of the data in Table III, Graph 2, is plotted in Figure 18, page 100. The procedure is identical with that used for the plots of the data on page 99.

The results indicated iron to have the lowest most probable value, aluminum an intermediate value and brass indicated the highest most probable value. This analysis was the same for both plots. It reduced to the same results as that accomplished by the Analysis of Variance method. The results of the two methods are summarized in the following table.

TABLE XVII. COMPARISON OF THE RESULTS OF DATA REDUCTION BY THE METHODS USED

	Analysis of Variance Method Multiple Range Test			Probability Graph Method		
	Fe	Al	Br	Fe	Al	Br
Group 1	138.00	139.20	143.10	137.81	139.00	143.10
Group 2	138.20	139.70	140.65	137.95	139.60	140.43

Corresponding Values in Decibels Converted from the above Attenuator Scale Readings using the Graph of Figure 16, page 67.

Group 1	28.6	29.0	30.0	28.5	29.0	30.0
Group 2	28.7	29.2	29.5	28.6	29.2	29.3

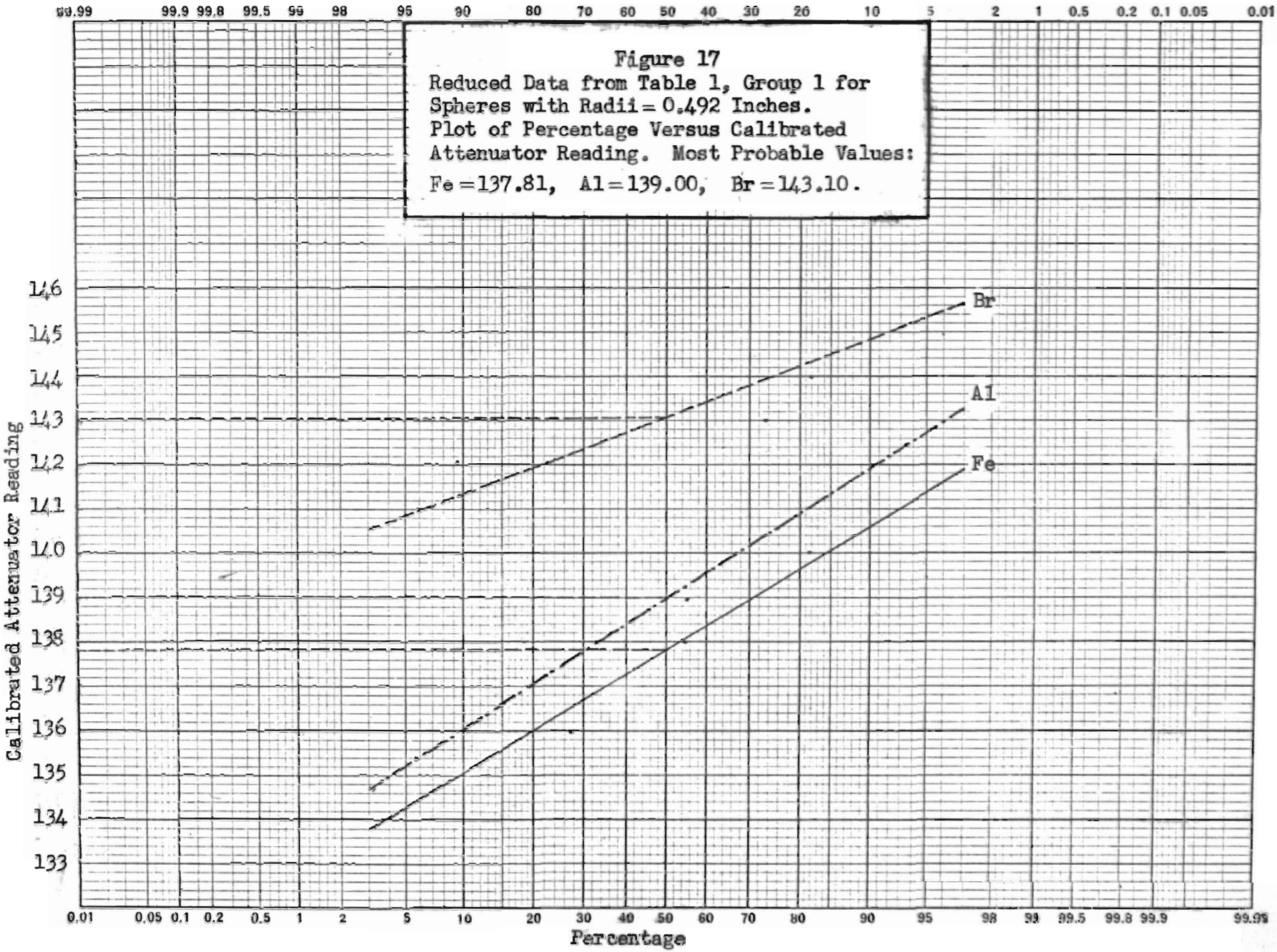
99.99 99.9 99.8 99.5 99 98 95 90 80 70 60 50 40 30 20 10 5 2 1 0.5 0.2 0.1 0.05 0.01
Figure 17
Reduced Data from Table 1, Group 1 for Spheres with Radii = 0.492 Inches.
Plot of Percentage Versus Calibrated Attenuator Reading. Most Probable Values:
Fe = 137.81, Al = 139.00, Br = 143.10.
Br
Al
Fe
Calibrated Attenuator Reading
146
145
144
143
142
141
140
139
138
137
136
135
134
133
0.01 0.05 0.1 0.2 0.5 1 2 5 10 20 30 40 50 60 70 80 90 95 98 99 99.5 99.8 99.9 99.99
Percentage

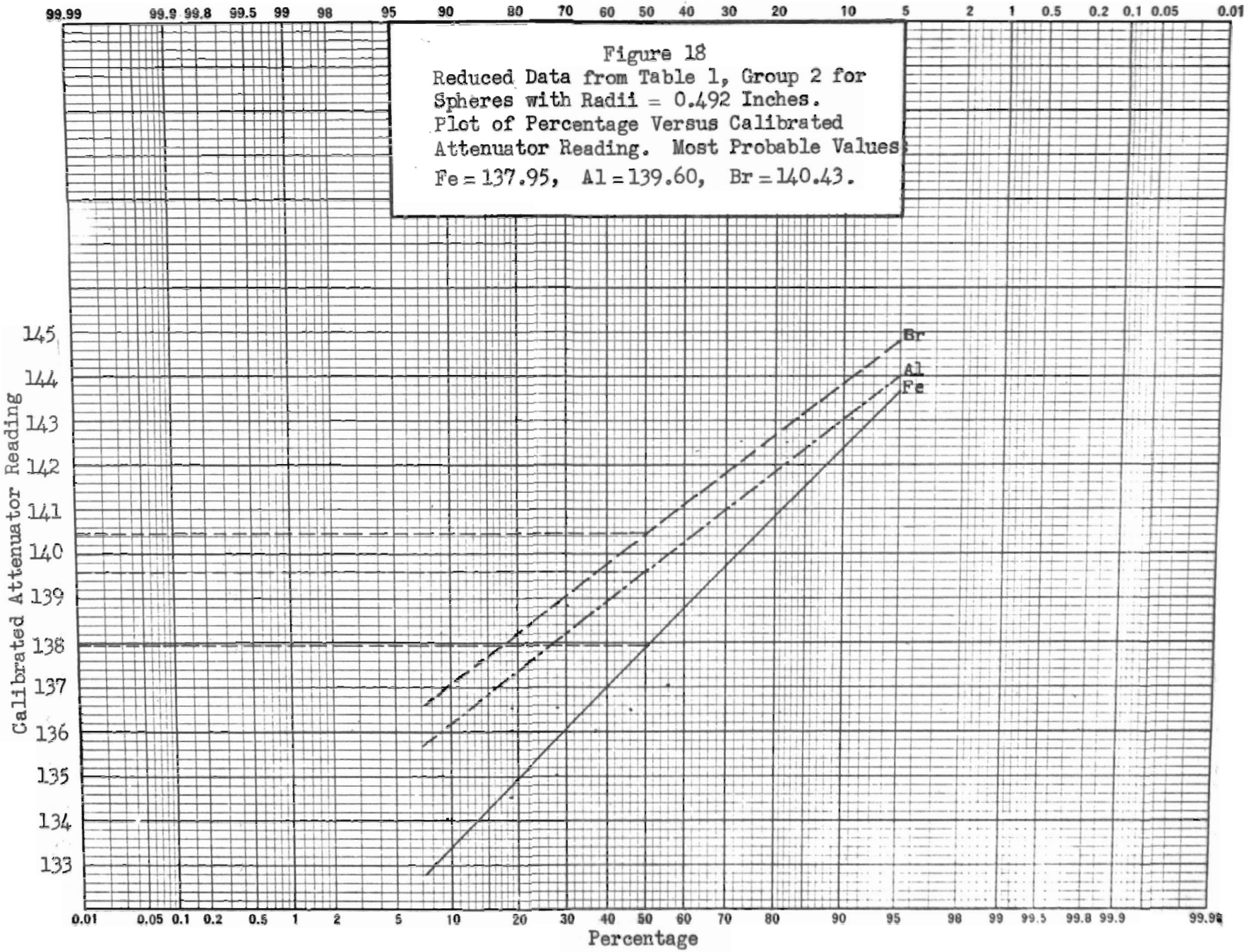
99.99 99.9 99.8 99.5 99 98 95 90 80 70 60 50 40 30 20 10 5 2 1 0.5 0.2 0.1 0.05 0.01
Figure 18
Reduced Data from Table 1, Group 2 for Spheres with Radii = 0.492 Inches.
Plot of Percentage Versus Calibrated Attenuator Reading. Most Probable Values
Fe = 137.95, Al = 139.60, Br = 140.43.
Br
Al
Fe
Calibrated Attenuator Reading
145
144
143
142
141
140
139
138
137
136
135
134
133
0.01 0.05 0.1 0.2 0.5 1 2 5 10 20 30 40 50 60 70 80 90 95 98 99 99.5 99.8 99.9 99.99
Percentage

Analysis of the Data in Reduced Form.

The concluding analysis will be based on the data, for spheres constructed of aluminum and iron. Correlation with theory related to the radar equation is demonstrated and error involved in lack of considering conductivity of the metal is shown. Further, the results demonstrate the merits of the equipment and technique designed for this research.

It is not known whether the bars of brass submitted to the National Bureau of Standards for resistivity determinations were representative of the material used in the construction of the spheres. This occured in the shops during the fabrication of the spheres. Due to this lack of exact information the final comparative analysis will be done considering only the aluminum and iron spheres. Also it should be noted that the values of conductivity for the aluminum samples were about one-half as large as values listed for aluminum in available tables[16,17]. This means the values for the aluminum and brass are more closely placed than would ordinarily be expected. This also places the conductivity values for iron and aluminum closer together, while usually they would be placed farther apart in value. The Analysis of Variance method will be applied to the data of groups 1 and 2, Table III, Chapter III, to get the desired reduced values for the iron and aluminum spheres.

---

[16] Ramo and Whinnery, p. 210.

[17] Stratton, p. 605.

TABLE XVIII. CONDENSED COMPUTATIONS FOR IRON AND ALUMINUM, GROUP 1

	Iron (Fe)	Aluminum (Al)
$\sum x_1$	1380.	1392.
n	10.	10.
$\bar{x}$	138.0	139.2
$\sum x_1^2$	190480.	193.788
c.f.	190440.	193.766
$\sum (x_1 - \bar{x})^2$	40.	22.
s_x^2	4.4444	2.4444
s_x	2.11	1.56
$s_{\bar{x}}$	0.667	0.494
$n-1 t_{0.05}$	2.262	2.262
$n-1 t_{0.05}\ s_{\bar{x}}$	1.509	1.117
ℓ_1	136.5	138.1
ℓ_2	139.5	140.3

TABLE XIX. ANALYSIS OF VARIANCE FOR GROUP 1

Source	Degree of Freedom(df)	Sum of Squares(ss)	Mean Square(ms)	F	Prl.
Total	19	69			
Treatments	1	7	7	2.03	0.21
Error	18	62	3.44		

Estimate of Standard Error of Treatment Mean, $SEM = \sqrt{\frac{EMS}{10}} = 0.590$

The F test suffices for the Multiple Range test when there are only 2 treatments.

$$Pr\left\{ -0.55 < \mu_{Al} - \mu_{Fe} < 2.953 \right\} = 0.05$$

Confidence Interval (5%) based on the difference of the means of Aluminum minus Iron, $(\mu_{Al} - \mu_{Fe}) = (1.2 \pm 1.75)$.

TABLE XX. CONDENSED COMPUTATIONS FOR IRON AND ALUMINUM, GROUP 2

	Iron (Fe)	Aluminum (Al)
Σx_i	1382.	1397.
n	10.	10.
$\bar{x}$	138.2	139.7
Σx_i^2	191115.50	195228.50
c.f.	190992.40	195160.90
$\Sigma(x_i-\bar{x})^2$	123.10	67.6
s_x^2	13.68	7.51
s_x	3.69	2.74
$s_{\bar{x}}$	1.170	0.867
$9\ t_{0.05}$	2.262	2.262
$9\ t_{0.05}\ s_{\bar{x}}$	2.647	1.961
l_1	135.55	137.74
l_2	140.85	141.66

TABLE XXI. ANALYSIS OF VARIANCE FOR GROUP 2

Source	Degree of Freedom(df)	Sum of Squares(ss)	Mean Square(ms)	F	PrL
Total	19	201.95			
Treatments	1	11.25	11.25	1.06	0.29
Error	18	190.70	10.59		

Estimate of Standard Error of Treatment Mean, $SEM=\sqrt{\frac{EMS}{10}}=1.028$

The F test suffices for the Multiple Range Test when there are only 2 treatments.

$$Pr\left\{-1.53 < \mu_{Al} - \mu_{Fe} < 4.55\right\}=0.05$$

Confidence interval (5%) based on the difference of the means of Aluminum minus Iron, $(\mu_{Al} - \mu_{Fe}) = (1.5 \pm 3.05)$.

TABLE XXII. CONDENSED COMPUTATIONS FOR COMBINED GROUPS 1 AND 2

	Iron (Fe)	Aluminum (Al)
Σx_1	2762.	2789.
n	20.	20.
$\bar{x}$	138.10	139.45
Σx_1^2	381595.50	389016.50
c.f.	381432.20	388926.05
$\Sigma(x_1-\bar{x})^2$	163.30	90.45
s_x^2	8.59	4.76
s_x	2.931	2.182
$s_{\bar{x}}$	0.655	0.4878
$9t_{0.05}$	2.093	2.093
$9t_{0.05}s_{\bar{x}}$	1.387	1.021
ℓ_1	136.71	138.43
ℓ_2	139.49	140.47

TABLE XXIII ANALYSIS OF VARIANCE FOR COMBINED GROUPS 1 AND 2

Source	Degree of Freedom(df)	Sum of Squares(ss)	Mean Square(ms)	F	PrL
Total	39	271.98			
Treatments	1	18.23	18.23	2.72	0.12
Error	38	253.75	6.68		

Estimate of Standard Error of Treatment Mean, $SEM = \sqrt{\frac{EMS}{10}} = 0.5779$

The F test suffices for the Multiple Range Test when there are only 2 treatments.

$$Pr\left\{ -0.31 < \mu_{Al} - \mu_{Fe} < 3.01 \right\} = 0.05$$

Confidence Interval (5%) based on the difference of the means of Aluminum minus Iron, $(\mu_{Al} - \mu_{Fe}) = (1.35 \pm 1.661)$.

The probability levels, P_rL, indicate the degree of

significance of the F value obtained. The combined data of Groups 1 and 2 show the treatment difference to be significant at the 88 per cent level, $(1-P_rL)$, that is, $Pr\{F_{1,18} \leq 2.72\}=0.88$, where $F_{1,18}$ means the tabular value of F for the degrees of freedom of 1 for the numerator and 18 for the denominator in the ratio for F. P_rL shows the value at which the statistic is significant. The reduction will be based on the values for $\bar{x}$ from the combined data which are Iron = 138.10 and Aluminum = 139.45. These values convert to 28.85 db for iron and 29.16 db for aluminum by using the attenuator calibration chart, Figure 16, page 67.

Application to the Radar Equation

For the case of the imperfect conductor, electric and magnetic fields may exist inside the conductor. An imperfect conductor may be treated[18] as a dielectric with a complex dielectric constant and with it's conductivity never appearing explicitly. With these concepts in mind consider the reduced data as related to the radar equation. The radar equation[19] may be stated in the form,

$$S = P \frac{G^2 \lambda^2 K}{(4\pi)^3 R^4}$$

where S is the received power

P is the transmitted power

λ is the wavelength

K is the radar cross-section

R is the distance from the source to the target.

---

[18]Ramo and Whinnery, p. 271.

[19]Kerr, p. 31

A value for the radar cross section, expressed in decibels, may be solved for in the following manner.

$$K = \frac{S}{P} \quad \frac{(4\pi)^3 R4}{G^2 \quad \lambda^2} \qquad (3\text{-}65)$$

$$K\,(db) = 10 \log K = 10 \log \frac{S}{P} + 30 \log 4\pi + 40 \log R - 20 \log G - 20 \log \lambda \qquad (3\text{-}65)$$

$$K\,(db) = 10 \log \frac{S}{P} + 30 \log 12.5664 + 40 \log 67.0 - 20 \log G - 20 \log 1.191$$

where: $-20 \log G = G(\text{transmit}) + G(\text{receive})$

$= 20.3 + 20.3 = 40.6$ db,

$R = 67.5$ cm,

and $$\lambda = \frac{Vc}{f} = \frac{2.9967 \times 10^{10}}{2.51625 \times 10^{10}} = 1.191 \text{ cm.} \qquad (3\text{-}66)$$

$$K\,(db) = \frac{S}{P}\,(db) + 64.034 \text{ db} \qquad (3\text{-}67)$$

The calibrated attenuator value may be expressed, using the notation of Chapter II, as

$$\text{Measured Value } b = \text{Total Gain in db} + \frac{S}{P}\,(db) \qquad (3\text{-}68)$$

$$\text{Measured Value } b = 91.5 \text{ db} + \frac{S}{P}\,(db)$$

$$\frac{S}{P}\,(db) = \text{Measured Value } b - 91.5 \text{ db}. \qquad (3\text{-}69)$$

Substituting this value for $\frac{S}{P}$ (db) into equation (3-67) gives

$$K\,(db) = b\,(db) - 91.5 \text{ db} + 64.034 \text{ db}. \qquad (3\text{-}70)$$

This is a convenient expression for the radar equation as applied to this research since all of the parameters are included in simplified form. This permits direct substitution of the measured values into the equation to solve for the desired values of the radar cros section, K (db), using 1.0 cm^2 as the reference and with the limiter cathode meter referred to 0.6 millamperes.

For the aluminum sphere with a radius of a = 1.25 cm.

$$K(db) = 29.16 \text{ db} - 27.466 \text{ db} = 1.694 \text{ db} . \qquad (3\text{-}71)$$

This value is indicated on the graph of Radar Cross-section of Metal Spheres for $\lambda = 1.191$ cm., Figure 19, page 108. This graph is a plot of radius in centimeters versus K in square centimeters and decibels for a metal sphere with perfect conductivity. This curve is a plot of backscattering values calculated by the exact solution for the case of a metallic sphere with infinite conductivity. The aluminum sphere has a relatively high conductivity and it's value of K = 1.694 db is a value that is placed in proximity to the curve according to the conductivity of the aluminum.

The iron sphere with a radius a = 1.25 cm. gives a different value from that of the aluminum sphere. This value is

$$K(db) = 28.85 \text{ db} - 27.466 \text{ db} = 1.384 \text{ db} . \qquad (3\text{-}72)$$

This value is farther displaced from the curve which demonstrates the effects of conductivity on the backscattering cross section.

Theoretical values for radar cross sections of perfectly conducting spheres have been calculated[20] by the exact solution and tabulated for the range of $\rho = \frac{2\pi a}{\lambda}$ from 0.00 to 10 in steps of 0.01 to 4 decimals. The radar cross section

---

[20] Scientific Computing Services, Ltd. of Ministry of Supply for R.R.D.E. "Radar Cross Section of Conducting Sphere", Table of ρ vs $\frac{K}{\pi a^2}$. See Appendix I.

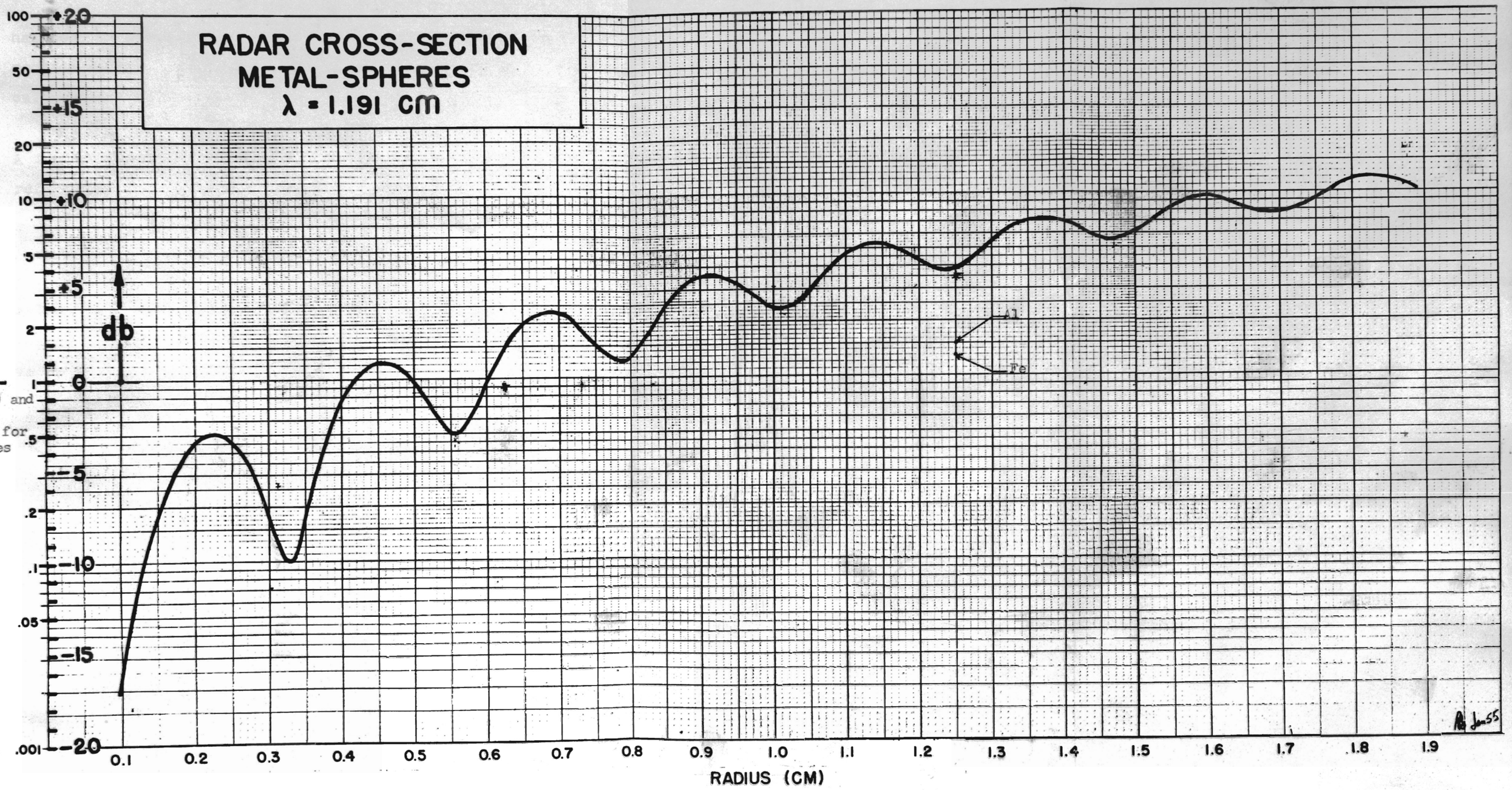

Figure 19. Radar Cross-section of metal spheres for λ = 1.191 cm.

has been considered as the ratio of the backscattering cross section to the optical cross section, expressed as $\frac{K}{\pi a^2}$. The calculated value for ρ in the case considered is

$$\rho = \frac{2\pi a}{\lambda} = \frac{2(3.1416)\ 1.25}{1.191} = 6.594. \qquad (3\text{-}73)$$

A corresponding value for $\rho = 6.594$ may be obtained from the referenced RRDE table for $\frac{K}{\pi a^2}$, to be 0.7762.

$$K = 0.7762 \times \pi a^2 \qquad (3\text{-}74)$$

$$K = 0.7762 \times 3.1416 \times (1.25)^2$$

$$K = 3.8072 \text{ cm}^2$$

Referring to the ordinate scales of Figure 19 the corresponding db reading for $K = 3.8072$, referred to 1 cm^2 is 5.6. This value may be used in the equation of $\frac{S}{P}$ (db) to get

$$\frac{S}{P} \text{ (db)} = -64.034 + 5.6 = 58.434 \text{ db}. \qquad (3\text{-}75)$$

With reference to equation (3-69) of $\frac{S}{P}$ (db)

$$b(\text{db}) = 91.5 \text{ db} - \frac{S}{P} \text{ (db)}$$

$$b(\text{db}) = 91.5 \text{ db} - 58.434 \text{ db} = 33.06 \text{ db}. \qquad (3\text{-}76)$$

This is a calculated value based on the theory. The values read from the attenuator after converting to decibels on the calibration curve, Figure 16, was 29.16 db and 28.85 db. Since the theoretical basis for the calculation is the infinitely conducting sphere, the aluminum and iron spheres with readings of 29.16 db and 28.85 db, respectively, differ from the point through which the curve of Figure 19 was plotted. A similar curve to that of Figure 19 could be plotted for aluminum spheres and iron spheres with each curve passing through the corresponding points illustrated.

for their values. A perfectly conducting sphere produces a value of K= 5.9db as shown on the curve. This value differs appreciably from those for spheres constructed from aluminum and iron.

The term conductivity has been used freely with reference to the extent with which an object absorbs and reflects electromagnetic energy. It is known and has been demonstrated in the section "Calibration of the System" that the wave of energy experiences a change of phase upon contact with the target. There has been no attempt to account for this change of phase. The values of power recorded are complex values but since only magnitudes are distinguished and the conditions are controlled to keep the respective phasors equal in value the powers may be assumed to be ones resulting from the effects of the different materials. The effects of sphericality of the transmitted and reflected waves have not been considered. These topics are ones of importance and should be good areas for investigation.

If the analysis of backscattering is to be complete, conductivity of the scattering object should be included. The operation of a conventional radar is not concerned with this type refinement but improved systems, particularly radar confusers must have every consideration in refinements that will contribute to their operation. Future developments of these are dependent upon considerations such as this to improve their employment and accomplish a most important job of reflectivity.

CHAPTER IV

SUMMARY AND CONCLUSIONS

An analysis of backscattering is incomplete when performed without due considerations of the effects of the conductivity of the target. The operation of a conventional radar is not concerned with this type of refinement but improved systems in the future, particularly radar tow targets and confusers must have every consideration in refinements that will contribute to an improved operation. Future developments of these is dependent upon what might be referred to as the fringe areas of improvision, to give the solutions to better employment and the accomplishment of a most important job of reflectivity.

A consideration of this type will aid in the analysis and evaluation of radar targets in the comparison of reflectors as radar confusers (chaff, rope, etc.), to observe surface conditions of materials and in the determination of the characteristics of materials and combinations of materials. Information on scattering behavior is of value in interpreting the natural modes of oscillation on complex structures. Essentially, the scattered radiation is a clue to the location and magnitude of unloaded currents on metal surfaces. The effect of coupling mechanisms such as slots on these currents is observed by corresponding changes in the scattering pattern and amplitude. Scattering measurements of this type are indirect determinations of current distributions and are

valuable where direct methods are difficult to employ.

By suitable scaling[1], reflection measurements may be conducted in a laboratory with minimum space. Making measurements at long wavelengths, which may characterize a given system, may be restricted due to the large space required and the inability to control the environmental and other conditions accompanying the system's characteristics. Scaling permits reduction in dimensions such that control of the elements effecting the accuracy of measurement may be determined, sufficiently analyzed and properly controlled permitting the desired overall accuracy of measurement. The system described may be adapted for this use.

Measurements, such as the ones made in this investigation, must be carefully controlled. The equipment arrangement and the techniques employed to make possible the reflection measurements were unique. Only with equipment of the prescribed sensitivity, accuracy and physical arrangement is research of this type possible.

The apparatus and procedure described in this paper were established to give maximum sensitivity and to produce a more precise method of measurement of backscattering from objects than has been developed by previous methods. External disturbances were eliminated, or their magnitudes established by performing the tests in a room of adequate size

---

[1]Donald D. King, Measurements at Centimeter Wavelengths, D. Van Nostrand Publishing Co., Inc., New York, 1952, p. 3.

with its interior constructed of low reflection material. The experimental measurement errors were reduced to a minimum.

By extending the research employing the image-plane to include backscattering values for all basic geometric configurations from different aspects, the information gathered could be used to great advantage. One example would be when backscattering from a particular aircraft or missile is desired. The vehicle may be reduced to the basic geometric configurations, these in turn may be measured on the image-plane by the technique described in this paper, then the resulting measured values can be combined to produce the overall backscattering value. The mathematical approach to this type solution has been done but the results become very extended and complicated. The inadequate sensitivity of equipments and the methods of measurements employed have restricted previous experimentation. This system could possibly be used to measure backscattering from non-rigid configurations such as a ribbon of metal if the image-plane were inverted to permit the ribbon to hang from it. Perhaps the measurements could be made in a laboratory test box. This would require one of adequate size and lined with an absorbent material. These are problems of interest and perhaps will be investigated in the near future. Research could be conducted on many objects to help gain more knowledge about radar cross sections and their analytical solutions.

SELECTED BIBLIOGRAPHY

Aden, A. L. "Electromagnetic Scattering From Metal and Water Spheres", Technical Report Number 106, Cruft Laboratory, Harvard University, Cambridge, Mass. August 1, 1950.

Bowkamp, C. J., "Diffraction Theory", Phillips research Laboratory, N. V. Phillips' Goleilampenfabrieken, Eindhoven, Netherlands, May, 1955.

Brillouin, L., "The Scattering Cross-Section of Spheres for Electromagnetic Waves", Journal of Applied Physics, Volume 20, Number 11, November 1949, pp. 1110-1125.

Cohen, M. H. and R. C. Fisher, "A Dual-Standard Echoing Body", AF Contract Number AF 18(600)-19, Ohio State University, Columbus, Ohio, 30 June 1954.

Cramer, H., The Elements of Probability Theory, John Wiley and Sons, Inc., New York, 1955.

Crumpler, T. B. and J. H. Yoe, Chemical Computations and Errors, John Wiley and Sons, Inc., New York, 1950 p. 1 and pp. 174-196.

Dike, S. H. and D. D. King, "The Absorption Gain and Backscattering Cross-Section of the Cylindrical Antenna", Proceedings of the Institute of Radio Engineers, Volume 40, July 1952, pp. 853-860.

Ehrlich, Morty, Unpublished Paper on Scattering Measurement Models, Microwave Instrumentation Company, 1953.

Fink, D. G., Radar Engineering, First Edition, McGraw-Hill Book Company, Inc., 1947, p. 232.

Fubini and Fails, "Methods of Measurement of Radar Cross Section", Report Number 380-1, Airborne Instrument Laboratories, Mineola, New York, January 1949.

Hagen and Rubens, "Reflection Coefficient Formulas", Annual Physik, 11, 1903, p. 873.

Hines, J. N. and T. E. Tice, "An Investigation of Reflection Measuring Equipment", Contract AF 18(600)-88, E. O. 112-61 SR-6f4, Antenna Laboratory, Ohio State University, Columbus, Ohio

Keller, J. B., "Reflection and Transmission of Electromagnetic Waves by Thin Curved Shells", AF Contract Number W 28-099-ac-172, Watson Laboratories, Red Bank, New Jersey, February 1948.

Kerr, D., Propagation of Short Radio Waves, McGraw-Hill Book Company, Inc., New York, 1951, pp.29-31 and pp. 445-448.

King, D. D., "The Measurement and Interpretation of Antenna Scattering", Proceedings of Institute of Radio Engineers, Volume 37, July 1949, pp. 770-777.

____. Measurements at Centimeter Wavelengths, D. Van Nostrand Company, Inc., 1952, p. 3, pp. 229-230 and pp. 291-295.

Kodis, R. D., "An Experimental Investigation of Microwave Diffraction", Technical Report Number 105, Cruft Laboratory, Harvard University, Cambridge, Mass., June 10, 1950.

Kouyoumjian, R. G., "The Calculations of the Echo Area of Perfectly Conducting Objects by the Variational Method", Ph. D. Thesis, Department of Physics, Ohio State University, Columbus, Ohio, 1948.

Kraus, J. D. Antennas, McGraw-Hill Book Company, Inc., 1950, p. 473.

Marchesano, J. E., "Hybrid Junctions", Philco Tech Rep Division Bulletin, Volume 5, Number 5, Philadelphia, Pa., September and October, 1955.

Mentzer, J. F. Scattering and Diffraction of Radio Waves, Pergamon Press, London and New York, 1955.

Ramo, S. and J. R. Whinnery, Fields and Waves In Modern Radio, Second Edition, John Wiley and Sons, Inc., 1953, p. 210, p. 234 and p. 271.

Ridenour, L. N., Radar System Engineering, McGraw-Hill Book Company, Inc., New York.

Sarbacher, R. I. and W. A. Edson, Hyper and Ultra-High Frequency Engineering, 8th Printing, John Wiley and Sons, Inc., New York, 1950, p. 403.

"Scattering From Spheres", Report Number 4, Navy Contract N7 onr- 29529, Antenna Laboratory, University of California, Berkely, California, 15 June 1950.

Schelkunoff, S., Electromagnetic Waves, D. Van Nostrand Company, Inc., New York, 1943, Chapter IX.

Sevik, J., "An Experimental Method of Measuring Back-Scattering Cross-Sections of Coupled Antennas", Technical Report Number 151, Cruft Laboratory, Harvard University, Cambridge, Mass., May 28, 1952.

Siegel, K. M. and H. A. Alperin and Associates, "Studies In Radar Cross-Sections", Report Numbers I through XI, Willow Run Research Center, Engineering Research Institute, University of Michigan, Willow Run, Mich.

Silver, S., Microwave Antenna Theory and Design, McGraw-Hill Book Company, Inc., New York, 1949, pp. 580-589.

Slater, J. C., Microwave Electronics, D. Van Nostrand Company, Inc., New York, 1950, pp. 62-168.

Snedcor, G. W., Statistical Methods, Fourth Printing. The Iowa State College Press, Ames, Iowa, 1950 pp. 60-65.

Spencer, R. C., "Backscattering From Conducting Surfaces", Report Number E 5070, AF Cambridge Research Center, Mass., April 1951.

Stratton, J. A., Electromagnetic Theory, McGraw-Hill Book Company, Inc., New York, 1941, pp. 504-508, p. 563 and p. 605.

"Test of Absorbent Material", Naval Research Laboratory Problem Number R11-14; Report On, Forwarding Of, Naval Research Laboratory, Washington, D. C., 24 June 1954.

Yarbrough, L. A., Laboratory Instruction Manual, ITUSAF, Revised Edition, 1955, Wright-Patterson AFB, Ohio, AF-WP-(B)-O-1, pp. 58-61.

APPENDIX I

RADAR CROSS SECTION OF CONDUCTING SPHERE

As computed by Scientific Computing Service, Ltd. of Ministry of Supply, (Table of $\sqrt{\frac{\pi K}{\lambda}}$ for $\frac{2\pi a}{\lambda}$ = 0.000(0.10) 10 to 4 decimals, $\rho = \frac{2\pi a}{\lambda}$).

ρ	$\frac{K}{\pi a^2}$	ρ	$\frac{K}{\pi a^2}$	ρ	$\frac{K}{\pi a^2}$
0.5	0.5294	3.7	1.4543	6.9	1.0466
0.6	1.0452	3.8	1.2419	7.0	1.1577
0.7	1.7704	3.9	0.9973	7.1	1.2250
0.8	2.5962	4.0	0.7854	7.2	1.2377
0.9	3.2938	4.1	0.6580	7.3	1.1923
1.0	3.6374	4.2	0.6422	7.4	1.1024
1.1	3.5474	4.3	0.7350	7.5	0.9931
1.2	3.1046	4.4	0.9063	7.6	0.8933
1.3	2.4543	4.5	1.1075	7.7	0.8288
1.4	1.7379	4.6	1.2844	7.8	0.8151
1.5	1.0755	4.7	1.3915	7.9	0.8542
1.6	0.5727	4.8	1.4031	8.0	0.9337
1.7	0.3115	4.9	1.3203	8.1	1.0314
1.8	0.3290	5.0	1.1688	8.2	1.1213
1.9	0.5936	5.1	0.9910	8.3	1.1798
2.0	1.0082	5.2	0.8336	8.4	1.1926
2.1	1.4446	5.3	0.7361	8.5	1.1576
2.2	1.7863	5.4	0.7207	8.6	1.0854
2.3	1.9568	5.5	0.7878	8.7	0.9960
2.4	1.9286	5.6	0.9160	8.8	0.9132
2.5	1.7201	5.7	1.0692	8.9	0.8585
2.6	1.3895	5.8	1.2057	9.0	0.8452
2.7	1.0228	5.9	1.2903	9.1	0.8754
2.8	0.7126	6.0	1.3026	9.2	0.9399
2.9	0.5336	6.1	1.2424	9.3	1.0208
3.0	0.5208	6.2	1.1279	9.4	1.0962
3.1	0.6627	6.3	0.9910	9.5	1.1466
3.2	0.9094	6.4	0.8677	9.6	1.1594
3.3	1.1892	6.5	0.7896	9.7	1.1323
3.4	1.4283	6.6	0.7753	9.8	1.0735
3.5	1.5675	6.7	0.8260	9.9	0.9992
3.6	1.5752	6.8	0.9258	10.0	0.9292

VITA

Lavern Andrew Yarbrough

Candidate for the Degree of

Doctor of Philosophy

Thesis: A STUDY OF K-BAND BACKSCATTERING COEFFICIENTS OF SYMMETRICAL TARGETS

Major Field: Electrical Engineering

Biographical:

Personal Data: Born at Tribbey, Oklahoma, September 22, 1920, the son of William A. and Pauline J. Yarbrough.

Education: Attended grade school at Harrah and Tribbey, Oklahoma; graduated from High School at Tribbey, Oklahoma in 1938; undergraduate studies at Univeristy of Oklahoma, Oregon State College, Yale University, Oklahoma Agricultural and Mechanical College where the Bachelor of Science degree was awarded with a major in Electrical Engineering, January 1951; received the Master of Science degree from Oklahoma Agricultural and Mechanical College, with a major in Electrical Engineering, in August 1951; completed requirements for the Doctor of Philosophy degree in August, 1957.

Organizations: Sigma Tau, Eta Kappa Nu, ASEE, IRE, AIEE, Registered Professional Engineer.

Professional Experience: Control Room Engineer at Radio Station WNAD, University of Oklahoma, June 1942 to September 1942. Entered active duty in Signal Corps, February 1943 after completion of Civil Service radio mechanic training. Completed in succession basic training, freshman and sophomore electrical engineering training, basic Cadet program and Communications Cadet program where a commission of Second Lieutenant was awarded in the United States Air Force in September, 1944. Awarded rating

of Electronics Countermeasures Observer in February 1943. Electronic Countermeasures operational employment in bomber aircraft from February 1943 to October 1945. Fighter-Interceptor Controller at Hollywood Control Center, October 1945 to April 1946. Television, radar and radio control operator in Crossroads Project, Atomic Bomb Research Project, Eniwetok, April 1946 to September 1946. Promoted to First Lieutenant and served in USAF Guided Missile Program, September 1946 to February 1947. Electronics Countermeasures, Radar and Communications Officer in USAF Strategic Air Command, February 1947 to September 1948. Student in Electrical Engineering under USAFIT program September 1948 to September 1951. Promoted to Captain and appointed Professor of Electrical Engineering at USAF Institute of Technology Resident College from September 1951 to October 1955. Served as Research and Development Administrator in Engineering Management of the Directorate of Nuclear Systems, Project 125 A, U. S. Air Force Research and Development Command Headquarters from October 1955 to June 1956. Student in Graduate Electrical Engineering under USAFIT program 1956 to August 1957. Appointed Professor of Electrical Engineering at U. S. Air Force Academy, August 1957.